ON THE SENSITIVITY OF COASTAL STORM SURGE TO ATMOSPHERIC FORCING

by

ALEXANDRA N. RAMOS VALLE

A dissertation submitted to the

School of Graduate Studies

Rutgers, The State University of New Jersey

In partial fulfillment of the requirements

For the degree of

Doctor of Philosophy

Graduate Program in Atmospheric Science

Written under the direction of

Enrique N. Curchitser

And approved by

_____

_____

_____

_____

New Brunswick, New Jersey

May, 2020

ABSTRACT OF THE DISSERTATION

On the Sensitivity of Coastal Storm Surge to Atmospheric Forcing

By ALEXANDRA N. RAMOS VALLE

Dissertation Director:

Enrique N. Curchitser

Storm surge represents a major threat for coastal communities in the United States, accounting for 50% of fatalities due to tropical cyclones (TCs) and causing significant economic losses. Cyclones along the Northeast United States have been some of the most destructive, partly due to their effect in regions with high population density. Hurricane Sandy was a high-impact event producing record-breaking storm surges around the Mid-Atlantic Bight region and causing billions of dollars in damages. Much of the impact from Hurricane Sandy is attributed to its atypical near-perpendicular angle of landfall. This event prompted the need to study a wide range of possible TC scenarios and to understand the role of atmospheric forcing in modulating storm surge. Motivated by the damages from TC-induced storm surge events, we seek to determine the sensitivity of storm surge to atmospheric forcing, in our attempt to contribute towards improved predictions and mitigation of storm surge impacts. Improvement of storm surge predictions can be accomplished by advancing and developing modeling systems, and by understanding the relation between storm surge and TC physical parameters. The work

in this dissertation seeks to determine the influence of different wind models on storm surge forecasts and to assess the sensitivity of storm surge to cyclone landfall angle.

To address these goals, we perform simulations of TCs, and their associated storm surge, by coupling state-of-the-art atmospheric and hydrodynamic models, namely the Weather Research and Forecasting model and the Advanced Circulation Model. The modeling framework facilitates the use of different wind models and the creation of synthetic cyclones that provide the desired spread in TC characteristics, particularly the angle of landfall. The coupled simulations are also used to inform an artificial neural network (ANN) model on the relationship between various TC parameters and storm surge, in our attempt to make accurate storm surge predictions at various station locations around the Mid-Atlantic Bight. We show that a higher resolution atmospheric simulation is not necessary to accurately depict the storm surge magnitude and spatial extent. While the sensitivity of storm surge and inundation to the TC impact angle varies along the coast, cyclones perpendicular to the coast generally produce the largest impacts. Results also emphasize the dependency of the storm surge impact to cyclone landfall location. We successfully train the ANN model to formulate timely storm surge predictions with a mean squared error of 0.08 m, demonstrating the potential of ANNs as forecasting tools.

We develop a modeling framework that can be employed to study the fundamental mechanisms modulating storm surge. Our results have important implications in how storm surge modeling can be improved, informing us on the current

limitations in storm surge assessment and on alternative methods for improved forecasts that will ultimately lead to a reduction of impacts from TC-induced storm surge.

ACKNOWLEDGEMENTS

I am extremely fortunate to have many people to thank for their support and encouragement during this adventure called grad school, and without whom the completion of this work would have not been possible. I would first like to extend my deepest gratitude to my mentor, Dr. Enrique Curchitser, who has provided me with invaluable advice and support during the past years. He has taught me to see every challenge as a new opportunity for growth, a lesson that I am very appreciative of. I am lucky to have had a mentor that supported my research endeavors (even when they were out of his own scope of research) and gave me so many opportunities to grow as a scientist and researcher. I would also like to extend my sincere gratitude to Dr. Cindy Bruyère, for her unconditional support, encouragement, and mentorship and for hosting me at the NCAR for the past four summers. I am deeply indebted to her for the time and dedication invested in mentoring me and teaching me everything I know about WRF- and the patience with which she did so. I am honored to have had such an amazing role model. I am also grateful to the other member of my dissertation committee, Dr. Tony Broccoli and Dr. Mark Miller, with whom I enjoyed many conversations on our research projects. I am grateful for their continued support since I began at Rutgers, both in the classroom setting and as committee members.

I would also like to thank some of the people at NCAR with whom I have had the pleasure of working with during my visits there. I am grateful to Kate Fossell, one of my co-authors, for everything she taught me about using the ADCIRC model and for always being available to answer my questions. I would also like to thank Abby Jaye and David

Ahijevych, both of whom shared their codes for model analysis with me and were always willing to help with the many issues that I encountered with the models. I would also like to express my gratitude to James Done, Andy Prein and the rest of the C3WE group at NCAR for taking an interest in my projects, our many conversations on ways to improve my analysis, and for always making me feel welcomed and part of the research group.

I would like to acknowledge Raphael Dussin for his incredible patience in assisting me through the installation process of my models and for his encouragement during the time we spent together at Rutgers. I am incredibly thankful to Dr. Ben Lintner for his interest in my professional development and the many opportunities he shared with me. I am also thankful to Bryan Raney for technical assistance. I would like to express my sincere thanks to Melissa Arnesen and Martha Pineda for their kindness and for always being available to give me advice and support. I would also like to acknowledge the assistance and encouragement from Simona Turcu and Gary Buschhorn at the School of Graduate Studies, who managed my fellowship.

I want to acknowledge my past research mentors, each of which contributed to my professional development before I even began graduate school: Arthur Taylor, Anne Myckow, David Enfield, Sang-Ki Lee, Jorge Capella and Mike Jensen.

I cherish the friendships and connections I made at DES and Rutgers. I specially want to thank my dear friends Nirmala and Natalie for the support and the advice they gave me- I love that we were able to go through the ups and downs of grad school together.

Leaving my home, friends and family in Puerto Rico to pursue my life-long dream of getting a Ph.D. is still one of the hardest things I have ever had to do. I truly cannot begin to express my gratitude to my family for their unconditional love and encouragement for me to pursue my dreams. Everything I have accomplished, I owe to my parents (Lourdes and Edwin), and my brother and sister-in-law (Alexis and Zashary), who have been my greatest source of inspiration and motivation. I would specially like to thank my partner, Giovanni, for his unconditional love, patience and understanding. Thank you for being with me every step of the way, for pushing me to give my absolute best and for encouraging me in moments when I doubted myself.

This material is based upon work supported by the National Science Foundation Graduate Research Fellowship Program under Grant No. DGE-1433187. Any opinions, findings, and conclusions or recommendations expressed in this material are those of the authors and do not necessarily reflect the views of the National Science Foundation. This work was also supported in part by the School of Environmental and Biological Sciences and the Institute of Earth, Ocean and Atmospheric Sciences at Rutgers University.

Parts of this dissertation have been previously published as follows:

1. Chapter 2 is published as:

   Ramos-Valle, A., Curchitser, E., Bruyère, C., & Fossell, K. (2018). Simulating Storm Surge I mpacts with a Coupled Atmosphere-Inundation Model with Varying Meteorological Forcing. *Journal of Marine Science and Engineering, 6*(2), 35. http://www.mdpi.com/2077-1312/6/2/35

2. Chapter 3 is published as:

Ramos-Valle, A. N., Curchitser, E. N., & Bruyère, C. L. (2020). Impact of Tropical Cyclone Landfall Angle on Storm Surge Along the Mid-Atlantic Bight. *Journal of Geophysical Research: Atmospheres*, e2019JD031796. https://agupubs.onlinelibrary.wiley.com/doi/abs/10.1029/2019JD031796

DEDICATION

To my loving parents –

You are my greatest inspiration and role models.

I could not have done this without your unconditional love and support.

TABLE OF CONTENTS

Abstract of the Dissertation ii

Acknowledgements v

Dedication ix

Table of Contents x

List of Tables xiv

List of Illustrations xv

CHAPTER 1: INTRODUCTION 1

1.1 Motivation 1

1.2 Background 4

1.3 Objectives 6

1.4 References 9

CHAPTER 2. SIMULATING STORM SURGE IMPACTS WITH A COUPLED ATMOSPHERE-INUNDATION MODEL WITH VARYING METEOROLOGICAL FORCING 12

2.1 Abstract 12

2.2. Introduction 12

2.3 Material and Methods 17

2.3.1 WRF Model Configuration 17

2.3.2 ADCIRC Model Description and Atmospheric Forcing Configuration 19

2.4 Results 23

2.4.1 WRF Model Evaluation 24

2.4.2 Control Storm Surge Simulation 30

2.4.3 WRF Simulated Cyclone Track-Forced Storm Surge Simulation 31

2.4.4 WRF Full Field-Forced Storm Surge Simulations 33

2.4.5 Inter-Comparison of Simulations with Varying Meteorological Forcing 35

2.5 Discussion 44

2.6 Conclusions 49

2.7 References 50

CHAPTER 3. IMPACT OF TROPICAL CYCLONE LANDFALL ANGLE ON STORM SURGE ALONG THE MID-ATLANTIC BIGHT 54

3.1 Abstract 54

3.2 Introduction 54

3.3 Material and Methods 57

3.3.1 HWCM configuration 58

3.3.2 Description of synthetic cyclone simulations with the HWCM 62

3.3.3 SWAN+ADCIRC Model Description and Atmospheric Forcing Configuration 64

3.4 Results 67

3.4.1 Evaluation of simulated synthetic tracks 67

3.4.2 HWCM+ADCIRC ensemble 68

3.4.3 The effect of TC landfall angle on storm surge 73

3.4.3.1 A case study along the coast of NJ 73

3.4.3.2 Ensemble simulations to assess the effect of cyclone landfall on storm surge 76

3.4.4. Clustering by storm surge scenarios 81

3.5 Discussion 85

3.6 Concluding remarks 88

3.7 References 89

CHAPTER 4. IMPLEMENTATION OF AN ARTIFICIAL NEURAL NETWORK FOR STORM SURGE FORECASTING 95

4.1 Abstract 95

4.2 Introduction 96

4.3 Data and Methods 99

4.3.1 Data 99

4.3.1.1 Synthetic Tropical Cyclones 99

4.3.1.2 Storm Surge Simulations 100

4.3.2 ANN Model Architecture 102

4.3.3 Performance Metrics 106

4.3.4 Metrics for ANN Model Interpretation 107

4.3.4.1 Permutation Feature Importance 107

4.3.4.1 Partial Dependence Plots 108

4.4 Results 108

4.4.1 Test for Model Predictability at Various Lead Times 108

4.4.2 Storm Surge Forecast 110

4.4.3 Feature Importance 113

4.5 Discussion 118

4.6 Conclusions 123

4.7 References 124

CHAPTER 5. SUMMARY 127

5.1 Summary and Implications 127

5.2 References 130

Appendix A: Supporting information for Chapter 3 132

LIST OF TABLES

Table 2-1. Model Configuration for Hurricane Sandy WRF 12-4km, WRF 12km and WRF 4km Simulations 19

Table 2-2. ADCIRC Model Configuration Parameters 22

Table 2-3. Description of Meteorological Forcing for Each Coupled Simulation 22

Table 2-4. Statistics for Water Elevation of Each Simulation 41

Table 3-1. Description of Parameters Chosen to Initialize the Real-World Simulations ... 63

Table 3-2. Range and Mean Values for Physical Parameters that Characterize the Cyclone Within Each Cluster 85

Table 4-1. Performance of the ANN Models Including MSE and Pearson Correlation Coefficient 109

LIST OF ILLUSTRATIONS

Figure 2-1. (a) Advanced Circulation Model (ADCIRC) finite element unstructured mesh used for the Federal Emergency Management Agency (FEMA) Region II Coastal Surge Study (FEMA, 2014). The mesh has been designed with higher resolution along the Hudson Bay, NJ, and NY coastal regions. The mesh has 604,790 nodes; (b) Zoom in for the white box in (a) of the NJ and NY coastline. Raritan Bay, Delaware Bay and Long Island Sound bays are identified 21

Figure 2-2. The Weather Research and Forecasting (WRF) model 12-4 km simulated hurricane Sandy track (black) initialized on 28 October 0000 UTC compared to National Hurricane Center (NHC) best track data (red). The simulated storm makes landfall on 30 October at 0000 UTC about 20 km south of hurricane Sandy's landfall location near Brigantine, NJ, USA. Track information is provided every 6 h. Insert: zoom in view of cyclone landfall location with track information provided every 3 h 25

Figure 2-3. Cyclone wind speed from NHC best track (dashed black line); WRF 12 km simulation (blue); and WRF 12-4 km simulation (green) 26

Figure 2-4. Same as Figure 2-2 except track is presented for the WRF 12 km simulation 27

Figure 2-5. Comparison of WRF 12-4 km simulated minimum pressure (top) and maximum wind (bottom) estimates with station observations for (a) Atlantic City, NJ, (b) The Battery, NY, (c) Bergen Point, NY, (d) Cape May, NJ, (e) Kings Point, NY and (f) New York Harbor Entrance, NY stations 29

Figure 2-6. Wind field analysis for 2100 UTC 29 October 2012 from (a) HWIND (source: NOAA/AOML/Hurricane Research Division); (b) WRF 12-4 km simulation 30

Figure 2-7. (a) Simulated maximum water levels above mean sea level (MSL) during the period of 23 October 0000 UTC through 30 October 1200 UTC for the CTL ADCIRC run forced with the NHC best track dataset. (b) Same as (a) except simulation is initialized on 28 October 0000 UTC to correspond with initialization period of WRF simulations. The black line indicates the track of Hurricane Sandy as it made landfall in New Jersey north of Atlantic City 31

Figure 2-8. (a) Simulated maximum water levels above MSL during the period of 28 October 0000 UTC through 30 October 1200 UTC for SCT12-4. The black line represents the track of the storm, which makes landfall closer to Atlantic City, south of the observed landfall location. (b) Difference between SCT12-4 and the control simulation 33

Figure 2-9. Simulated maximum water levels during the period of 28 October 0000 UTC through 30 October 1200 UTC for (a) FWP12-4; (b) FWP12; and (c) FWP4 34

Figure 2-10. Differences from the control simulation for the (a) FWP12-4; (b) FWP12; and (c) FWP4 simulations 35

Figure 2-11. Difference in maximum water elevation between FWP12-4 and SCT12-4 (i.e., between track-forced simulation and the simulation forced with the full wind and pressure field output from WRF simulations of the same resolution) 38

Figure 2-12. Times series of all simulations including a short CTL simulation for (a) Atlantic City NJ station; (b) The Battery NY station; and (c) Montauk NY station. The WRF-ADCIRC simulation estimates have been shifted by 3 h ahead of time to correspond with the peak

of the observed water level and are shown for (d) Atlantic City NJ station; (e) The Battery NY station; and (f) Montauk NY station 39

Figure 2-13. Maximum water elevation with ADCIRC wind vector output on 29 October 2300 UTC for (a) CTL; (b) SCT12-4; (c) FWP12-4; (d) FWP12; and (e) FWP4. The length of the 30 ms^{-1} wind vector is provided as reference 43

Figure 3-1. Atmospheric vertical profile used to characterize the environment in the ideal and real simulations. Values were interpolated to account for missing data at various pressure levels. The atmospheric temperature and dewpoint are shown in the red and green lines, respectively 59

Figure 3-2. (a) Depiction of the FEMA Region II mesh spacing for the NJ-NY coastal region. (b) Bathymetric heights along the NJ-NY coast. The location of various points of interest are highlighted 64

Figure 3-3. (a) Synthetic cyclone tracks for the 198 TCs resulting from the HWCM ensemble. Synthetic cyclone tracks are shown at 6-hr intervals for 60 hr after cyclone placement in the real-world domain. (b) The landfall location density map is shown 69

Figure 3-4. Distribution of (a) wind speed (m/s), (b) minimum pressure (mb), (c) translation speed (m/s), and (d) radius of maximum winds (km) for the 198 HWCM simulated synthetic cyclones 70

Figure 3-5. (a) Ensemble average of maximum water level. (b) Zoom in of (a) along the New Jersey coast. (c) Maximum water elevation forecasted at each node. (d) Zoom in of (c) along the New Jersey coast 72

Figure 3-6. (a) Case study to explore relationships between TC landfall angle and storm surge. Maximum wind speed fields for the (b) perpendicular, (c) diagonal, and (d) parallel cases …… 74

Figure 3-7. Maximum storm surge levels for the (a) perpendicular, (b) diagonal and (c) parallel tracks in the case study. Tracks are plotted near landfall at 3-hr intervals ……. 76

Figure 3-8. The tracks that made landfall in NJ were considered to investigate the effect of TC landfall angle and location on storm surge. The clustering resulted in (a) 59 perpendicular tracks, (b) 43 diagonal tracks, and (c) 11 parallel tracks with respect to the NJ coast. (d-f) The corresponding maximum storm surge levels, showing the differences in offshore extent ……..…… 77

Figure 3-9. Distribution of (a) wind speed (m/s), (b) minimum pressure(mb), (c) radius of maximum winds (km), (d) translation speed, (e) inundation area (km^2), and (f) inundation volume(km^3). The distributions are normalized by the number of storms per category ..79

Figure 3-10. Simplified tracks for the storms that produced the top 10 highest storm surges for each of the categories at (a) Atlantic City and (b) The Battery stations. The tracks are identified based on the magnitude of the peak storm surge …….. 80

Figure 3-11. Tropical cyclone and storm surge properties identified by clusters. (a) Landfall location of storms, (b) maximum wind speed at landfall, (c) estimates of inundation volume, and (d) translation speed. TC data in (b)-(d) have been sorted by increasing latitude coordinate at landfall …….. 83

Figure 4-1. Tracks for the 198 synthetic cyclones used for training and testing of the ANN. These cyclones were simulated with the HWCM model (Ramos-Valle et al., 2020) ……. 100

Figure 4-2. Region of study. The location of the stations examined in this study are highlighted. The ANN model is trained with storm surge levels at these five stations … 101

Figure 4-3. (a) Schematic of the architecture of a simple ANN with a single hidden layer. The input and their associated weights are combined into a net input function, as represented in Equation 1, and passed through the activation function to produce an output (Equation 2). (b) Schematic of an ANN with two hidden layers and multi-dimensional output as implemented in the current study. Source: Sahoo and Bhaskaran (2019) ……. 103

Figure 4-4. Distribution of various TC parameters for the 149 TCs used for training …… 105

Figure 4-5. Taylor diagram showing relative performance of each ANN models in Table 4-1. Point A denotes the target model …… 110

Figure 4-6. Scatter plots showing the ADCIRC model predictions vs the ANN model predictions. The dataset presented included every time step of the 49 cases in the testing set (N = 3,528 data points). The best fit line (dashed gray line) and the identity line (solid gray line) are plotted for reference ……. 111

Figure 4-7. Storm surge time series for one of the TC test cases. The ANN storm surge time series prediction is compared to the verification data, the ADCIRC model predication, at (a) Atlantic City, (b) Sandy Hook, (c) The Battery, and (d) Orient Harbor stations …… 113

Figure 4-8. Feature permutation importance as given by the MSE loss function. The input variables are sorted in decreasing order of importance …… 115

Figure 4-9. Correlation matrix between the input variables used in the ANN …….. 115

Figure 4-10. Partial dependence plots for the input variables: (a) latitude, (b) longitude, (c) pressure (mb), (d) R_{max} (km), (e) translation speed (m/s) and (f) maximum wind speed (m/s), examined at The Battery station …… 117

Figure 4-11. Partial dependence plots for the input variables: (a) latitude, (b) longitude, (c) pressure (mb), (d) R_{max} (km), (e) translation speed (m/s) and (f) maximum wind speed (m/s), examined at Montauk station …… 118

Figure A-1. Depicts the cases used to test for model variability in the HWCM. The DFI scheme, with integration time of 0.5, 1, 2 and 3 hours, was implemented within the HWCM to removed initial model instabilities by reducing high-frequency features. TC intensity is shown per each 3-hr time step …… 132

Figure A-2. K-means cluster analysis for the maximum storm surge distributions of the 113 cyclones in the HWCM ensemble that make landfall along the NJ coastline. The analysis resulted in the use of the four clusters presented here. (Left) Tracks for the associated storm in each cluster and (right) the average maximum storm surge distributions are shown for Cluster 1, Cluster 2, Cluster 3 and Cluster 4, respectively … 133

Figure A-3. Rainfall totals for the (a) perpendicular, (b) diagonal and (c) parallel tracks in the case study presented in section 3.5 …… 134

CHAPTER 1. INTRODUCTION

1.1 Motivation

Tropical cyclones (TCs), which are associated with heavy rains, extreme winds and floods, represent a major threat for coastal communities in the United States. The overall damages from weather-related disaster events in the US is dominated by losses resulting from TCs (Smith, 2018). Specifically, in the Atlantic basin one out of every five to six TCs causes loss of life (Rappaport, 2014). Storm surge, defined as an abnormal rise of water generated by a storm, above and beyond the predicted astronomical tides, represents the most damaging aspect of a TC. Storm surge impacts often result in significant loss of life and property. Rappaport (2014) quantified the loss of life directly resulting from Atlantic TCs and reported that 50% of fatalities were attributed to storm surge.

An example of a high-impact TC is Hurricane Katrina (2005), which drove a storm surge of about 7.6 m along the coast of Mississippi, causing a total of more than $125 billion in losses and multiple fatalities (Lin et al., 2010). Along the Northeast US, where cyclones are less frequent, the “Long Island Express” cyclone of 1983, produced flooding of up to 3.5 m in New York (NY) (Lin et al., 2010). Another notable case is that of Hurricane Sandy which produced major floods in New York City and damages of at least $50 billion (Blake et al., 2013).

Population expansions in coastal cities will only serve to increase the community’s exposure to these devastating TC and storm surge events. Climate change is expected to exacerbate storm surge and coastal flood impacts from TCs (Colle et al., 2008; Lin et al., 2012). The combined effect of changes in cyclone climatology along with the expected

rise in sea level is projected to shorten storm surge flooding return periods (Garner et al., 2017; Lin et al., 2012; Reed et al., 2015). For areas like New York City, this translates to a projected reduction in the return period of the 100-year surge flood to occur between 3-20 years (Lin et al., 2012), and a decrease in the return period of the 500-year flood event to approximately a 25-year return period (Reed et al., 2015).

The magnitude of the storm surge impacts is known to depend on TC characteristics such as the cyclone intensity (Weisberg & Zheng, 2006), size (Irish et al., 2008), and forward speed (Hussain et al., 2017; Rego & Li, 2009; Thomas et al., 2019), as well as on local geographic and bathymetric features (Bloemendaal et al., 2019). While the physics of storm surge are relatively well known (Kohno et al., 2018), uncertainties remain regarding the level of sensitivity to these TC parameters. These relationships and dependencies are difficult to assess due to the limited historical record. The limitation in the observed record, as well as the quality of the data, presents difficulties in our ability to assess and understand the expected storm surge impact from different TC scenarios (i.e. different combinations of cyclone features).

A recent study by Needham et al. (2015), accounted for water level records for 389 TCs in the western North Atlantic Basin. A total of 17 events affected islands in the Caribbean, while 242 events occurred along the U.S Gulf Coast. Out of a total of 110 events that impacted the U.S. Atlantic Coast, 22% occurred along the coastline from Virginia to Maine (Needham et al., 2015). The Northeast US is characterized by low-frequency and high-impact events. Cyclones affecting the Northeast US have been some

of the most destructive, partly due to their impact in densely populated areas in low laying coastal regions (Hallegatte et al., 2013; Klotzbach et al., 2018; Yin et al., 2016).

A classic and historical example of a high-impact event in the Northeast US is that of Hurricane Sandy, which made landfall in Brigantine, New Jersey (NJ) on October 2012. Hurricane Sandy ranks as the fourth costliest TC to impact the US (NCEI, 2018)- most of the damages being attributed to the magnitude of the storm surge impacts (Neumann et al., 2015). Hurricane Sandy caused major disruptions in transportation and long-term damages to the housing market. It caused unprecedented storm surges in NJ and NY, between 3 and 4 m above mean sea level (Blake et al., 2013; Reed et al., 2015). While other factors were involved in generating such impacts (e.g. storm size), much of the damages are attributed to Hurricane Sandy's rare near-perpendicular angle of landfall relative to the NJ coast. While the return period of a TC with a track similar to that of Hurricane Sandy's is estimated to be more that 700 years (Hall & Sobel, 2013), the damages it produced reflected the magnitude of the impacts this type of track can have, emphasizing the need to study and assess a wider range of possible TC scenarios. Hurricane Sandy served as an example of how a combination of different factors, including TC characteristics and impact area, can amount to such extensive damages, prompting the need to further understand and quantify the sensitivity of storm surge to TC parameters and atmospheric forcing in general.

This research is motivated by the impacts of extreme TC and storm surge events on communities, and our goal of mitigating the risk from these natural threats. Hazards associated with TCs, including but not limited to coastal flooding from storm surge, have

a virtually incalculable impact on people's quality of life, that transcends the physical aspects of these natural phenomena. From a socio-economic perspective, in the aftermath of these events there is a general loss of essential services, with disruptions in the education, transportation, communication and health services. Additionally, these events have long-lasting impacts on people's mental health. In the aftermath of major cyclones, there is an increased risk for posttraumatic stress disorder, anxiety and depression (Scaramutti et al., 2019), which challenges people's ability to cope and adapt to other natural events.

In this work, we focus on the physical aspects of TC-induced storm surge to contribute to the improvement of storm surge forecasting, as a step toward making coastal communities more resilient to TCs and the associated flood hazard.

1.2 Background

Atmospheric forcing is the primary driver of storm surge (Dietrich et al., 2017; Lakshmi et al., 2017), and it is one the main sources of uncertainties in storm surge modeling (Gonzalez et al., 2019; Mayo & Lin, 2019). Previous studies have examined the sensitivity of storm surge to cyclone intensity, size, forward speed and location (Hussain et al., 2017; Irish et al., 2008; Thomas et al., 2019). Weisberg and Zheng (2006) studied the impact of various storm parameters on storm surge in Tampa Bay and found that storm surge heights increased in proportion to the cyclone wind speed. Peak storm surge was found to increase proportionally with storm size (as given by the radius of maximum winds, R_{max}) for a set of synthetic cyclones simulated in the Gulf of Mexico (Irish et al., 2008).

While the relationship between storm surge and some of the storm parameters are more straightforward to determine, others such as the effect of storm translational speed and angle of landfall on storm surge have proven to be more complicated and difficult to assess. Rego and Li (2009) conducted a case-study of Hurricane Rita in the Gulf of Mexico and found that increasing translational speed increased peak surge by about 7%, but decreased the flooding volume. Comparably, Thomas et al. (2019) found that faster cyclones were responsible for producing higher storm surge along the open coast but less flooding. Hussain et al. (2017) found different regimes when assessing the impact of storm translational speed on storm surge while relating to the radius of maximum winds. They found this relationship to differ depending on whether the location assessed is outside or within the R_{max}, with increasing translation speed producing lower surge heights within the storm's R_{max} and higher surge heights beyond the R_{max}.

The sensitivity of storm surge to landfall angle around New York City has been assessed in various studies (Galarneau et al., 2013; Gurumurthy et al., 2019; Lin et al., 2010). Their results indicate that for New York City, specifically at the Battery station, the optimal wind direction for maximum storm surge is generally southeasterly. Some of these studies were limited by the model capability and the neglect of spatial variations in storm surge and inland flood assessment, which are necessary to accurately account for the impact and risk from different TCs.

These storm surge assessments and sensitivity studies are often conducted with numerical storm surge models. Atmospheric forcing in these models is provided in the form of surface pressure and surface wind fields from various sources and configurations.

These can include the use of cyclone track-based data implemented in parametric vortex models to represent TC winds, as well as the use 3D full-physics atmospheric models. Each model presents their own strengths and limitations. There is often a trade-off between model efficiency and their predictive skill and accuracy. Parametric vortex models use a simple set of TC parameters, including the cyclone location, maximum wind speed, minimum pressure, and translation speed, to derive the TC wind field. As such, the use of parametric models enables timely storm surge predictions at the expense of less accuracy in the TC wind field, in contrast to what can be achieved with numerical weather prediction models.

More recently, data-driven methods, including machine learning methods such as artificial neural networks (ANNs), have been implemented for forecasting storm surge. ANNs rely on historical or simulated TC datasets to learn the relationships between the atmospheric forcing parameters and the resulting storm surge, enabling them to make predictions of storm surge outcomes based on a given set of input parameters.

Sensitivity studies are further constraint by the limited TC and storm surge historical records. Due to the length limitations of the historical TC record, additional methods have been developed to simulate possible storm tracks or synthetic cyclones. The use of these models in simulating synthetic cyclones, linked with hydrodynamic models, facilitates the studies of different hurricane scenarios and their expected storm surge impact.

1.3 Objectives

Recent major TC-induced storm surge events have revolutionized storm surge studies and prompted the need for improved storm surge forecasts. Improvement of storm surge

forecasts can be achieved by consideration of: (i) the advancement and understanding of model coupling (e.g. atmospheric, hydrodynamics and hydrological components), (ii) a comprehensive understanding of the sensitivity of storm surge to different cyclone characteristics, and (iii) the availability of timely and accurate water level forecasts. This study is guided and motivated by these areas of improvement in storm surge assessment and forecasting. The overarching goal of this study is to contribute to the improvement of storm surge forecasts and risk reduction from this hazard by understanding the role of atmospheric forcing on storm surge, from a physical and modeling standpoint. From the modeling standpoint, the approach is to determine how different model configurations affect storm surge and identify optimal modeling practices for storm surge assessment. From the physical stance the objective is to gain a better intuition into the relation between the atmospheric drivers of storm surge and the resulting impact to determine how different TC parameters modulate storm surge.

The field of storm surge studies is moving towards integrating multiple storm hazards by building a comprehensive model for storm surge assessment that includes fully-coupled atmospheric, hydrodynamic, hydraulic and hydrological models. Model coupling presents a challenge as multiple processes run at different spatial and temporal scales (Elko et al., 2019). A step in this direction is to understand how each of these components interact with each other and the modeling limitations for each of the interactions. In Chapter 2, we addressed the need for improved understanding of model coupling between the atmospheric and hydrodynamic components. We compared the use of different wind field models as atmospheric forcing to the hydrodynamic model.

Additionally, we evaluated the sensitivity of the atmospheric model resolution in accurately depicting storm surge spatial patterns. Quantifying the spatial resolution needed for accurate and timely forecasts is identified as one of the top research priorities in improving storm surge forecasting methods (Elko et al., 2019). Our aim is to understand the model limitations and determine an accurate coupled-model configuration that can be employed for storm surge assessment.

The need for a comprehensive understanding of the underlying processes contributing to the storm surge impact is addressed in Chapter 3. We implemented a newly developed atmospheric model that allows us to simulate synthetic cyclones, addressing the limitations imposed by the historical record. Our approach is to simulate a wider range of TC scenarios that will allow us to assess variations of storm surge magnitude, spatial distribution and inland flooding as a function of cyclone landfall angle. We designed a modeling framework that can be applied for other physical problems and to other regions. For example, the regional atmospheric circulation during storm surge events has been shown to be linked to the magnitude of the surge impact (Catalano & Broccoli, 2018; Montreuil et al., 2016). Different environmental and climatic conditions lead to different magnitudes of storm surge impact. The framework presented can be applied to explore and test these mechanisms, including the expected changes due to projected climate conditions.

Chapter 4 presents the implementation of an ANN in producing accurate and timely water level predictions. Data from the ensemble of synthetic cyclones generated in Chapter 3 was used to inform the neural network model of the relationship between

different TC characteristics and storm surge. Our aim in implementing an ANN is to build a model capable of producing timely and accurate results, that in addition can provide information on the degree of sensitivity of storm surge to various cyclone parameters. In Chapter 5, we present a summary of the methodologies implemented and the key findings of this work.

1.4 References

(NCEI), N. N. C. f. E. I. (2018). U.S. Billion-Dollar Weather and Climate Disasters. Retrieved from https://www.ncdc.noaa.gov/billions/

Blake, E. S., Kimberlain, T. B., Berg, R. J., Cangialosi, J. P., & Beven II, J. L. (2013). Tropical cyclone report: Hurricane sandy. *National Hurricane Center, 12*, 1-10.

Bloemendaal, N., Muis, S., Haarsma, R. J., Verlaan, M., Irazoqui Apecechea, M., de Moel, H., et al. (2019). Global modeling of tropical cyclone storm surges using high-resolution forecasts. *Climate Dynamics, 52*(7), 5031-5044. https://doi.org/10.1007/s00382-018-4430-x

Catalano, A. J., & Broccoli, A. J. (2018). Synoptic characteristics of surge-producing extratropical cyclones along the northeast coast of the United States. *Journal of Applied Meteorology and Climatology, 57*(1), 171-184.

Colle, B. A., Buonaiuto, F., Bowman, M. J., Wilson, R. E., Flood, R., Hunter, R., et al. (2008). New York City's vulnerability to coastal flooding: Storm surge modeling of past cyclones. *Bulletin of the American Meteorological Society, 89*(6), 829-841.

Dietrich, J., Muhammad, A., Curcic, M., Fathi, A., Dawson, C., Chen, S., & Luettich Jr, R. (2017). Sensitivity of Storm Surge Predictions to Atmospheric Forcing during Hurricane Isaac. *Journal of Waterway, Port, Coastal, and Ocean Engineering, 144*(1), 04017035.

Elko, N., Dietrich, C., Cialone, M., Stockdon, H., Bilskie, M. W., Boyd, B., et al. (2019). Advancing the understanding of storm processes and impacts. *Shore & Beach, 87*(1), 37.

Galarneau, T. J., Davis, C. A., & Shapiro, M. A. (2013). Intensification of Hurricane Sandy (2012) through extratropical warm core seclusion. *Monthly Weather Review, 141*(12), 4296-4321.

Garner, A. J., Mann, M. E., Emanuel, K. A., Kopp, R. E., Lin, N., Alley, R. B., et al. (2017). Impact of climate change on New York City's coastal flood hazard: Increasing flood heights from the preindustrial to 2300 CE. *Proceedings of the National Academy of Sciences, 114*(45), 11861-11866.

Gonzalez, V. M., Nadal-Caraballo, N. C., Melby, J. A., & Cialone, M. A. (2019). *Quantification of Uncertainty in Probabilistic Storm Surge Models: Literature Review*. Retrieved from Vicksburg, MS: https://apps.dtic.mil/dtic/tr/fulltext/u2/1067548.pdf

Gurumurthy, P., Orton, P. M., Talke, S. A., Georgas, N., & Booth, J. F. (2019). Mechanics and Historical Evolution of Sea Level Blowouts in New York Harbor. *Journal of Marine Science and Engineering, 7*(5), 160.

Hall, T. M., & Sobel, A. H. (2013). On the impact angle of Hurricane Sandy's New Jersey landfall. *Geophysical Research Letters, 40*(10), 2312-2315. Article. <Go to ISI>://WOS:000328840200076

Hallegatte, S., Green, C., Nicholls, R. J., & Corfee-Morlot, J. (2013). Future flood losses in major coastal cities. *Nature climate change, 3*(9), 802.

Hussain, M. A., Tajima, Y., Hossain, M. A., & Das, P. (2017). Impact of Cyclone Track Features and Tidal Phase Shift upon Surge Characteristics in the Bay of Bengal along the Bangladesh Coast. *Journal of Marine Science and Engineering, 5*(4), 52. http://www.mdpi.com/2077-1312/5/4/52

Irish, J. L., Resio, D. T., & Ratcliff, J. J. (2008). The influence of storm size on hurricane surge. *Journal of Physical Oceanography, 38*(9), 2003-2013. Article.

Klotzbach, P. J., Bowen, S. G., Pielke Jr, R., & Bell, M. (2018). Continental United States Hurricane Landfall Frequency and Associated Damage: Observations and Future Risks. *Bulletin of the American Meteorological Society*(2018).

Kohno, N., Dube, S., K., Entel, M., Fakhruddin, S., H. M., Greenslade, D., Leroux, M.-D., et al. (2018). Recent progress in storm surge forecasting. *Tropical Cyclone Research and Review, 7*(2), 128-139. https://hal.archives-ouvertes.fr/hal-01727930

Lakshmi, D. D., Murty, P., Bhaskaran, P. K., Sahoo, B., Kumar, T. S., Shenoi, S., & Srikanth, A. (2017). Performance of WRF-ARW winds on computed storm surge using hydodynamic model for Phailin and Hudhud cyclones. *Ocean Engineering, 131*, 135-148.

Lin, N., Emanuel, K., Oppenheimer, M., & Vanmarcke, E. (2012). Physically based assessment of hurricane surge threat under climate change. *Nature Climate Change, 2*(6), 462-467. Article.

Lin, N., Emanuel, K. A., Smith, J., & Vanmarcke, E. (2010). Risk assessment of hurricane storm surge for New York City. *Journal of Geophysical Research: Atmospheres, 115*(D18).

Mayo, T., & Lin, N. (2019). The Effect of the Surface Wind Field Representation in the Operational Storm Surge Model of the National Hurricane Center. *Atmosphere, 10*(4), 193. http://www.mdpi.com/2073-4433/10/4/193

Montreuil, A.-L., Elyahyioui, J., & Chen, M. (2016). Effect of Large-Scale Atmospheric Circulation and Wind on Storm Surge Occurrence. *Journal of Coastal Research, 75*(sp1), 755-759, 755. https://doi.org/10.2112/SI75-152.1

Needham, H. F., Keim, B. D., & Sathiaraj, D. (2015). A review of tropical cyclone-generated storm surges: Global data sources, observations, and impacts. *Reviews of Geophysics, 53*(2), 545-591.

Neumann, J. E., Emanuel, K., Ravela, S., Ludwig, L., Kirshen, P., Bosma, K., & Martinich, J. (2015). Joint effects of storm surge and sea-level rise on US Coasts: new economic estimates of impacts, adaptation, and benefits of mitigation policy. *Climatic Change, 129*(1), 337-349. journal article. https://doi.org/10.1007/s10584-014-1304-z

Rappaport, E. N. (2014). Fatalities in the United States from Atlantic tropical cyclones: New data and interpretation. *Bulletin of the American Meteorological Society, 95*(3), 341-346.

Reed, A. J., Mann, M. E., Emanuel, K. A., Lin, N., Horton, B. P., Kemp, A. C., & Donnelly, J. P. (2015). Increased threat of tropical cyclones and coastal flooding to New York City during the anthropogenic era. *Proceedings of the National Academy of Sciences of the United States of America, 112*(41), 12610-12615. Article. <Go to ISI>://WOS:000363130900029

Rego, J. L., & Li, C. (2009). On the importance of the forward speed of hurricanes in storm surge forecasting: A numerical study. *Geophysical Research Letters, 36*(7). https://agupubs.onlinelibrary.wiley.com/doi/abs/10.1029/2008GL036953

Scaramutti, C., Salas-Wright, C. P., Vos, S. R., & Schwartz, S. J. (2019). The mental health impact of Hurricane Maria on Puerto Ricans in Puerto Rico and Florida. *Disaster medicine and public health preparedness, 13*(1), 24-27.

Smith, A. B. (2018). *2017 US billion-dollar weather and climate disasters: a historic year in context*. Retrieved from https://www.climate.gov/news-features/blogs/beyond-data/2017-us-billion-dollar-weather-and-climate-disasters-historic-year

Thomas, A., Dietrich, J., Asher, T., Bell, M., Blanton, B., Copeland, J., et al. (2019). Influence of storm timing and forward speed on tides and storm surge during Hurricane Matthew. *Ocean Modelling, 137*, 1 - 19. http://www.sciencedirect.com/science/article/pii/S1463500318302609

Weisberg, R. H., & Zheng, L. (2006). Hurricane storm surge simulations for Tampa Bay. *Estuaries and Coasts, 29*(6), 899-913.

Yin, J., Lin, N., & Yu, D. P. (2016). Coupled modeling of storm surge and coastal inundation: A case study in New York City during Hurricane Sandy. *Water Resources Research, 52*(11), 8685-8699. <Go to ISI>://WOS:000393318600017

CHAPTER 2. SIMULATING STORM SURGE IMPACTS WITH A COUPLED ATMOSPHERE-INUNDATION MODEL WITH VARYING METEOROLOGICAL FORCING

2.1 Abstract

Storm surge events have the potential to cause devastating damage to coastal communities. The magnitude of their impacts highlights the need for increased accuracy and real-time forecasting and predictability of storm surge. In this study, we assess two meteorological forcing configurations to hindcast the storm surge of Hurricane Sandy, and ultimately support the improvement of storm surge forecasts. The Weather Research and Forecasting (WRF) model is coupled to the Advanced CIRCulation Model (ADCIRC) to determine water elevations. We perform four coupled simulations and compare storm surge estimates resulting from the use of a parametric vortex model and a full-physics atmospheric model. One simulation is forced with track-based meteorological data calculated from WRF, while three simulations are forced with the full wind and pressure field outputs from WRF simulations of varying resolutions. Experiments were compared to an ADCIRC simulation forced by National Hurricane Center best track data, as well as to station observations. Our results indicated that given accurate meteorological best track data, a parametric vortex model can accurately forecast maximum water elevations, improving upon the use of a full-physics coupled atmospheric-surge model. In the absence of a best track, atmospheric forcing in the form of full wind and pressure field.

2.2 Introduction

Tropical cyclones (TCs), and their associated storm surge, are some of the most damaging natural phenomena (Smith & Katz, 2013). The magnitude of the resulting storm

surge is dependent on geographical and bathymetric features, as well as TC characteristics including intensity, size, translational speed, and the direction in which the TC approaches the coast at landfall. The lack of availability of observations and accuracy of these properties prior to landfall, and the limitations in the characterization of the TC wind structure prove a challenge for real-time forecasting of storm surge impacts. When trying to understand how storm surge impacts will affect coastal regions, it is imperative to have a clear understanding of the factors that have influenced storm surge estimates in the past. Yet, as is the case with TCs, historical data on storm surge events is limited (Resio & Westerink, 2008).

Based on a recent review on TC induced storm surges, maximum water level data is available for 389 TCs in the western North Atlantic Basin, with 17 events on Caribbean Islands, 242 events along the U.S Gulf Coast and 110 events along the U.S. Atlantic Coast (Needham et al., 2015). Only 22% of the events observed along the U.S Atlantic Coast occurred along the coastline from Virginia to Maine (Needham et al., 2015). Some of these TC and extratropical cyclone (ETC) induced storm surge events have been highly destructive, partly because their landfall location has been around densely populated areas in states such as New York (NY) and New Jersey (NJ) (Klotzbach et al., 2018). In this study, we considered one of such events as a case study. Hurricane Sandy is a TC known for its unique development and track, as well as the magnitude of the damages it caused. Despite being a unique case, Hurricane Sandy is an example of the vast impact TCs can have, and how a combination of factors can amount to such extensive damages (Colle et al., 2015). As such, Hurricane Sandy is chosen as our case of interest.

Hurricane Sandy is now ranked as the fourth costliest storm to impact the US (NCEI, 2018). The damages produced were primarily caused by the large extent of the TC's wind field (Blake et al., 2013), the near perpendicular landfall angle (Hall & Sobel, 2013), and the consequent storm surge produced by the combination of these factors. The storm surge observed reached up to 3.85 m above normal tide level at Kings Point, NY, USA (Barnes et al., 2013; Blake et al., 2013). Moreover, having reached unprecedented storm surge heights, Hurricane Sandy tested the resilience of the NJ and NY coastal infrastructure to storm surge. Events such as Hurricane Sandy highlight the importance of understanding the physical processes behind storm surge and improving modeling techniques, and as such, this remains an active topic of research.

Atmospheric forcing is the principal driver of storm surge (Dietrich et al., 2017; Lakshmi et al., 2017). In storm surge models, atmospheric forcing is provided in the form of surface pressure and near-surface wind fields from various sources and configurations. These can include the use of cyclone track-based data implemented in parametric vortex models, as well as the use of wind reanalysis products and 3D atmospheric models.

Parametric vortex models use a simple set of storm parameters to represent the wind and pressure fields. These models range in complexity in their representation of the TC wind field, which can be represented as a simple symmetric vortex (Holland, 1980) or can more accurately describe the wind field by accounting for wind asymmetries (Gao et al., 2013; Mattocks et al., 2006). Some storm surge models such as the Sea, Lake and Overland Surges from Hurricanes (SLOSH) allow for the use of symmetric vortex models, with spatially constant radius of maximum wind (Rmax), to characterize the TC wind field

for a given track dataset. However, a recent study comparing multiple meteorological forcing for the case of Hurricane Rita found that due to uncertainties in the wind field, an asymmetric model outperforms the symmetric model in forecasting storm surge (Akbar et al., 2017).

The parameters needed for implementation in the parametric vortex model include the storm location, minimum central pressure, maximum wind velocity and radius of maximum winds (Dietrich et al., 2017; Lakshmi et al., 2017). These parameters are available as part of the National Hurricane Center (NHC) forecast advisories issued every 6 h throughout the storm's lifetime. The availability of these storm parameters and the computational efficiency of parametric vortex models provide for timely storm surge forecasts. As such, the use of parametric vortex models is suitable for real-time forecasting of storm surge. However, these models are a simplification of the TC wind field and fail to capture important dynamic processes such as weakening and distortion of the TC wind field after interaction with topography. Full physics atmospheric models can more accurately represent these processes and interactions in the TC wind field and have been used for storm surge assessment. As storm surge modeling shifts into real-time coupling of inundation and full-physics atmospheric models, it becomes relevant to study and evaluate the coupled model performance in predicting storm surge. Understanding of the limitations of these coupled systems will contribute to further development in the field.

Recent studies have researched the effect of using various meteorological forcing for storm surge or wave assessment. Akbar et al. (2017) performed a hindcast of

Hurricane Rita to study the effect of varying wind fields on storm surge estimates, including meteorological forcing from the National Oceanic and Atmospheric Administration (NOAA)/Hurricane Research Division's (HRD) Real-time Hurricane Wind Analysis System (HWIND; Powell et al., 1998), the Dynamic Holland Model (Holland, 1980), and the Asymmetric Holland Model (Mattocks et al., 2006). Results from the study indicate that HWIND performed better than both the Dynamic and Asymmetric Holland Models. The sensitivity of storm surge to different meteorological forcing types for the case of Hurricane Isaac (2012) in the Gulf of Mexico has also been studied. Dietrich et al. (2017) showed that provided availability of accurate forecast advisories, in a hindcast scenario, a parametric vortex model results in reasonable storm surge estimates. Bennett and Mulligan (2017) compared the effect of wind fields from two parametric models and a 3D atmospheric model on the generation of surface waves by Hurricane Sandy and concluded that the 3D atmospheric model, which has the best description of the storm wind field, is most suitable for their assessment.

Studies comparing different atmospheric forcing make use of NHC forecast advisories or NHC-BT datasets in their parametric vortex model implementations, and compare them to storm surge forecasts forced by full-physics atmospheric models or wind reanalysis products (e.g., Akbar et al. (2017), Dietrich et al. (2017) and Bennett and Mulligan (2017)). That is, the comparisons are not exclusive of atmospheric forcing method but also account for accuracy of the data used. In this study, we perform similar comparisons but aim to isolate the effectiveness of using a parametric vortex model in contrast to a full-physics atmospheric model. To achieve this, we explore the use of a

single dataset produced by an atmospheric model and format the output according to the forcing method of interest. The surface pressure and near-surface wind fields from an atmospheric model are directly implemented as atmospheric forcing. In addition, we process the output of the atmospheric model to obtain a track file similar to the NHC-BT and implement it using the Generalized Asymmetric Holland Model (GAHM; Gao et al., 2013) described in Section 2.3.2. This method allows us to perform a more direct comparison between both atmospheric forcing configurations. The methodology of extracting a track dataset from a full-physics atmospheric model highlights an alternative way of incorporating these models for hindcasting and real-time forecasting purposes.

The model configurations, model coupling details and an overview of the simulations performed are described in Section 2.3. Results from the control simulation and the coupled model simulations are described in Section 2.4. The implications and limitations of the study are discussed in Section 2.5. Finally, conclusions are provided in Section 2.6.

2.3 Material and Methods

2.3.1 WRF Model Configuration

Sixty-hour simulations of Hurricane Sandy, initialized at 0000 UTC on 28 October 2012, were performed using the Weather Research and Forecasting (WRF) model (Skamarock et al., 2008) version 3.8. Simulations initialized prior to this time result in significant storm track error at landfall. Similar results were reported in Galarneau et al. (2013), where simulations of Hurricane Sandy initialized at 0000 UTC 23–27 October showed substantial track error at landfall. The spread of landfall locations extended

between the Maryland/Delaware coast to the northern NJ and NY coastal area. Simulations were made using (i) a 12-km horizontal resolution domain that covered the western North Atlantic Ocean basin and the eastern US, (ii) a 4-km horizontal resolution domain with the same outer extent, and (iii) a two-way nested configuration with a 12-km horizontal resolution outer domain and a smaller, vortex following nest of 4 km. The simulations ran with 38 vertical levels and a model top at 50 mb. To allow for model stabilization and adjustment in the 12-4 km vortex-following simulation, the nested domain was prescribed to start tracking the vortex after 1 h of the simulation start time.

Initial and boundary conditions were provided by the European Centre for Medium-Range Weather Forecasts (ECMWF) ERA-Interim reanalysis data (ECMWF, 2009) and were updated every 6 h. The physical parameterizations implemented were those used by the National Center for Atmospheric Research's real-time hurricane simulations for domains comparable to the 12- and 4-km resolution used in this study. The parameterization schemes used include (Table 2-1): WRF Single-moment 6-class microphysics scheme (Hong & Lim, 2006), Yonsei University boundary layer scheme (Hong et al., 2006), Tiedke cumulus parameterization (Tiedtke, 1989), RRTMG for shortwave and longwave radiation parameterization (Iacono et al., 2008), and the NOAH land surface model (Chen & Dudhia, 2001). The simulation was initialized with sea surface temperature (SST) values from ERA-Interim for 28 October 2012 0000 UTC and was not updated throughout the simulation. The SST profile varied spatially but not temporally. Observed SST along the storm track remained approximately constant at around 25 C until

Sandy moved away from the Gulf Stream and towards the NJ coast and encountered cooler waters.

Table 2-1. Model configuration for Hurricane Sandy WRF 12-4km, WRF 12km and WRF 4km simulations.

Model Parameter	Configuration
Time step (s)	60 [1]
Cumulus convection	Tiedke
Boundary layer	Yonsei University (YSU)
Microphysics	WRF single-moment 6-class scheme (WSM6)
Land surface	Noah land surface model
Radiation	Rapid Radiative Transfer Model for GCMs (RRTMG)

[1] Simulations ran with the same configuration except for the WRF 4 km with time step of 30 s.

The simulated cyclone track data, including the location, maximum wind speed and minimum pressure of the storm were directly output from WRF and used for model evaluation.

2.3.2 ADCIRC Model Description and Atmospheric Forcing Configuration

To hindcast the storm surge from Hurricane Sandy, WRF output was used as forcing for the two-dimensional depth integrated (2DDI) implementation of the ADCIRC hydrodynamic model (Luettich & Westerink, 2004; Luettich et al., 1992). ADCIRC has been used for various storm surge impact studies for cases in the Gulf of Mexico (Dietrich et al., 2010; Dietrich et al., 2017; Forbes et al., 2010; Fossell et al., 2017), along the eastern US coast (Lin et al., 2010) and more specifically for the NJ and NY coastal region (Cialone et al., 2017; Colle et al., 2015; Colle et al., 2008; Lin et al., 2010; Yin et al., 2016). ADCIRC uses a finite element unstructured triangular grid allowing for higher resolution near the coast and coarser resolution in the deep ocean. In this study, simulations were performed

on a grid developed by the Federal Emergency Management Agency (FEMA) as part of the Region II Coastal Storm Surge Study (FEMA, 2014). The mesh domain of the FEMA grid is shown in Figure 2-1 and includes the U.S. Atlantic Coast, the Gulf of Mexico, and the Caribbean with higher resolution along the NJ and NY coastlines (inland spacing 80–500 m; 30 m in limited areas). This mesh was originally used for the case of Hurricane Sandy and has since been implemented in storm surge modeling studies for this case as well as other tropical and extratropical systems (Orton et al., 2015; Yin et al., 2016). Details of the model configuration are described in Table 2-2.

Tides-only simulations were performed and initialized 10 days prior to the first time-record in the NHC-BT (23 October 0000 UTC) for the control simulation, and prior to the WRF initialization time (28 October 0000 UTC) for the WRF-ADCIRC simulations. This time difference results from a delayed initialization of the WRF simulations. Recall that for our case study, WRF simulations initialized earlier than 28 October 0000 UTC resulted in large track errors at landfall (Section 2.3.1). All simulations were forced with 7 tidal constituents: M2, N2, K2, S2, K1, O1, Q1 along the open boundary.

After the tides-only simulations, five 60 h simulations with meteorological forcing were carried out. The control ADCIRC simulation (CTL) was conducted with forcing provided from the 6-hourly NHC-BT data for Hurricane Sandy. Atmospheric forcing for CTL was implemented with the GAHM parametric model. Given that the NHC-BT dataset is a post-storm analysis, CTL estimates of water elevation are considered the closest to truth or observed values.

The CTL experiment was followed by four WRF-ADCIRC simulations. The four WRF-ADCIRC simulations are characterized as follows (Table 2-3): (i) forcing with hourly Simulated Cyclone Track (SCT) data from the outer domain of the two-way nested WRF 12-4 km simulation (SCT12-4), (ii) forcing with 3 h Full Wind and Pressure fields (FWP) from the WRF 12-4 km simulation (FWP12-4), (iii) forcing with 3 h full wind and pressure fields from the WRF 12 km simulation (FWP12), and (iv) forcing with 3 h full wind and pressure fields from the WRF 4-km simulation (FWP4).

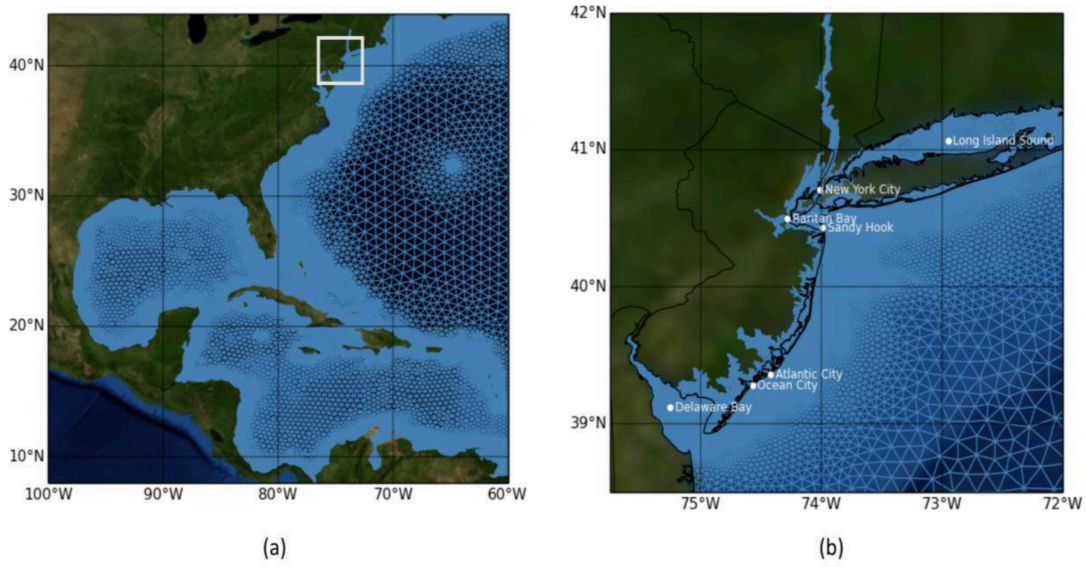

Figure 2-1. (a) Advanced Circulation Model (ADCIRC) finite element unstructured mesh used for the Federal Emergency Management Agency (FEMA) Region II Coastal Surge Study (FEMA, 2014). The mesh has been designed with higher resolution along the Hudson Bay, NJ, and NY coastal regions. The mesh has 604,790 nodes; (b) Zoom in for the white box in (a) of the NJ and NY coastline. Raritan Bay, Delaware Bay and Long Island Sound bays are identified.

Table 2-2. ADCIRC model configuration parameters.

Parameter	Description	Value
NOLIBF	Bottom stress	1; quadratic bottom friction law
NCOR	Coriolis parameter	1; spatially variable
NWS	Atmospheric forcing	20; Generalized Asymmetric Holland Model format 12; forcing in rectangular grid format
NRAMP	Ramp option parameter	1; hyperbolic tangent ramp function
DRAMP	Days to apply ramp function	7 days

Table 2-3. Description of meteorological forcing for each coupled simulation.

Case	Forcing	Source
CTL	Best track	NHC
SCT12-4	Simulated cyclone track	D01 from WRF 12-4 km
FWP12-4	Full wind and pressure fields	WRF 12-4 km
FWP12	Full wind and pressure fields	WRF 12 km
FWP4	Full wind and pressure fields	WRF 4 km

The SCT12-4 simulation is comparable to the CTL simulation but includes a different atmospheric forcing source. The SCT12-4 simulation is forced with cyclone track data obtained from the 12-4 km nested WRF simulation, for which the forcing is applied through a parametric vortex model. Prior to implementing the track-based meteorological forcing into ADCIRC, WRF data is processed to recalculate track data. In addition, wind structure information is calculated since the WRF model output does not explicitly contain this information. Wind structure data obtained from post-processing include the radius of maximum winds (Rmax) and the wind radii for the 34-, 50- and 64-kt isotachs. Wind radii for each isotach is obtained by calculating the weighted average with respect to the diagonal in each of the quadrants.

Since TCs often exhibit asymmetries in their structure, in this study, we use the implementation of ADCIRC which allows the use of an asymmetric model to characterize the wind field in the CTL and SCT12-4 simulations. The model used is the GAHM, which is an adaptation from the asymmetric Holland model (Holland, 1980) but modified to use information from all available isotachs. Wind structure information includes the radius of maximum winds for the 34-, 50- and 64-kt isotachs. Gao et al. (2013) and Dietrich et al. (2017), provide a comprehensive description of the parametric vortex model implementation. In the following we provide an overview of the atmospheric forcing implementation. GAHM, built-in within ADCIRC, is used to model the TC wind and pressure fields. It calculates the wind velocity and surface pressure at each mesh node, directly coupling to ADCIRC. GAHM is designed to fit multiple isotachs in each of the four storm quadrants and as such produces a hurricane vortex with spatially varying Rmax (Gao et al., 2013). The use of multiple isotachs provides for a better representation of the full wind field and of the TC wind field asymmetries.

The three remaining simulations (FWP12-4, FWP12, and FWP4) are forced with the 10 m wind and surface pressure field outputs from WRF simulations. The wind and atmospheric pressure fields are spatially interpolated onto the ADCIRC model domain and temporally interpolated to correspond with the model time step.

2.4 Results

The WRF-ADCIRC simulations were compared to CTL, and to water elevation observations at various stations. The FWP12-4 simulation was directly compared to SCT12-4 to determine differences arising from the use of varying meteorological forcing

methods. Finally, a sensitivity test based on model resolution was performed for the simulations forced with the full-physics atmospheric model.

2.4.1 WRF Model Evaluation

Prior to the WRF-ADCIRC coupling the accuracy of the simulated TC was evaluated. Evaluation of the WRF model simulations were performed by comparing the track and intensity of the simulated storms with data from the NHC-BT dataset. The discussion will be focused mainly on the WRF 12-4 km simulation, except in situations that warrant further analysis.

The two-way nested WRF 12-4 km model simulation proved skillful in predicting the observed track and landfall location. At the time of initialization, the simulated storm track was located about 46 km to the right of the observed BT location (Figure 2-2). The track error increased to a maximum of about 110 km, with the simulated track shifting to the left of the observed location on 29 October 0600 UTC. The track then followed the same trend as the NHC-BT observations and took Hurricane Sandy's characteristic Northwest turn towards the NJ coast. After 29 October 1600 UTC, the track error was reduced to about 32 km. The simulated storm remained to the left of the observed track and made landfall south of Brigantine, NJ, USA with a track error at the time of landfall at 2330 UTC on 29 October of 21.5 km (Figure 2-2).

In terms of the minimum sea level pressure at landfall, the simulated hurricane was only fractionally weaker (3.6 mb) than the observed. The lifetime minimum pressure obtained by our simulation was 948.5 mb at 0000 UTC 30 October, while the observed hurricane reached a minimum pressure of 940 mb at 1800 UTC 29 October. The slightly

weaker nature of the simulated storm is evident when comparing the maximum winds (Figure 2-3). The maximum wind of the simulated storm at landfall was 4.48 ms^{-1} less than observations, but the error is still within the range of NHC's annual average intensity error for a 48 h forecast of about 5.45 ms^{-1} (10.6 kts per 2016 standards; Cangialosi & Franklin, 2017). Despite the weaker maximum wind at landfall, our simulation reached the secondary intensity peak of 43.5 ms^{-1} which nearly matches the observed maximum of 44 ms^{-1}. The simulated storm reached its maximum early at 0600 UTC on 29 October, which is approximately 6 h prior to the observed peak for Hurricane Sandy.

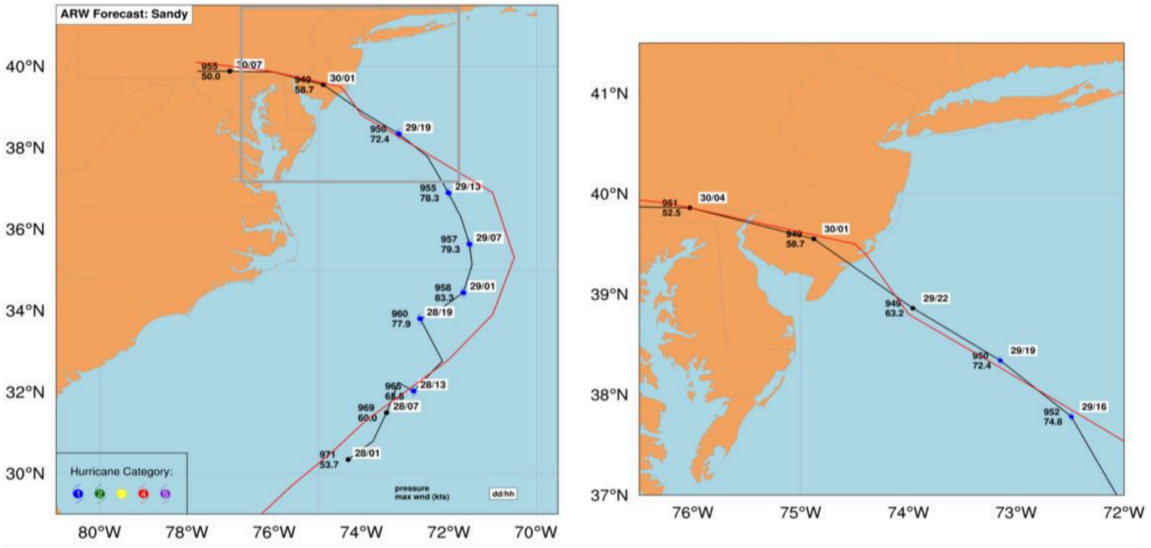

Figure 2-2. The Weather Research and Forecasting (WRF) model 12-4 km simulated hurricane Sandy track (black) initialized on 28 October 0000 UTC compared to National Hurricane Center (NHC) best track data (red). The simulated storm makes landfall on 30 October at 0000 UTC about 20 km south of hurricane Sandy's landfall location near Brigantine, NJ, USA. Track information is provided every 6 h. Insert: zoom in view of cyclone landfall location with track information provided every 3 h.

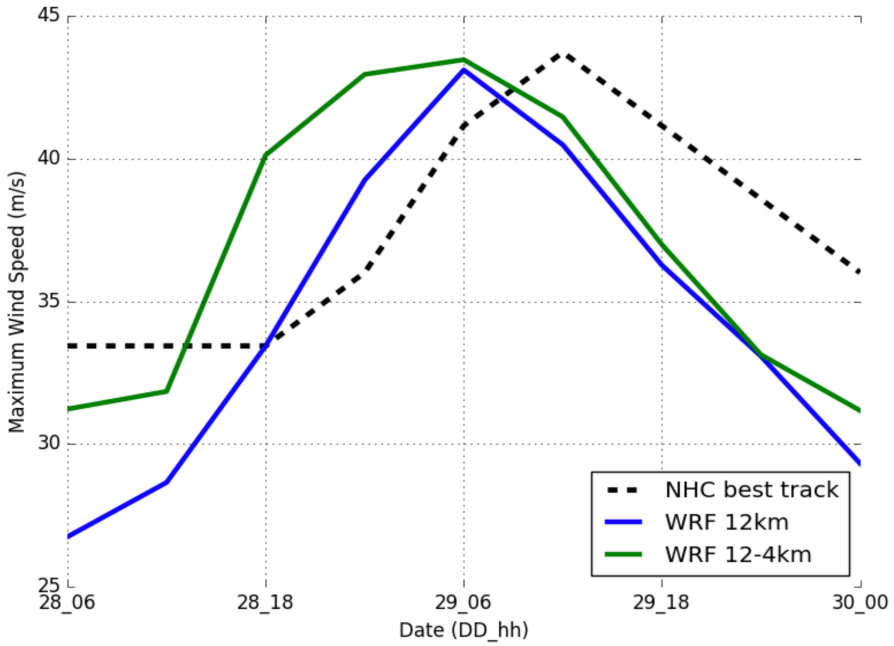

Figure 2-3. Cyclone wind speed from NHC best track (dashed black line); WRF 12 km simulation (blue); and WRF 12-4 km simulation (green).

The single-nested WRF 12 km simulation on the other hand, followed the general observed track but showed signs of instability along the track, prior to recurving to the left (Figure 2-4). The track error is less than that of the WRF 12-4 km simulation in the hours prior to landfall but increases to about 37 km as it approaches the coast and makes landfall north of the observed location. The WRF 12 km simulated TC was in general weaker than the WRF 12-4 km. In this case, the lifetime minimum pressure occurring near landfall on 30 October 0100 UTC, was 949.8 mb. The storm also reached a maximum intensity of 43.1 ms^{-1} on 29 October at 0600 UTC. As shown in Figure 2-3, the storm starts with a lower intensity than the WRF 12-4 km simulated TC, remaining as such for the entire simulation until reaching peak intensity and weakening faster than the former after landfall.

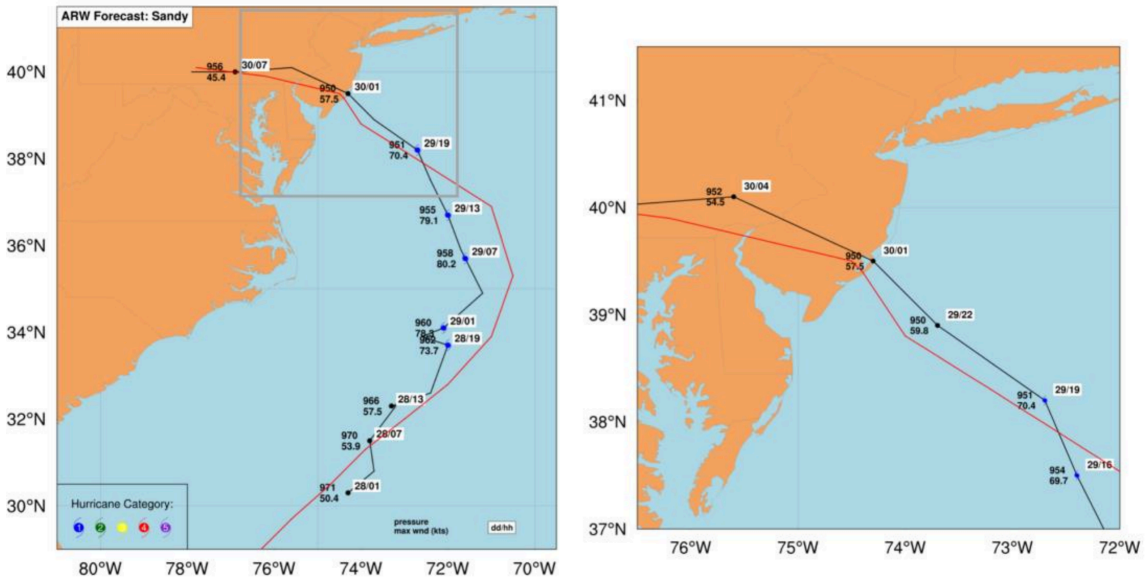

Figure 2-4. Same as Figure 2-2 except track is presented for the WRF 12 km simulation.

Wind patterns and minimum pressure estimates were further explored for the WRF 12-4 km simulation by comparing observations from the NOAA National Data Buoy Center buoys and weather stations along the coast of NJ and NY to the WRF simulations (http://www.ndbc.noaa.gov/). Nevertheless, the comparisons provide additional insight into the WRF 12-4 km simulated wind and pressure field patterns. Unlike many stations in the vicinity, the New York Harbor Entrance Station recorded wind and pressure data throughout the entire analysis period (Figure 2-5f). The simulated pressure pattern matched well with observations and accurately captured the pressure drop at the buoy, with a significant correlation coefficient of 0.995. The simulated wind patterns followed the same general behavior as the observed winds, although the simulated winds appear to be slightly overestimated at this station (correlation of 0.952). Other stations examined followed a similar pattern of significant correlation between pressure and wind estimates. Minimum pressure was well simulated in all stations (Figure 2-5). Wind speed time series

for the Cape May, NJ and Kings Point, NY stations (Figure 2-5d–e) showed more discrepancies. In these stations the simulated winds are overestimated, however the peak wind speed is accurately captured in the Cape May station.

For storm surge assessment, it is important that the atmospheric simulations can reproduce the structure and location of maximum intensity observed for TCs, but more so it requires that the overall wind fields are accurately depicted (i.e., extent and asymmetries). We compared the wind field from the HWIND product for various forecast times before and during landfall to the WRF 12-4 km simulation. We determined that the WRF 12-4 km simulation could capture the main features in structure and intensity observed for Hurricane Sandy, with maximum wind intensities both on the left and right side of the track, characteristic of extratropical cyclones. Our comparison shows that at 2100 UTC 29 October, 2 h prior to landfall, the model simulation reproduced the annular/semi-annular structure of the TC, as well as the location and intensity of the maximum winds in the lower TC quadrants (Figure 2-6). After landfall at 0000 UTC 30 October, the model simulation was also able to capture the weakening and dissipation of the TC as it started losing definition of its structure when interacting with land and topography.

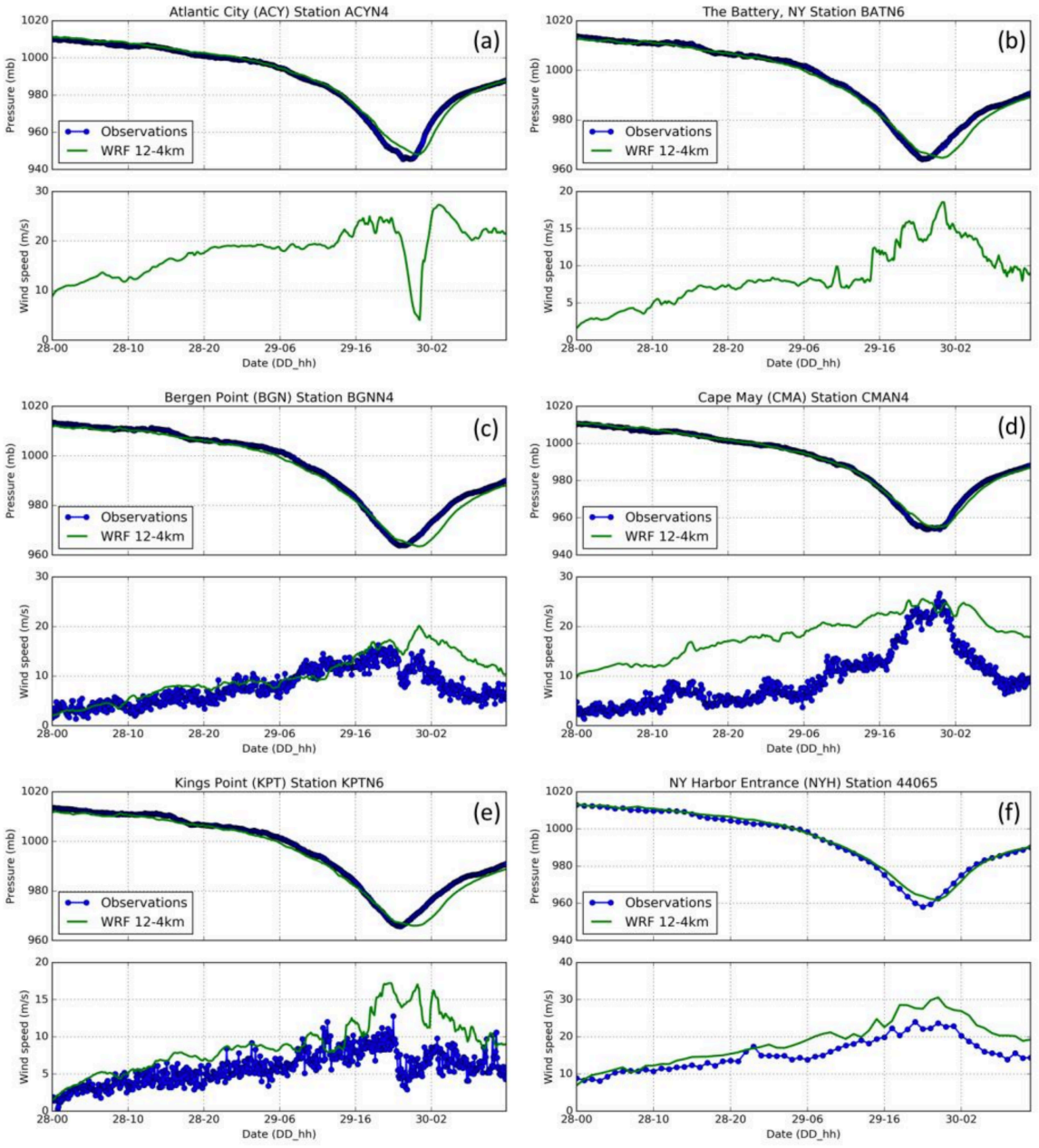

Figure 2-5. Comparison of WRF 12-4 km simulated minimum pressure (top) and maximum wind (bottom) estimates with station observations for (a) Atlantic City, NJ, (b) The Battery, NY, (c) Bergen Point, NY, (d) Cape May, NJ, (e) Kings Point, NY and (f) New York Harbor Entrance, NY stations.

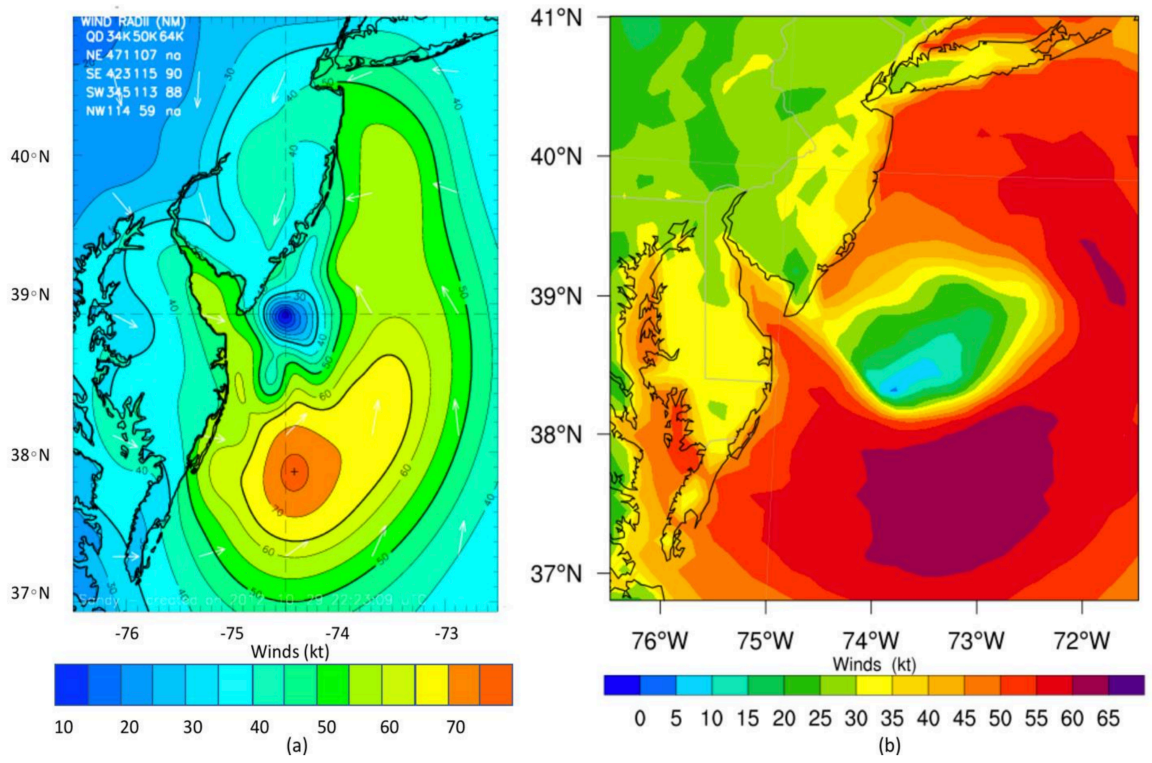

Figure 2-6. Wind field analysis for 2100 UTC 29 October 2012 from (a) HWIND (source: NOAA/AOML/Hurricane Research Division); (b) WRF 12-4 km simulation.

2.4.2 Control Storm Surge Simulation

Figure 2-7 shows the maximum water elevation for the CTL run, where ADCIRC was forced with the NHC-BT data for Hurricane Sandy and implemented with the GAHM. The NHC-BT should have marginal track and intensity errors, and per ADCIRC model configuration, should be the closest representation to actual observations. In the WRF12-4 km simulation of Hurricane Sandy strong winds prevail on both sides of the storm tracks, as discussed in Section 2.4.1. The maximum water elevation estimates reached the maximum observed storm tide (storm surge + tide) of about 4 m. High water elevations are observed in areas right of the storm track including the NY Harbor and Long Island Sound regions. Opposite results are seen to the left of the storm track, where storm surge

was lowest overall. Maximum water elevation estimates on the southern coast of NJ and in the Delaware Bay range between 1–2 m. Near Brigantine and Atlantic City water elevation estimates were moderate, ranging between 1.5 and 2.5 m.

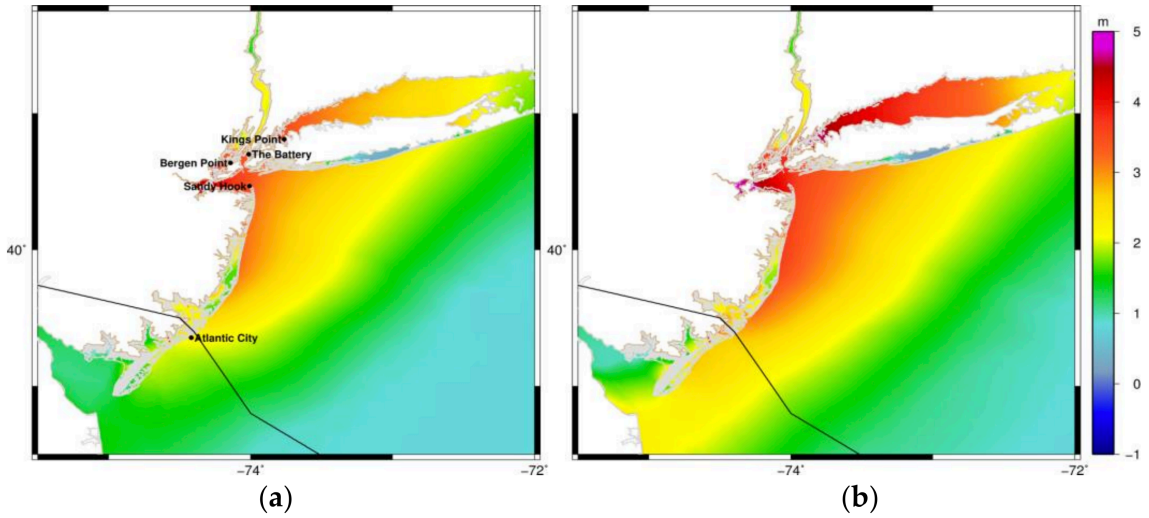

Figure 2-7. (a) Simulated maximum water levels above mean sea level (MSL) during the period of 23 October 0000 UTC through 30 October 1200 UTC for the CTL ADCIRC run forced with the NHC best track dataset. (b) Same as (a) except simulation is initialized on 28 October 0000 UTC to correspond with initialization period of WRF simulations. The black line indicates the track of Hurricane Sandy as it made landfall in New Jersey north of Atlantic City.

2.4.3 WRF Simulated Cyclone Track-Forced Storm Surge Simulation

The WRF-ADCIRC SCT12-4 simulation results show maximum water elevation estimates that do not reach the maximum observed storm tide for Hurricane Sandy (Figure 2-8a). One of the causes to consider is the simulated TC size. On 28 October 0000 UTC the NHC-BT data indicate that Hurricane Sandy's 34-kt wind radii extent for the NE, SE, SW and NW quadrants are 480, 300, 300 and 280 nm, respectively. The 34-kt wind

radii calculated for SCT12-4 were generally smaller than observations, particularly in the NE quadrant, with a 241-, 276-, 298- and 326-nm extent for the NE, SE, SW, and NW quadrants, respectively. The simulated storm in SCT12-4 is smaller than was observed for Hurricane Sandy and is not expected to have that significant of an effect on maximum water elevations.

Water elevation in the NY Harbor, Raritan Bay and Long Island Sound areas mainly ranged between 2 and 3 m, while estimates in the Delaware Bay were lower and ranged between 1 and 2 m. When compared to the CTL run, the simulated maximum elevation gradient resembles that of the CTL, with highest surge in the NY Harbor and Long Island Sound regions. However, the maximum water elevation estimate in the NY Harbor was largely underestimated by the SCT12-4 simulation with differences ranging between about 0.75 and 1.5 m (Figure 2-8b). SCT12-4 overestimates maximum water elevation in the Delaware Bay. Near the area of landfall in Brigantine, NJ the differences between the CTL and SCT12-4 are the lowest. Differences range between 0.0 and 0.5, owing to similarities in track and intensity between the WRF12-4 simulated storm and observations for Hurricane Sandy near landfall.

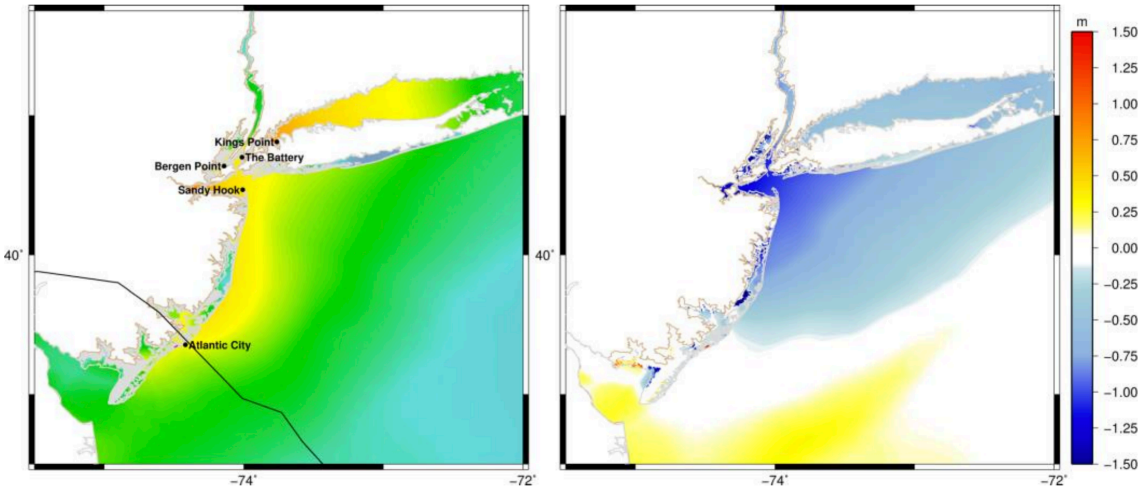

Figure 2-8. (a) Simulated maximum water levels above MSL during the period of 28 October 0000 UTC through 30 October 1200 UTC for SCT12-4. The black line represents the track of the storm, which makes landfall closer to Atlantic City, south of the observed landfall location. (b) Difference between SCT12-4 and the control simulation.

2.4.4 WRF Full Field-Forced Storm Surge Simulations

One of the main features evident in the FWP12-4 simulation, is high maximum water elevation in Long Island Sound (Figure 2-9a), where maximum water elevations in this region reached up to 4 m, overestimating CTL by about 1 m. Compared to CTL, the FWP12-4 simulation underestimates the maximum water elevation along the NY Harbor and Raritan Bay areas by about 0.4–1.0 m (Figure 2-10a), as expected for a storm with winds between 5 and 8 m/s weaker than observations. Meanwhile it overestimates water elevations by about 0.4 m in the coastal region south of Atlantic City, NJ, USA.

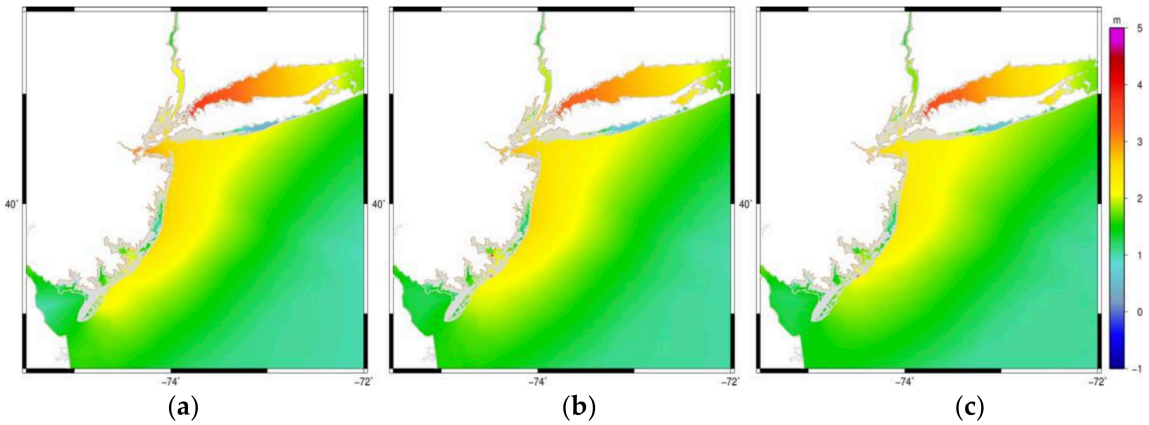

Figure 2-9. Simulated maximum water levels during the period of 28 October 0000 UTC through 30 October 1200 UTC for (a) FWP12-4; (b) FWP12; and (c) FWP4.

The area where the maximum water elevation ranged between 2 and 3 m is broader in this simulation, extending further east into the Atlantic Ocean than in the SCT12-4 simulation. This area of higher water elevation also extends further south along the NJ coastline in FWP12-4 than both the CTL and SCT12-4 simulations, pointing to a larger TC wind field representation in the full-physics model compared to the parametric wind model. Also, evident in this simulation are higher estimates along the Hudson River where the maximum water elevation reached above 2 m. The increased surge along the Hudson River is a feature that could not be captured in the previous track-forced simulation (SCT12-4) but is present in the CTL run. These discrepancies could point to significant differences in wind speed and direction along the narrow river.

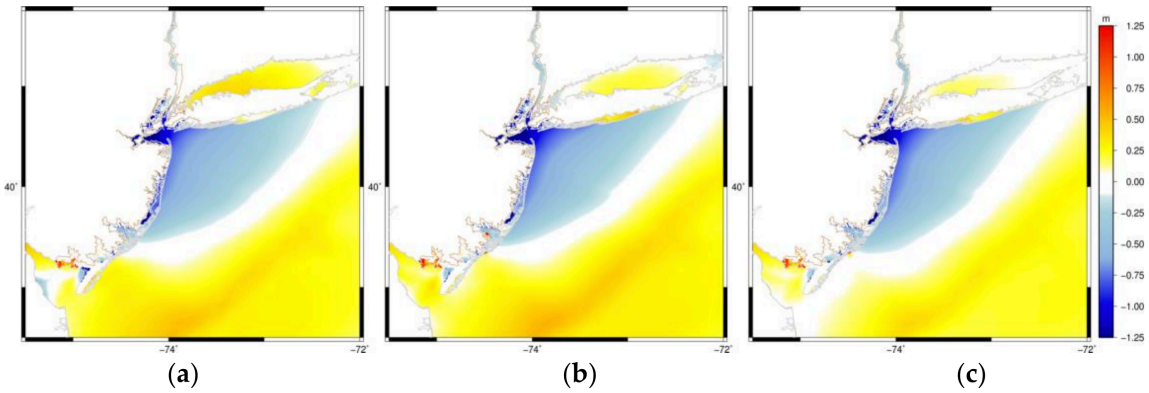

Figure 2-10. Differences from the control simulation for the (a) FWP12-4; (b) FWP12; and (c) FWP4 simulations.

The sensitivity of storm surge estimates to differences in horizontal resolution of the meteorological input data in the form of full wind and pressure fields were also explored. The FWP12 produces similar maximum water elevation estimates when compared to the FWP12-4. Maximum water elevation for FWP12 are generally lower than FWP12-4 in the New York Harbor and Long Island Sound region. When comparing FWP12 to the CTL, differences are reduced in Long Island Sound (Figure 2-10b). A similar maximum elevation pattern is observed for FWP4, where maximum elevations in Long Island Sound compare closer to the CTL with differences around 0.3 m (Figure 2-10c). However, FWP4 underestimates water elevations in the NY Harbor region by 1.2–2.0 m.

2.4.5 Inter-Comparison of Simulations with Varying Meteorological Forcing

All simulations exhibit higher storm tide to the right of the TC track, and a lower storm tide estimate to the left of track. This result is expected for TCs with wind maxima on the right-hand side of the storm. The fact that ETCs can exhibit two regions of wind maximum on either side of the track has notable implications for this case. With strong offshore winds to the left of the track, more water is moved offshore, reducing storm

surge on the left side of the track. Observations, as well as all model simulations, show this pattern of higher storm tide along the northern NJ coast and Long Island (right of track), and lower estimates along the southern NJ coast (left of track).

Figure 2-11 shows the difference in modeled maximum water elevation between SCT12-4 and FWP12-4. Results indicate that much of the difference observed between these simulations is within Long Island Sound. In this region, FWP12-4 estimates water elevations that are generally between 0.8 and 1.0 m above the SCT12-4 estimates. Meanwhile, the opposite is observed in the Delaware Bay, where SCT12-4 estimates a storm surge about 0.4 m higher than FWP12-4, pointing to possible differences in wind field extent. Overall, differences were within the 1 m range, with FWP12-4 overestimating maximum elevation in most of the area of study, when compared to SCT12-4. Nevertheless, the track-forced SCT12-4 simulation had higher correlation and lower RSME than the FWP12-4 simulation.

We then compared all simulations to maximum water elevation hourly time series from various NOAA Tides and Currents (NOAA/NOS/CO-OPS) stations marked on Figure 2-7. Results point to a reduction in the extent of the inundation area, as discussed in results from Akbar et al. (2017). Out of the seven stations considered, three stations are projected to be dry, one station is projected to dry after initial inundation, and 3 others are wet throughout the entire simulation. These three stations are discussed here and include Atlantic City, NJ station (ID: 8534720), The Battery, NY station (ID: 8518750) and Montauk, NY station (ID: 8510560). Results from the time series comparisons indicate a phase lag between modeled and observed data, with all WRF-ADCIRC simulations peaking

3–4 h prior to observations (Figure 2-12a–c). It was hypothesized that the lag in the peak water levels was caused by the difference in the length of the simulations. To test the effect of the differences in initialization time of the meteorological forcing for the case of Hurricane Sandy, an additional simulation was performed with the same configurations as CTL but beginning on 28 October 0000 UTC. The phase lag observed between the WRF-ADCIRC simulations and the station observations of about 3–4 h, was also apparent for the shorter CTL simulation. However, time-series for this simulation indicate that the shorter time configuration causes overestimation of the maximum water elevation at all station locations. This overestimation is thought to be a product of abruptly adding a very large TC as meteorological forcing for ADCIRC (see Section 2.4.3).

These results from the shorter CTL simulation therefore indicate sensitivity to the initialization time of the meteorological forcing and points to the cause of the observed phase shift in the WRF-ADCIRC simulations. The shorter CTL simulation was performed for purposes of testing, and henceforth we will only refer to the original CTL simulation initialized on 23 October 0000 UTC. Furthermore, hurricane Sandy was a slow-moving TC and the sensitivity to initialization time could be heightened by this factor, as the effect of the winds acting on the surface and generating surge are longer lasting for slower storms. It would prove interesting to examine other cases and explore this sensitivity of the simulated storm tracks to initialization time.

To further understand the coupled model characteristics, we shifted all the WRF-ADCIRC time series by 3 h (Figure 2-12d–f) so that the peak water levels would coincide with observations. This allowed for a better assessment of the magnitude of the water

level each simulation could capture. For evaluation purposes the Pearson correlation coefficient (p) and the root mean square error (RMSE) were calculated for each simulation (Table 2-4). The coefficients of correlation between shifted modeled and observed water level estimates ranged between 0.76 and 0.93. Although the CTL simulation underestimated the water elevation at all stations, the strongest correlations are observed for this simulation with an average across stations of 0.91. Following the CTL simulation, FWP12 had the highest correlation and lowest RMSE averaging to 0.82 and 0.46 m, respectively, for all stations. Similarly, the FWP4 simulation had an average correlation of 0.78 and average RMSE of 0.49 m. The SCT12-4 simulation had an average correlation of 0.80 for all stations, and generally underestimated the water levels, specifically near the time of landfall.

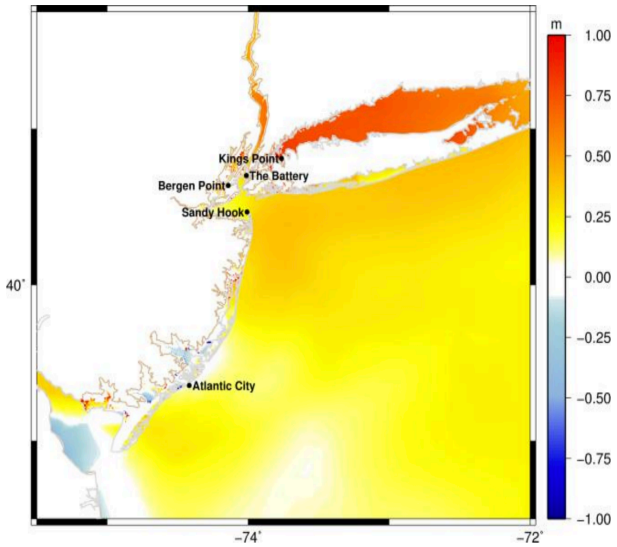

Figure 2-11. Difference in maximum water elevation between FWP12-4 and SCT12-4 (i.e., between track-forced simulation and the simulation forced with the full wind and pressure field output from WRF simulations of the same resolution).

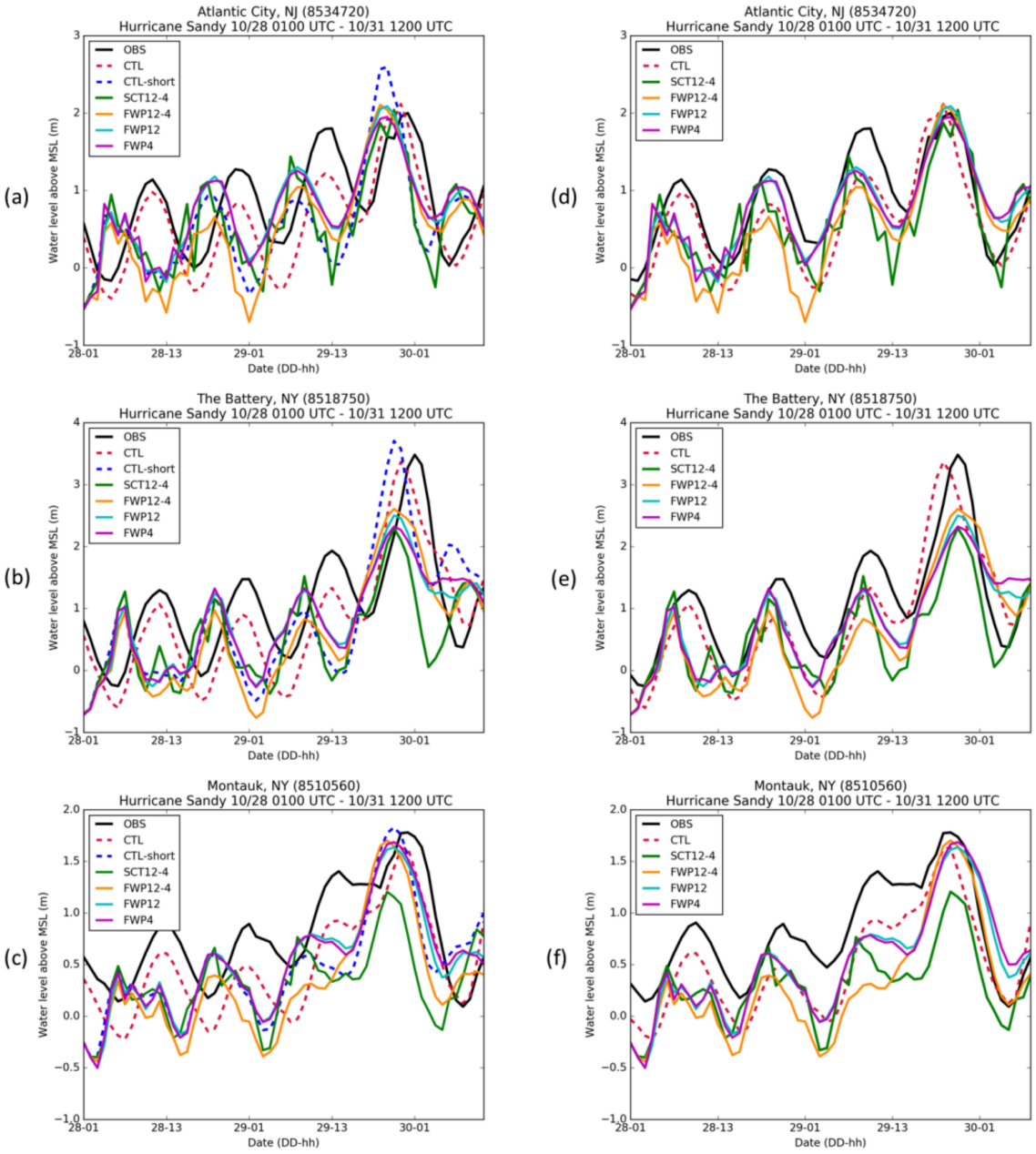

Figure 2-12. Times series of all simulations including a short CTL simulation for (a) Atlantic City NJ station; (b) The Battery NY station; and (c) Montauk NY station. The WRF-ADCIRC simulation estimates have been shifted by 3 h ahead of time to correspond with the peak of the observed water level and are shown for (d) Atlantic City NJ station; (e) The Battery NY station; and (f) Montauk NY station.

Investigation of the wind field structure for SCT12-4 shows that the wind radii estimates for the 34-, 50-, and 64-kt winds in the WRF12-4 km simulation are underestimated in comparison to wind structure data from the NHC-BT. These results highlight modeled storm surge sensitivity to wind structure and radii of maximum winds. The use of a track dataset, such as in SCT12-4, would rely on having accurate and consistent wind radii estimates. We should keep in mind that the NHC-BT data set is a post-storm analysis that uses various observational methods for assessment and reanalysis. On the contrary, the tracking algorithm used in this study to obtain track and wind radii estimates from the WRF simulation is based solely on the WRF model output. The incorporation of observations, as in NHC-BT, is omitted in SCT12-4 and can thus contribute to the errors discussed.

The FWP12-4 simulation usually estimated peaks that were lower in magnitude than both track-forced simulations: CTL and SCT12-4. However, near the time of landfall this pattern was altered. Although the water elevations for FWP12-4 remained lower than station observations, this simulation was able to capture the observed peak better than the SCT12-4 in all three stations (Figure 2-12d–f). Consideration should be given to the WRF 12-4 km simulation configuration. Near the time of landfall, the high-resolution vortex following nest (4 km) is positioned over the region where the stations are located. This pattern and the unexpected result of lower error in the SCT12-4 simulation implied that it may be a construct of including a moving nest in the WRF simulations, and of possible model grid interpolation problems. This hypothesis is further validated when we

consider that the effect is minimized in Montauk station, which is the farthest station from the center of the TC and of the high-resolution domain.

Table 2-4. Statistics for water elevation of each simulation.

Simulation	Station	*p*	RMSE (M)
CTL	MTK	0.93	0.35
	BAT	0.89	0.52
	ACY	0.92	0.37
	Average	0.91	0.41
SCT12-4	MTK	0.81	0.58
	BAT	0.82	0.75
	ACY	0.76	0.51
	Average	0.8	0.61
FWP12-4	MTK	0.79	0.59
	BAT	0.8	0.77
	ACY	0.76	0.58
	Average	0.78	0.65
FWP12	MTK	0.8	0.43
	BAT	0.83	0.59
	ACY	0.82	0.37
	Average	0.82	0.46
FWP4	MTK	0.76	0.45
	BAT	0.79	0.64
	ACY	0.8	0.38
	Average	0.78	0.49

Figure 2-13 shows the wind vector output from ADCIRC for the CTL, SCT12-4, FWP12-4, FWP12 and FWP4 simulations for 29 October 2300 UTC. At the time of landfall, the CTL simulation shows the highest water level estimates in the NY Harbor among all five simulations (Figure 2-13a). The WRF-ADCIRC simulations exhibit lower water elevation estimates at landfall. In the CTL simulation, strong winds are angled perpendicular to the coast in the direction of the New York Harbor area. This is not the case for the WRF-ADCIRC simulations, where a combination of weaker northeasterly

winds prevails in the New York Harbor coastal region. Results in Figure 2-13 also highlight the discrepancy in landfall timing, where the simulated TCs in the WRF-ADCIRC simulations make landfall after the observed time. This effect is more pronounced for the FWP4 simulation as observed in Figure 2-13e. Another important result illustrated in Figure 2-13 is the depiction of weaker winds over land for all the WRF-ADCIRC simulations. This difference in the wind field structure is not observed for CTL.

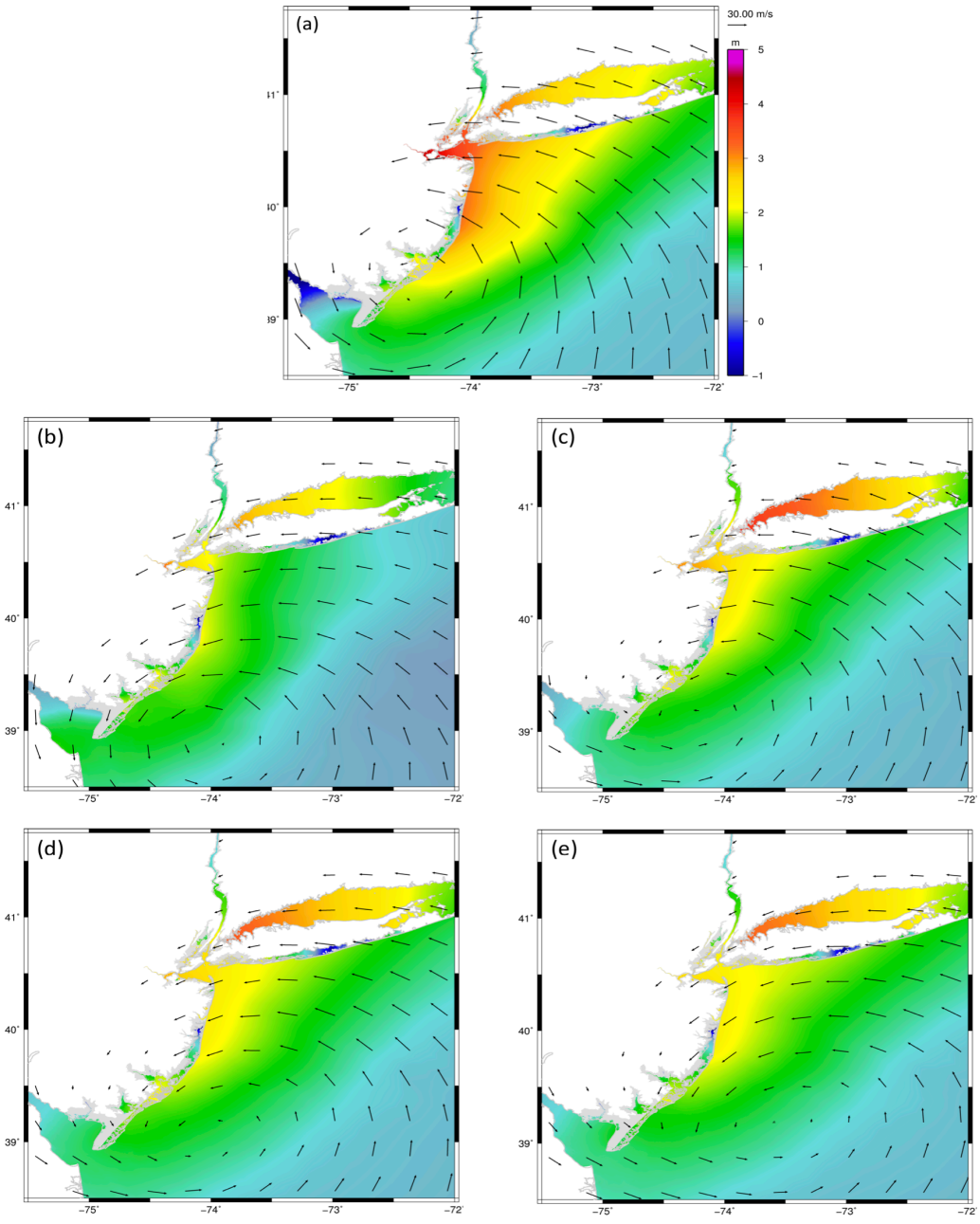

Figure 2-13. Maximum water elevation with ADCIRC wind vector output on 29 October 2300 UTC for (a) CTL; (b) SCT12-4; (c) FWP12-4; (d) FWP12; and (e) FWP4. The length of the 30 ms^{-1} wind vector is provided as reference.

2.5 Discussion

Accurate meteorological data is a critical factor in effectively capturing storm surge impacts. The simulated minimum pressure and winds from the WRF simulations corresponded well with station observations for Hurricane Sandy. However, discrepancies in wind speed were seen in some meteorological stations. The station time-series analysis however, presented some limitations. The corresponding station locations in WRF are given by the closest grid point to the station, and thus our results are not precise point-to-point comparisons. Errors in distance between the WRF station location with respect to their actual location ranged between 3.3 and 6.4 km for the New York Harbor Entrance and the Bergen Point stations.

Much of the error in the coupled WRF-ADCIRC simulations can be attributed to differences in the wind representation in each of the models. In terms of the maximum water elevation, generally, higher values are observed in areas right of the storm track, as is expected for TCs given their characteristic right-of-track wind maximum pushing water ashore. ETCs however, as is the case for Hurricane Sandy, can exhibit wind maxima on both sides of the track. Given the angle at which Hurricane Sandy approached the coast near landfall, wind maxima to the left of the track forces more water away from the coast reducing the observed storm surge in the region south of landfall. This was the case for the WRF simulated TCs. Moreover, in the CTL simulation, as it was observed for Hurricane Sandy, the perpendicular direction of the winds on the right of the track, is allowing more water to be pushed onshore. As illustrated in Figure 2-13, this is not the case for the WRF-ADCIRC simulations. These results motivate the need to understand what the storm surge

response would have been if the winds were to be weaker or stronger and directed in alternative angles. The response of storm surge to varying TC characteristics is the subject of ongoing research.

Results from our time-series comparisons indicate a phase lag between modeled and observed data, with all WRF-ADCIRC simulations peaking 3–4 h prior to observations (Figure 2-12a–c). This result is not uncommon, and it has been shown to occur in other studies. For example, Colle et al. (2015), showed that in their WRF ensemble experiment, some members predicted peak storm surge up to 12 h too soon. In our case, the WRF simulations have a lag of their own with maximum winds peaking about 6 h prior to observations (Section 2.4.1). Part of this error is expected to propagate into the ADCIRC storm surge estimates. Moreover, Akbar et al. (2017) discussed the effect of bottom friction as another potential source of error in storm surge simulations. Their results show early peak arrival for simulations with decreased bottom friction parameter and the opposite effect for increased bottom friction. Results from the CTL simulation, forced with NHC-BT data, do not exhibit the shift in peak arrival. It is worth highlighting the differences in initialization time of the meteorological forcing between the CTL simulation and the WRF-ADCIRC simulations. The CTL simulation was initialized on 23 October 0000 UTC, at the start of the NHC-BT record. To minimize errors in the simulated storm the WRF simulations were initialized 5 days after on 28 October 0000 UTC, and the atmospheric forcing in ADCIRC thus began at that time. Although the time evolution of the storm is important to capture the finer storm surge details at landfall, the track errors for simulations initialized prior to the chosen date had a left-of-track bias, as was also found

by Galarneau et al. (2013). Studies have shown that for tracks that make landfall within 150 km of the observed landfall location, storm surge forecasts can be underestimated by 0.5–1.0 m (Colle et al., 2015). Thus, we selected the configuration that minimized this error at landfall and best depicted the characteristics of Hurricane Sandy. In our simulations, the choice of initialization time seems to be the biggest factor influencing the shift in peak surge arrival.

Based on our results, we would rank (in decreasing order) the performance of our models as follows: CTL, FWP12, FWP4, SCT12-4 and FWP12-4. The time-series analysis showed that the CTL simulation forced with NHC-BT data compared well with observations, indicating a suitable ADCIRC model setup. This implies that we can reproduce accurate storm tide estimates with the best possible meteorological data available using a simplified parametric model. Yin et al. (2016), found similar results in their storm surge assessment of Hurricane Sandy. Results showed the effectiveness of their simulation in accurately predicting the timing and magnitude of the peak surge. However, some discrepancies were observed before and after the peak surge, which they have attributed to the use of a simplified parametric vortex model for their wind field representation.

Time-series results from the WRF-ADCIRC simulations show discrepancies when compared to CTL. Discrepancies were more evident at The Battery, NY station where none of the WRF-ADCIRC simulations could accurately capture the magnitude of the peak storm surge (Figure 2-12e). Colle et al. (2015), showed similar results of underestimated water levels for various of their WRF ensemble simulations. However, their control simulation

which is most comparable in terms of configuration to our FWP12-4 simulation, captured the peak surge at The Battery. It overestimated the observed water elevations by 0.20 m. An important distinction between both studies is the implementation of wave coupling in their assessment, which has been neglected for the purposes of this study.

Statistical results in Table 2-4 indicate that the track-forced SCT12-4 simulation has a higher average correlation coefficient and lower average RMSE than the FWP12-4 simulation. However, simulations with meteorological forcing in the form of wind and pressure fields from full-physics atmospheric models are assumed to contribute less error than track-forced simulations that make use of parametric wind models. Parametric wind models can have between 10% and 20% higher random error (Resio & Westerink, 2008), an assumption based on the fact that these do not account for details in the wind structure as atmospheric models do. Parametric wind models also fail to capture interactions with topography and TC dynamics and feedbacks, which are important in storm surge modeling. The FWP12 and FWP4 simulations show improvement over the track-based simulations, which leads us to conclude that the improvement of SCT12-4 over FWP12-4 is a construct of including a vortex-following nest in the WRF 12-4 km simulation. The sensitivity of storm surge simulations to atmospheric forcing resolution in the FWP simulations was also investigated. When comparing the FWP simulations, results indicate that for our case the coarser horizontal resolution simulation (WRF 12 km) is sufficient to forecast storm surge estimates and there is no need for increased resolution.

Although storm surge predictions from CTL can be considered as a standard for the real case, the values might be an overestimate, given the lack of interaction with topography acting to weaken the storm. In their study, Dietrich et al. (2017) found similar results for simulations forced with NHC advisories and implemented within GAHM. The maximum wind speed for their simulation remained relatively constant at landfall and retained a larger wind field extent when compared to HWIND. The larger wind field caused higher water elevations for the track-based simulation. The weakening of winds caused by the interaction with land and topography, is evident in the FWP12-4 simulation, as shown by decreased wind speed over land in Figure 2-13c–d compared to CTL (Figure 2-13a). The methodology of directly extracting the TC properties used by the parametric models from the full-physics models can, to a certain degree, reduce this limitation by adding to the realism and complexity of the TC wind field. Moreover, these results point to the utility of using full physics models for forecasting storm surge. It implicitly accounts for weakening of winds and distortion of the wind field by the interaction with land.

The results of this study are not uncommon. Bennett and Mulligan (2017) found that a 3D atmospheric model was more suitable for hindcasting the waves of Hurricane Sandy when compared to the Holland Model and the GAHM. However, one noticeable difference to our study is their use of an atmospheric model with data assimilation. A similar study by Dietrich et al. (2017) highlighted the value in using parametric vortex models for hindcasting purposes but encouraged the use of full-physics coupled models for storm surge forecasting of Hurricane Isaac. Although results have been similar for various cases and geographic regions, the studies performed are location-dependent,

thus prompting the need for a systematic study of the effect in the choice of atmospheric forcing.

2.6 Conclusions

In this study, we compare four WRF-ADCIRC simulations to determine the best choice in meteorological forcing for storm surge studies. For real-time forecasting of storm surge or in the absence of a best track data set, it is important to identify a suitable model configuration that can provide accurate atmospheric and surge forecasts. In this work, we explore ways of improving this modeling framework.

One of the simulations consisted of using track data estimated from a full-physics WRF 12-4 km simulation as meteorological forcing for the ADCIRC model. The GAHM was then implemented within the ADCIRC model to determine the wind field in the domain. The remaining three simulations directly used the full wind and pressure field output from the full-physics WRF 12-4 km, WRF 12 km and WRF 4 km simulations as meteorological forcing. All simulations were compared to a control run using the NHC-BT data for Hurricane Sandy.

Results indicate that our initial choice of meteorological forcing for estimating storm surge would depend on data availability. A best track data set appears to be the best meteorological forcing option for our configuration of the ADCIRC model. However, when a best track is not available, our results would indicate that we could primarily rely on using full wind and pressure field output from a 12 km resolution WRF simulation.

The results of this study have encouraged the authors to further understand the sensitivity of storm surge impacts to atmospheric forcing and to varying storm

characteristics. Ongoing research focuses on the sensitivity of storm surge to the track, intensity, and size of tropical cyclones in a coupled atmosphere, storm surge and wave modeling framework.

2.7 References

Akbar, M. K., Kanjanda, S., & Musinguzi, A. (2017). Effect of Bottom Friction, Wind Drag Coefficient, and Meteorological Forcing in Hindcast of Hurricane Rita Storm Surge Using SWAN+ ADCIRC Model. *Journal of Marine Science and Engineering, 5*(3), 38.

Barnes, E. A., Polvani, L. M., & Sobel, A. H. (2013). Model projections of atmospheric steering of Sandy-like superstorms. *Proceedings of the National Academy of Sciences, 110*(38), 15211-15215.

http://www.pnas.org/content/110/38/15211.abstract

Bennett, V. C., & Mulligan, R. P. (2017). Evaluation of surface wind fields for prediction of directional ocean wave spectra during Hurricane Sandy. *Coastal Engineering, 125*, 1-15.

Blake, E. S., Kimberlain, T. B., Berg, R. J., Cangialosi, J. P., & Beven II, J. L. (2013). Tropical cyclone report: Hurricane sandy. *National Hurricane Center, 12*, 1-10.

Cangialosi, J. P., & Franklin, J. L. (2017). *Forecast Verification Report: 2016 Hurricane Season*.

Chen, F., & Dudhia, J. (2001). Coupling an advanced land surface-hydrology model with the Penn State-NCAR MM5 modeling system. Part I: Model implementation and sensitivity. *Monthly Weather Review, 129*(4), 569-585. <Go to ISI>://WOS:000168253900001

Cialone, M. A., Grzegorzewski, A. S., Mark, D. J., Bryant, M. A., & Massey, T. C. (2017). Coastal-storm model development and water-level validation for the North Atlantic Coast Comprehensive Study. *Journal of Waterway, Port, Coastal, and Ocean Engineering, 143*(5).

Colle, B. A., Bowman, M. J., Roberts, K. J., Bowman, M. H., Flagg, C. N., Kuang, J., et al. (2015). Exploring water level sensitivity for metropolitan New York during Sandy (2012) using ensemble storm surge simulations. *Journal of Marine Science and Engineering, 3*(2), 428-443.

Colle, B. A., Buonaiuto, F., Bowman, M. J., Wilson, R. E., Flood, R., Hunter, R., et al. (2008). New York City's vulnerability to coastal flooding: Storm surge modeling of past cyclones. *Bulletin of the American Meteorological Society, 89*(6), 829-841.

Dietrich, J., Bunya, S., Westerink, J., Ebersole, B., Smith, J., Atkinson, J., et al. (2010). A high-resolution coupled riverine flow, tide, wind, wind wave, and storm surge

model for southern Louisiana and Mississippi. Part II: Synoptic description and analysis of Hurricanes Katrina and Rita. *Monthly Weather Review, 138*(2), 378-404.

Dietrich, J., Muhammad, A., Curcic, M., Fathi, A., Dawson, C., Chen, S., & Luettich Jr, R. (2017). Sensitivity of Storm Surge Predictions to Atmospheric Forcing during Hurricane Isaac. *Journal of Waterway, Port, Coastal, and Ocean Engineering, 144*(1), 04017035.

ECMWF. (2009). ERA-Interim Project. Retrieved 07 Sep 2016, from European Centre for Medium-Range Weather Forecasts https://doi.org/10.5065/D6CR5RD9

FEMA. (2014). Region II Storm Surge Project: Mesh Development. In. Washington, DC.

Forbes, C., Luettich Jr, R. A., Mattocks, C. A., & Westerink, J. J. (2010). A retrospective evaluation of the storm surge produced by Hurricane Gustav (2008): Forecast and hindcast results. *Weather and Forecasting, 25*(6), 1577-1602.

Fossell, K. R., Ahijevych, D., Morss, R. E., Snyder, C., & Davis, C. (2017). The Practical Predictability of Storm Tide from Tropical Cyclones in the Gulf of Mexico. *Monthly Weather Review, 145*(12), 5103-5121.

Galarneau, T. J., Davis, C. A., & Shapiro, M. A. (2013). Intensification of Hurricane Sandy (2012) through extratropical warm core seclusion. *Monthly Weather Review, 141*(12), 4296-4321.

Gao, J., Luettich, R., & Fleming, J. (2013). *Development and Initial Evaluation of A Generalized Asymmetric Tropical Cyclone Vortex Model in ADCIRC.* Paper presented at the ADCIRC Users Group Meeting, Vicksburg, MS.

Hall, T. M., & Sobel, A. H. (2013). On the impact angle of Hurricane Sandy's New Jersey landfall. *Geophysical Research Letters, 40*(10), 2312-2315. Article. <Go to ISI>://WOS:000328840200076

Holland, G. J. (1980). An analytic model of the wind and pressure profiles in hurricanes. *Monthly weather review, 108*(8), 1212-1218.

Hong, S.-Y., & Lim, J.-O. J. (2006). The WRF single-moment 6-class microphysics scheme (WSM6). *J. Korean Meteor. Soc, 42*(2), 129-151.

Hong, S.-Y., Noh, Y., & Dudhia, J. (2006). A new vertical diffusion package with an explicit treatment of entrainment processes. *Monthly Weather Review, 134*(9), 2318-2341.

Iacono, M. J., Delamere, J. S., Mlawer, E. J., Shephard, M. W., Clough, S. A., & Collins, W. D. (2008). Radiative forcing by long-lived greenhouse gases: Calculations with the AER radiative transfer models. *Journal of Geophysical Research: Atmospheres, 113*(D13).

Klotzbach, P. J., Bowen, S. G., Pielke Jr, R., & Bell, M. (2018). Continental United States Hurricane Landfall Frequency and Associated Damage: Observations and Future Risks. *Bulletin of the American Meteorological Society*(2018).

Lakshmi, D. D., Murty, P., Bhaskaran, P. K., Sahoo, B., Kumar, T. S., Shenoi, S., & Srikanth, A. (2017). Performance of WRF-ARW winds on computed storm surge using hydodynamic model for Phailin and Hudhud cyclones. *Ocean Engineering, 131*, 135-148.

Lin, N., Emanuel, K. A., Smith, J., & Vanmarcke, E. (2010). Risk assessment of hurricane storm surge for New York City. *Journal of Geophysical Research: Atmospheres, 115*(D18).

Lin, N., Smith, J. A., Villarini, G., Marchok, T. P., & Baeck, M. L. (2010). Modeling extreme rainfall, winds, and surge from Hurricane Isabel (2003). *Weather and forecasting, 25*(5), 1342-1361.

Luettich, R. A., & Westerink, J. (2004). *Formulation and Numerical Implementation of the 2D/3D ADCIRC Finite Element Model Version 44.XX*. Retrieved from Chapel Hill, NC: http://www.unc.edu/ims/adcirc/adcirc_theory_2004_12_08.pdf

Luettich, R. A., Westerink, J. J., & Scheffner, N. W. (1992). ADCIRC: An Advanced Three-Dimensional Circulation Model for Shelves, Coasts, and Estuaries. Report 1. Theory and Methodology of ADCIRC-2DDI and ADCIRC-3DL. In *Dredging Research Program Technical Report DRP-92-6* (pp. 137). Vicksburg, MS: COASTAL ENGINEERING RESEARCH CENTER.

Mattocks, C., Forbes, C., & Ran, L. (2006). *Design and implementation of a real-time storm surge and flood forecasting capability for the State of North Carolina*. Retrieved from Chapel Hill, NC:

Needham, H. F., Keim, B. D., & Sathiaraj, D. (2015). A review of tropical cyclone-generated storm surges: Global data sources, observations, and impacts. *Reviews of Geophysics, 53*(2), 545-591.

National Center for Environmental Information (NCEI) (2018). U.S. Billion-Dollar Weather and Climate Disasters. Retrieved from https://www.ncdc.noaa.gov/billions/

NOAA/NOS/CO-OPS. Tides and Currents. Retrieved from https://tidesandcurrents.noaa.gov

Orton, P., Vinogradov, S., Georgas, N., Blumberg, A., Lin, N., Gornitz, V., et al. (2015). New York City panel on climate change 2015 report chapter 4: dynamic coastal flood modeling. *Annals of the New York Academy of Sciences, 1336*(1), 56-66.

Powell, M. D., Houston, S. H., Amat, L. R., & Morisseau-Leroy, N. (1998). The HRD real-time hurricane wind analysis system. *Journal of Wind Engineering and Industrial Aerodynamics, 77*, 53-64.

Resio, D. T., & Westerink, J. J. (2008). Modeling the physics of storm surges. *Physics Today*(9), 33-38.

Skamarock, W., Klemp, J., Dudhia, J., Gill, D., Barker, D., Duda, M., et al. (2008). A description of the Advanced Research WRF Version 3, NCAR technical note,

Mesoscale and Microscale Meteorology Division. *National Center for Atmospheric Research, Boulder, Colorado, USA*.

Smith, A. B., & Katz, R. W. (2013). US billion-dollar weather and climate disasters: data sources, trends, accuracy and biases. *Natural Hazards*. http://link.springer.com/article/10.1007/s11069-013-0566-5

Tiedtke, M. (1989). A comprehensive mass flux scheme for cumulus parameterization in large-scale models. *Monthly Weather Review, 117*(8), 1779-1800.

Yin, J., Lin, N., & Yu, D. P. (2016). Coupled modeling of storm surge and coastal inundation: A case study in New York City during Hurricane Sandy. *Water Resources Research, 52*(11), 8685-8699. <Go to ISI>://WOS:000393318600017

CHAPTER 3. IMPACT OF TROPICAL CYCLONE LANDFALL ANGLE ON STORM SURGE ALONG THE MID-ATLANTIC BIGHT

3.1 Abstract

Storm surge impact depends on coastal geographical and bathymetric features as well as various tropical cyclone characteristics including the size, intensity, and impact angle of the storm. Although the factors contributing to storm surge are well studied, uncertainties remain regarding the level of sensitivity to these parameters. This work seeks to contribute to the current knowledge of storm surge by studying the sensitivity to tropical cyclone landfall angle. We perform an ensemble of synthetic tropical cyclones using a newly developed modeling capability derived from the Weather Research and Forecasting (WRF) model, the Hybrid WRF Cyclone Model. Wind and atmospheric pressure field outputs from 200 synthetic cyclones are used as atmospheric forcing for the Advance Circulation (ADCIRC) model. We study the sensitivity of storm surge offshore extent and inundation to tropical cyclone impact angle. The extent of the impact area around the landfall location is sensitive to the cyclone landfall angle. Cyclones with tracks perpendicular to the coast are shown to produce the highest water levels and broadest inland and offshore extent. Results also indicate a heterogeneity in the sensitivity to landfall angle along the coast, highlighting the importance of both cyclone impact angle and location.

3.2 Introduction

Tropical cyclones (TCs) represent the most destructive atmospheric events in the United States (Smith & Katz, 2013). Often, the resulting TC-induced storm surge has more

of a destructive impact than have precipitation and winds alone. The potential damages due to storm surge depends on local geographic and bathymetric features, as well as on TC characteristics such as intensity, size, speed, and angle of landfall with respect to the coast. The lack of accurate meteorological observations prior to landfall makes the understanding, assessment, and prediction of storm surge challenging. Previous hindcast storm surge modeling studies (Dietrich et al., 2011a, 2011b; FEMA, 2011, 2014; Mayo & Lin, 2019) have provided accounts of errors from the hydrodynamic models typically used such as the Sea, Lake and Overland Surges from Hurricanes (SLOSH) model (Jelesnianski et al., 1992) and the Advanced Circulation (ADCIRC) model (Luettich & Westerink, 2004; Luettich et al., 1992). Mayo and Lin (2019) found that on average the SLOSH model, used by the National Weather Service for operational storm surge forecasting, tends to underestimate peak storm surge levels by 22%. For the case of Hurricane Gustav, Dietrich et al. (2011a) used ADCIRC and found an overall error of 0.14 m. For the New Jersey-New York (NJ-NY) region, average ADCIRC model peak storm surge error is found to be 0.32 m (FEMA, 2011, 2014b).

An added complicating factor in assessing storm surge impacts is the limited North Atlantic TC and water elevation record. A recent review on TC-induced storm surge accounts for availability of water level data for 110 cases along the entire U. S. Atlantic Coast since 1880 (Needham et al., 2015). Only 22% of the 110 events occurred along the coastline from Virginia to Maine (Needham et al., 2015). Despite their relatively infrequent occurrence along the northern portion of the U.S. Atlantic Coast, these surge events have produced substantial damages. In particular, the NJ-NY region is

characterized by these low-frequency and high-impact TC and extratropical (Booth et al., 2016; Colle et al., 2008; Lin et al., 2019; Needham et al., 2015) cyclone-induced storm surge events. Most notable are the Long Island Express Hurricane (1983), which produced storm surge of 3.0-3.5 m in Long Island (Lin et al., 2010), and more recently Hurricane Sandy (2012), a transitioning extratropical cyclone that tested the resilience of the NJ-NY coastal region with typical storm surge heights of about 3-4 m (Blake et al., 2013).

The vulnerability of such regions highlights the need for improved understanding of the underlying processes contributing to storm surge impacts. Atmospheric forcing is a primary driver of storm surge, and it represents one of the main sources of uncertainty in storm surge modeling (Gonzalez et al., 2019; Kohno et al., 2018; Lin & Chavas, 2012; Mayo & Lin, 2019). Therefore, determining the sensitivity of storm surge to different TC physical parameters is an important step in increasing forecasting accuracy. Previous studies examined the impact on storm surge from changes in TC intensity (Weisberg & Zheng, 2006), size (Irish et al., 2008), forward speed (Hussain et al., 2017; Rego & Li, 2009; Thomas et al., 2019; Weisberg & Zheng, 2006) and location (Fossell et al., 2017; Galarneau et al., 2013). The relationship between storm surge and some of the storm parameters are more straightforward to determine, but others such as the effect of storm translational speed and angle of landfall on storm surge have proven to be more complicated and difficult to assess.

Historically, the behavior observed along the NJ region, and more broadly along the eastern United States, is for cyclones to move northward along the coast (Hall and Sobel, 2013). However, Hurricane Sandy was an example of the possibility of storms

impacting land from other directions. While various factors contributed to its record-breaking storm surge, part of the impact is attributed to its rare near-perpendicular angle of landfall (Hall & Sobel, 2013). As such, Hurricane Sandy put into perspective the need to determine storm surge sensitivity to storm track and landfall angle in the NJ-NY coastal region. The impact of changing a TC's landfall angle on storm surge has not been studied in as much detail as other cyclone parameters. Moreover, studies specific to the NJ-NY region are lacking in this respect. In this study, we seek to address the uncertainty in the impact of TC landfall angle on storm surge in the NJ-NY coastal region.

The model specifications, coupling details and a summary of the simulations performed are provided in section 3.3. Results from the atmospheric and storm surge ensembles are presented in section 3.4, and their implications are discussed in section 3.5. Finally, a summary and conclusions from the study are available in section 3.6.

3.3 Materials and Methods

Simulations of synthetic cyclones were performed with the Hybrid Weather Research and Forecasting (WRF) Cyclone Model (HWMC) and used as meteorological forcing for the Simulating Waves Nearshore (SWAN; Booij et al., 1999) and ADCIRC (SWAN+ADCIRC; Dietrich et al., 2011b) coupled surge-wave model (Ramos-Valle, 2019). A case study of three synthetic cyclones with different landfall angles was conducted to examine the impact of approach angle on storm surge. The case study was expanded to include the analysis of a large number of synthetic cyclones along the NJ coastline. The synthetic cyclones were grouped into three categories, as given by the general direction of their tracks. The average storm surge produced by these scenarios was analyzed and

vulnerable coastal locations were identified. Finally, a clustering algorithm was performed on the storm surge model simulations for a more detailed assessment of the factors influencing the different storm surge responses. In the following section, the model techniques used for the work presented are described.

3.3.1 HWCM Configuration

Simulations of TCs were conducted with the HWCM; an extension of the WRF (Skamarock et al., 2008) model that enables the simulation of synthetic cyclones in a real-world domain. Bruyère et al. (2019) provide an in-depth description and evaluation of the HWCM model setup. Here an overview of the model and its configuration to simulate synthetic TCs is provided. The simulation process was split into two steps as the HWCM makes use of both the real and idealized components of WRF (for details on the configuration of idealized cyclones in WRF, see Rotunno et al., 2009). To set up the HWCM simulations, a cyclone was spun up in an idealized configuration. This cyclone was then placed in a real-world domain where it could dynamically develop and propagate.

To achieve the first step, a weak initial vortex was placed within an idealized atmosphere, which was defined as the 10-year average September climatology for the Western North Atlantic region bounded within latitudes 33°N and 41°N and longitudes -70.0°W and -75.5°W. The initial atmospheric conditions were spatially constant throughout the simulation domain. The atmospheric vertical profile was constructed with data from the National Centers for Environmental Prediction/National Center for Atmospheric Research Reanalysis 1 (Kalnay et al., 1996). Low-level instabilities in the vertical profile (Figure 3-1) were smoothed out to ensure that the resulting environment

was supportive of cyclone formation and development. In practice, the background environment can be provided by any profile-based data set. Using a 10-year September climatological mean ensures a realistic environment able to sustain TC development throughout the length of the simulation.

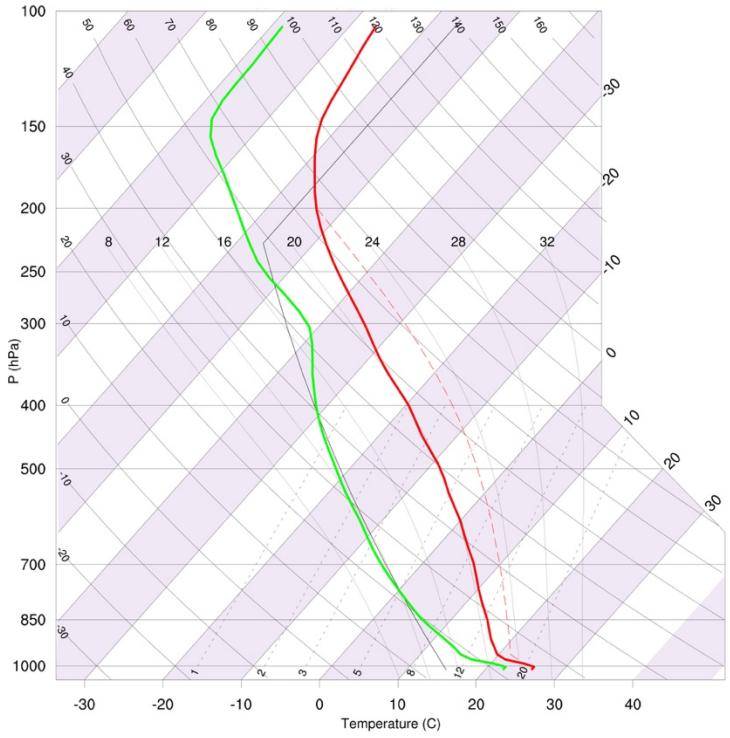

Figure 3-1. Atmospheric vertical profile used to characterize the environment in the ideal and real simulations. Values were interpolated to account for missing data at various pressure levels. The atmospheric temperature and dewpoint are shown in the red and green lines, respectively.

The initial vortex was set up to represent a TC-like axisymmetric vortex with tropical depression strength (maximum wind speed of 15 m/s), outer radius of 412.5 km and radius of maximum winds of 150 km, based on the vortex derived by Rotunno and Emanuel (1987). The extent of the radius of maximum winds was increased from the

default value of 82.5 km to account for larger cyclones. The simulation uses a spatially constant Coriolis parameter of 5.0E-5 s^{-1}, corresponding to 20°N. The TC was positioned in the center of the domain and spun up for a period of 12 days in the idealized domain with constant sea surface temperatures (SSTs) of 28°C. The horizontal resolution was set to 12-km. No lateral boundary conditions were needed for this step as periodic boundaries were used.

Once a mature TC was established in the idealized plane, the first step in the simulation process was completed. As a second step, the cyclone was then placed in a real-world domain. As described by Bruyére et al. (2019), the real-world domain is characterized as a β-plane with real coastlines and topography. The real-world domain contained all the characteristics inherent to real simulations in WRF such as prescribed land mask, terrain height, land use type, and albedo.

As in typical real-case simulations, the TC was allowed to dynamically evolve in response to the imposed atmospheric and sea surface conditions. The initial environmental conditions were similar to those used in the idealized configuration. Additionally, in the real-world simulations, the background wind flow was prescribed and set up to provide a constant flow at the boundaries. The HWCM allows for adjustment of the placement of the TC in the real-world domain, and of the speed and direction of the background wind flow. The ability to vary these properties allow for a degree of control of the TC landfall location, angle of landfall, and TC translation speed, while still permitting the TC to dynamically evolve, propagate, and interact with the surrounding environment and topography (Bruyère et al., 2019).

Four-day simulations of synthetic TCs were performed using the real simulation capabilities of the WRF model v3.8. The simulations were performed on a 12-km horizontal resolution grid (same as in the idealized simulation) and ran with 38 vertical levels and model top at 50 mb. The horizontal resolution used, while somewhat coarser than suggested to accurately capture TC intensity (Lakshmi et al., 2017; Mori et al., 2014), was chosen to balance the need for sufficient accuracy with our ability to simulate a large number of cyclones (Bruyère et al., 2019). The physical parameterizations implemented were previously tested on a similar domain and model configuration for the case of Hurricane Sandy (Ramos-Valle et al., 2018) and were used by the National Center for Atmospheric Research for hurricane simulations for domains of comparable horizontal resolution to that of 12-km used in this study (Galarneau et al., 2013). The parameterization schemes used include the following: WRF single-moment 6-class microphysics scheme (Hong & Lim, 2006), Yonsei University boundary layer scheme (Hong et al., 2006), Tiedtke cumulus parameterization (Tiedtke, 1989), RRTMG for shortwave and longwave radiation parameterization (Iacono et al., 2008), and the Noah land surface model (Chen & Dudhia, 2001). The SST remained time invariant and spatially uniform at 28°C (Bruyère et al., 2019; Kimball, 2008; Li et al., 2015). As reported by Bruyère et al. (2019), a constant SST does not negatively impact the development of cyclones, and on the contrary, its effect is that of sustaining a stronger TC throughout the simulation. The choice of a constant SST adds the benefit for less complexity by simplifying the differences between the simulated TCs and allowing for a more direct comparison between simulations. Since a cyclone was effectively transposed from one environment to another,

a 2-hr digital filter initialization (Peckham et al., 2016) scheme was implemented to reduce initial model instabilities and allow the simulations additional spin-up time.

Alternative approaches are available to simulate synthetic cyclones for storm surge applications, including the use of parametric vortex models (e.g., Dynamic Holland Model; Holland, 1980) and statistical-deterministic TC models (Emanuel et al., 2006; Lin et al., 2012). Track-based data are implemented within parametric models, which allows for easy manipulation of storm characteristics to study the individual impact of storm parameters. Various studies have compared the use of parametric models with more realistic wind field representations (Akbar et al., 2017; Bennett & Mulligan, 2017; Ramos-Valle et al., 2018; Torres et al., 2018), including the use of the WRF model. Full physics atmospheric models have proven to be more accurate, albeit at a larger computational cost (Ramos-Valle et al., 2018). The use of the HWCM ensures fidelity in generating physically plausible storms that dynamically interact and respond to their surroundings, with more accurate wind field representations. Not only does the HWCM present the advantage of allowing a high degree of control over cyclone parameters, but it also allows for sensitivity studies of climate change (by variation of SST or other environmental factors). The methodology is applicable to other regions, facilitating sensitivity studies in other areas. We present the first application of the HWCM for storm surge assessment.

3.3.2 Description of Synthetic Cyclone Simulations With the HWCM

The HWCM allows flexibility in adjusting various parameters when placing a TC in the real-world domain. By solely changing the speed and direction of the background steering flow, as well as the initial location of the TC in the real-world domain, a range of

possible evolution scenarios for the same initial TC can be simulated. In this study, three different initial cyclones with intensities representative of Category- 2, -3, and -4 storms were examined. For each case, one of three parameters were varied at a time: the initial location of the TC in the real-world domain, the speed of the background wind flow, and the direction of the wind flow (Table 1).

Table 3-3. Description of Parameters Chosen to Initialize the Real-World Simulations.

Initial TC category	Initial TC intensity (m/s)	Initial TC location	Background wind speed (m/s)
Category 2	46	Point A: 38.7358, -68.8555	8
Category 3	54	Point B: 36.5861, -69.5870	10
Category 4	61	Point C: 34.9458, -73.5707	12

Three points were selected as initial locations for the placement of the TCs. The locations of these points were chosen to allow for coverage of a large portion of the domain in order to simulate probable TC tracks. While the average tracks of North Atlantic TCs are often north-northeastward (Hall & Sobel, 2013), the choice of the initial cyclone location in this study promotes the simulation of cyclones from various directions and landfall impact angle that may not be observed in the historical records but nevertheless are physically plausible. It is important to highlight that these points do not represent cyclogenesis locations, as the TCs were fully developed by the time they were placed at each point in the real-world domain. Additionally, the speed of the background wind flow was chosen to vary between 8-, 10- and 12 m/s. All directional wind angles in 45° intervals were tested. The directional angle frequency was increased by 5° intervals within the bounds that produced landfalling TCs. Since the focus of the study is primarily on storms

that have a direct impact on the coast, only the TCs that made landfall along the NJ-NY coastline were considered. This method produced between 2 and 12 tracks for each of the 27 configurations.

3.3.3 SWAN+ADCIRC Model Description and Atmospheric Forcing Configuration

Coastal impacts from the synthetic storms were assessed by using the two-dimensional depth integrated (2DDI) implementation of the ADCIRC hydrodynamic model (Luettich & Westerink, 2004; Luettich et al., 1992), coupled with the SWAN wave model (SWAN+ADCIRC). The SWAN model includes processes such as wave growth due to wind and action loss due to white capping, surf breaking, and bottom friction.

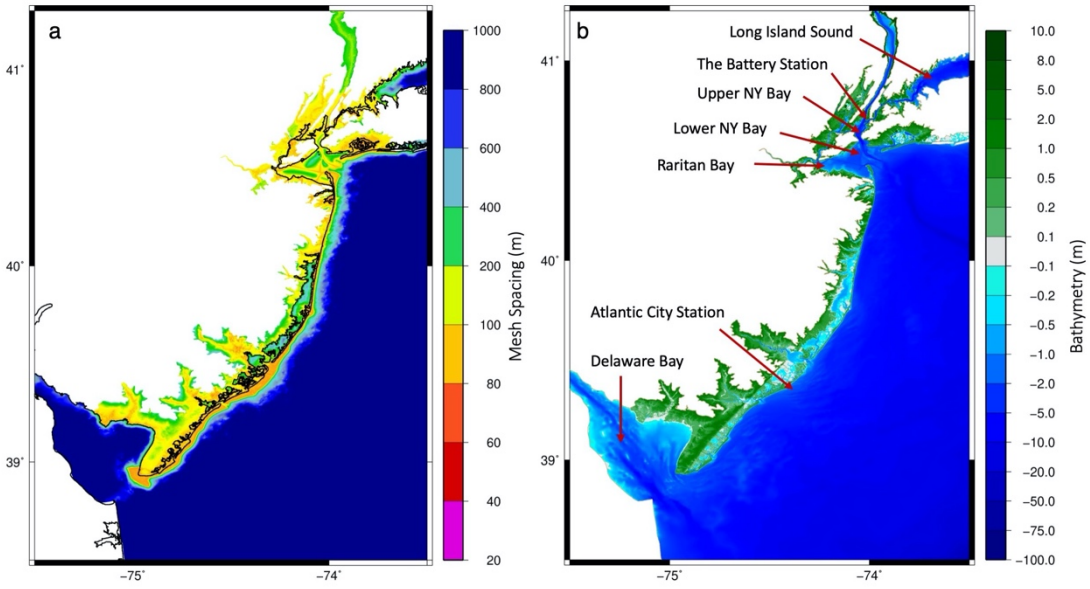

Figure 3-2. (a) Depiction of the FEMA Region II mesh spacing for the NJ-NY coastal region. (b) Bathymetric heights along the NJ-NY coast. The location of various points of interest are highlighted.

ADCIRC has been implemented for various coastal studies in the region of interest along the NJ-NY coastal area (Cialone et al., 2017; Colle et al., 2015; Lin et al., 2010;

Ramos-Valle et al., 2018; Yin et al., 2016). The ADCIRC model uses a finite element unstructured triangular grid allowing for higher resolution near the coast and coarser resolution in the deep ocean. The ADCIRC mesh is made up of elements, each of which contains three nodes or vertices where water heights are computed. In this study, simulations were performed on a grid developed by the Federal Emergency Management Agency (FEMA) as part of the Region II Coastal Storm Surge Study (FEMA, 2014a). Various studies have validated and implemented the use of this mesh to study TCs and extratropical cyclones (Orton et al., 2015; Ramos-Valle et al., 2018; Yin et al., 2016). The mesh domain contains a total of 604,790 nodes and includes the U.S. Atlantic Coast, the Gulf of Mexico, and the Caribbean. Increased resolution is found in areas including the Delaware Bay, the Hudson River Valley, New York City, and Long Island Sound (LIS) (Figure 3-2). The mesh inland extent was constructed based on the 25-ft NAVD88 contour (FEMA, 2014a), resulting in a broader inland extent in southern NJ and a narrower extent in northern NJ. The inland extent of the mesh (Figure 3-2) can be interpreted as the potential or maximum inundation area.

The hourly 10-m winds and surface pressure fields obtained from the HWCM-simulated storms were used as atmospheric forcing to the hydrodynamic and wave models (i.e., one-way coupling between atmospheric and oceanic components). The wind and atmospheric pressure fields were spatially interpolated onto the SWAN+ADCIRC model domain and temporally interpolated to correspond with the SWAN+ADCIRC model time step of 1 s. SWAN+ADCIRC have been tightly coupled to run on the same unstructured grid, and information passes between the two every 10-min without the

need for further interpolation (Dietrich et al., 2011b, 2012). SWAN is driven by wind speeds, water levels, and currents computed by ADCIRC after the implementation of the atmospheric forcing. The coupled SWAN+ADCIRC model has been tested and validated and has been used extensively in storm surge studies (Akbar et al., 2017; Dietrich et al., 2012; Marsooli & Lin, 2018). While the experimental design prevents the comparison of simulated storm surge to observed water level, both the computational mesh and the coupled model setup have been previously tested (FEMA, 2014a; Ramos-Valle et al., 2018). Moreover, uncertainties in atmospheric forcing are addressed by performing the HWCM ensemble of synthetic tracks.

The bottom friction in the model is parametrized using the quadratic bottom friction law. The Garratt (1977) wind drag formulation was used to calculate the wind drag coefficient with a cap at 0.0035. The density of air was set to the model default at 1.15 kg/m^3, and the Coriolis parameter was set to vary spatially throughout the domain. For simplicity, and with the purpose of isolating the effect of storm landfall angle on storm surge, tidal forcing was not included in this study. As the synthetic cyclones are not associated with a specified date/time, these would occur at a random stage of a chosen tidal cycle. Additionally, the influence of nonlinear tidal-surge effects, which have been found to be large in the NJ-NY Harbor (NYH) region (Lin et al., 2010), would have had to be considered in the attempt of isolating the effect of landfall angle on storm surge. Tidal effects must be considered for real cases and in the application of the results presented herein.

The storm surge scenarios produced by coupling the HWCM ensemble of synthetic cyclones with the SWAN+ADCIRC modeling system were assessed. The extent of the inland flooding produced by the storms was estimated over the region bounded within latitudes 38.9°N and 41.5°N and longitudes -72.0°W and -75.7°W. The potential inundation area was calculated by inspecting the dry nodes in the mesh, within the specified bound, prior to the start of the simulation. Elements with more than two nodes inundated at any point throughout the simulation were accounted for in the estimate of the inundation area. The estimates for inundation volume were calculated by multiplying the average maximum water elevation within each element by the area of the element. The volume estimates can then be interpreted as a volume potential.

3.4 Results

3.4.1 Evaluation of Simulated Synthetic Tracks

The method presented relied on the effective implementation of the HWCM model in simulating synthetic storms. Although an extensive validation of the HWCM is beyond the scope of this paper, we evaluated the use of this methodology by assessing whether the behavior of the synthetic tracks was a response of model internal variability or if it was in fact a response to the external forcing imposed.

Figure A-1 in appendix A shows the resulting tracks from the test case for two HWCM synthetic storms. Details of the simulations are provided in appendix A (text A-1). The cyclones are subjected to the effect of the model internal variability due to the nonlinear nature of the system. However, the behavior observed from the synthetic tracks is indicative of a response that is mainly due to the external forcing imposed at the

lateral boundaries, which dominates the overall movement and behavior of the cyclones. We used this feature to create an ensemble of storms, that provide the desired spread in landfall locations and impact angle, which would have not been generated by solely exploiting the internal variability of the model.

3.4.2 HWCM+ADCIRC Ensemble

We performed more than 300 simulations using the HWCM during the testing phase of the model configuration. A total of 198 simulated tracks were chosen as a subset to create the ensemble of synthetic tracks (shown in Figure 3-3a). The tracks selected included those cyclones that made landfall at any point along the NJ-NY coastline. Even though an equal number of simulations were tested for each of the three initial storm locations, the resulting ensemble produced fewer number of landfalling synthetic tracks originating from the southernmost point (Point C in Table 1). These tracks are categorized as parallel moving tracks relative to the NJ coast and have been known historically to be more common than tracks moving from offshore at more slanted angles. The combination of TC initial location and background wind flow resulted in fewer parallel landfalling cyclones. The simulation resulted in 97 tracks originating from point A, 73 from point B, and 28 from point C.

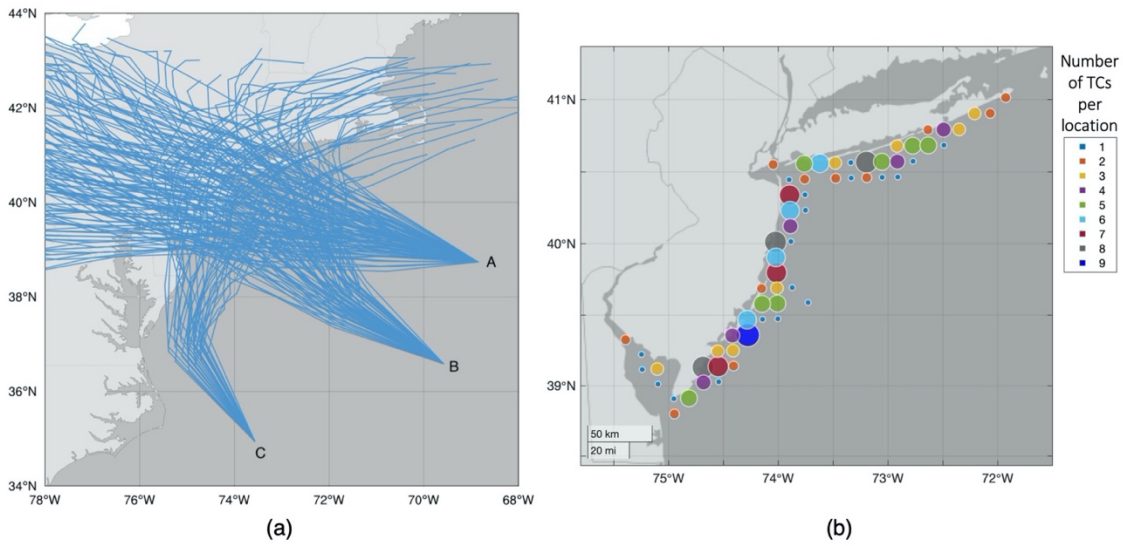

Figure 3-3. (a) Synthetic cyclone tracks for the 198 TCs resulting from the HWCM ensemble. Synthetic cyclone tracks are shown at 6-hr intervals for 60 hr after cyclone placement in the real-world domain. (b) The landfall location density map is shown.

The density map in Figure 3-3b shows the extent and ample coverage of the ensemble members along the entire NJ-NY coastline. The average distance between adjacent landfall points is 12 km.

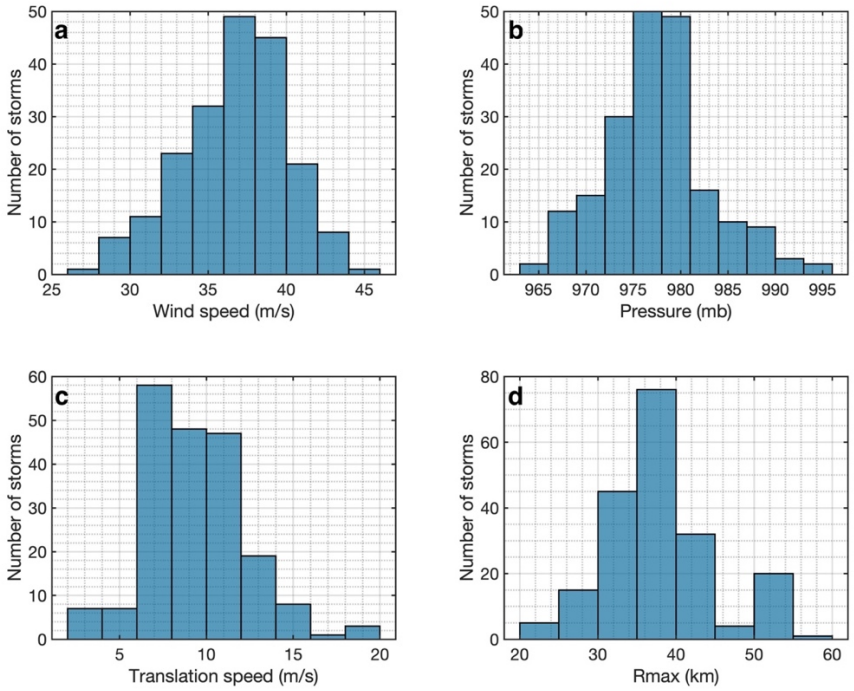

Figure 3-4. Distribution of (a) wind speed (m/s), (b) minimum pressure (mb), (c) translation speed (m/s), and (d) radius of maximum winds (km) for the 198 HWCM simulated synthetic cyclones.

The distribution of storm parameters (Figure 3-4) were examined and compared to the historical record. Henceforth, we identify each track by the maximum wind speed, minimum pressure, radius of maximum wind (R_{max}), and translation speed at the time step prior to landfall.

The range of TC intensities, as given by the maximum wind speed at landfall, varies from 26 to 46 m/s (i.e., tropical storm to Category 2 intensity). About 85% of the cases in the ensemble fall within the range of 33-42 m/s (i.e., Category 1). Generally, the intensity of TCs that make landfall in the U.S. North Atlantic Coast is rarely higher than that of a Category 1 storm (Marsooli & Lin, 2018). Even though the initial vortices inserted in the

real-world domain ranged from Category 2 to 4 intensity, the environment did not sustain these intensities throughout the storm's lifetime and by landfall the storms had weakened to mostly Category 1 cyclones. This is an expected outcome since in addition to weakening at landfall, the TCs weaken as they stabilize after being transposed to the real-world domain. The ensemble distribution of maximum wind speed falls within the probability density function of maximum intensity at landfall for North Atlantic TCs, which peaks at around 43 m/s (Landsea et al., 2015).

The range of translation speed in the probability density function for North Atlantic TCs (1989-2000) varies from 0 to 18 m/s with a peak between 4 and 6 m/s (Kaplan & DeMaria, 2003). The translation speed for the HWCM ensemble members is consistent with the North Atlantic TC record as storm motion ranges between 3 and 19 m/s, with a similar peak in the distribution between 6 and 8 m/s. The mean R_{max} of Atlantic Basin TCs from 1988 to 2008 is estimated to be around 64 km with a standard deviation of 39.6 km (Quiring et al., 2011). The radius of maximum winds for the HWCM ensemble has a narrower range in the distribution (20 - 60 km) and is generally characterized by smaller TCs, with the majority of the storms having an R_{max} within the range 30-40 km.

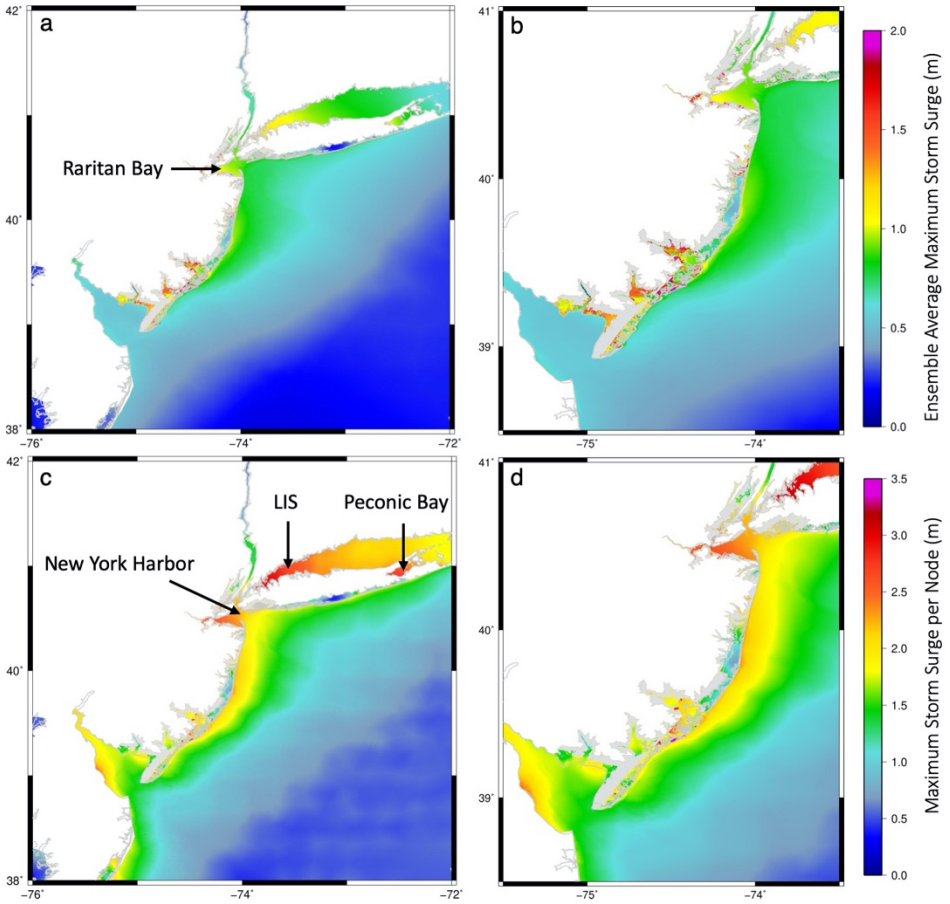

Figure 3-5. (a) Ensemble average of maximum water level. (b) Zoom in of (a) along the New Jersey coast. (c) Maximum water elevation forecasted at each node. (d) Zoom in of (c) along the New Jersey coast.

The ensemble average maximum storm surge (Figures 3-5a and 3-5b) is above 1.5 m in various locations along the coast including regions of southern NJ and Raritan Bay, highlighting these areas' vulnerability and sensitivity to different types of storms. Extreme scenarios are shown in Figure 3-5c and 3-5d, where the maximum elevation per node is contoured. In these scenarios, some areas such as the NYH (encompassing the Upper New York Bay, Lower New York Bay, and Raritan Bay), LIS, Peconic Bay, and the inlets along the south coast of NJ experienced a maximum storm surge of over 2.5 m for given cases.

These areas represent high vulnerability regions with an increased likelihood of experiencing substantial storm surge impact.

3.4.3 The Effect of TC Landfall Angle on Storm Surge

3.4.3.1 A Case Study Along the Coast of NJ

The density map of landfall locations shown in Figure 3-3b allowed us to determine sites where multiple TCs made landfall. We examined various cases where cyclones approached the selected landfall locations from various directions. Henceforth, the tracks are categorized according to their general direction with respect to the NJ coast; thus, they are based on the initial storm placement in the real world (i.e., points A-C in Table 1). To isolate the effect of landfall angle and allow for a more direct comparison between the cyclones, we minimized the differences among the TC's physical parameters. The TC selection process began with identifying the tracks that crossed any given location within a 20-km radius centered on a point of reference near the coast. From this initial selection, we only included the TCs that had maximum wind, translational speed and R_{max} within $\pm$ 0.5σ of the mean of all storms crossing the 20-km radius. Various points along the NJ coastline were examined, and similar results were found among these test cases. Only one of the cases is presented here (Figure 3-6a).

The tracks chosen for this reference point intersect along the coast as they make landfall, approximately 23 hr after the simulation was initialized. From Figures 3-6b - 3-6d the similarities among the wind field structures are shown. For all three cases, the lifetime maximum wind speed occurred on the right-hand side of the TCs during the first forecast hours of the simulation. The range of maximum wind speed at landfall for the three tracks

is narrow, ranging between 34.5 and 35 m/s. The difference with respect to the TC maximum wind speed parameter mean was calculated for each of the tracks per hourly time step. The average difference in maximum wind speed within the first 24 hr was 0.38, 0.43, and -0.81 m/s for the perpendicular, diagonal, and parallel tracks, respectively, while the actual differences fluctuated to $\pm$ 3.0 m/s close to landfall time. The estimated difference in maximum wind speeds began to diverge after the storm had made landfall, ensuring similarities between the storms up to that point. Similarities in the TC size are also highlighted in Figures 3-6b - 3-6d. The TCs are characterized by R_{max} within the range of 33-37 km. The diagonal track has the highest R_{max} of 37 km, while the perpendicular and parallel tracks both have an R_{max} estimated at 33 km at landfall. The variation in translation speed is also subtle varying between 6.47, 7.23, and 9.15 m/s for the parallel, perpendicular, and diagonal tracks, respectively.

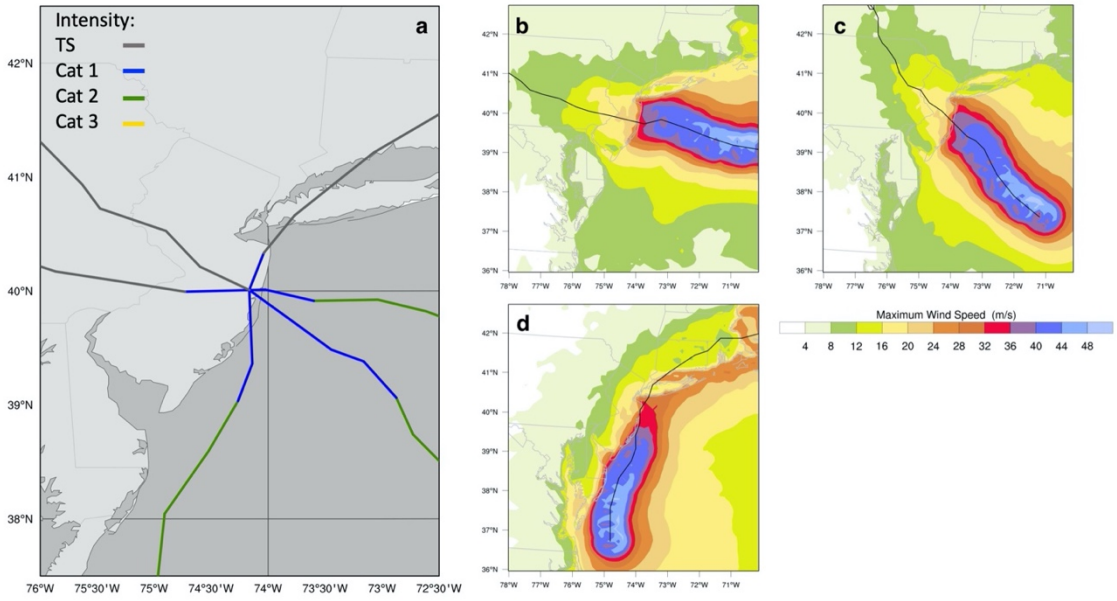

Figure 3-6. (a) Case study to explore relationships between TC landfall angle and storm surge. Maximum wind speed fields for the (b) perpendicular, (c) diagonal, and (d) parallel cases.

While the differences among the synthetic cyclone characteristics were minimized, the maximum storm surge patterns in Figure 3-7 highlights the differences in impact area as well as the differences in offshore surge extent. At the Battery, the peak storm surge ranged from 1.06, 1.09, and 0.72 m for the perpendicular, diagonal and parallel tracks, respectively. Most of the impacts from the parallel track (Figure 3-7c) were observed in the Delaware Bay and along the southern coast of NJ, coinciding with regions of intense winds. As the storm advanced along the coast, the strongest winds were often directed toward the coast. The parallel case also produced the highest inundation volume, estimated at about 0.6059 km^3. For the diagonal track in Figure 3-7b, storm surge heights above 1.0 m are more localized and centered more closely to the landfall location than those for the other two cases. Due to its more oblique angle, as the storm moved towards the coast, the strongest winds in the right-hand side of the TC remained over open ocean for a longer period of time. Closer to landfall, NE winds directed toward the coast caused high storm surge in this area. As the storm continued its movement, easterly winds were directed into the NYH area. The inundation volume for the diagonal case was 0.2153 km^3. The perpendicular case shows the extent of stronger winds over the LIS and NYH regions, corresponding with the locations where maximum storm surge was generated. As the TC approached land, a shift from N/NE winds to purely easterly winds along the fetch direction over the LIS caused a buildup of water as inferred from Figure 3-7a. Similarly to

the diagonal case, easterly winds are directed toward the NYH region. In both cases, the direction and magnitude of the winds force water into small areas, suggesting a larger potential for inland flooding. While the perpendicular track had a broader offshore impact and extent than had the other two tracks, it had the lowest estimated volume of 0.1574 km^3.

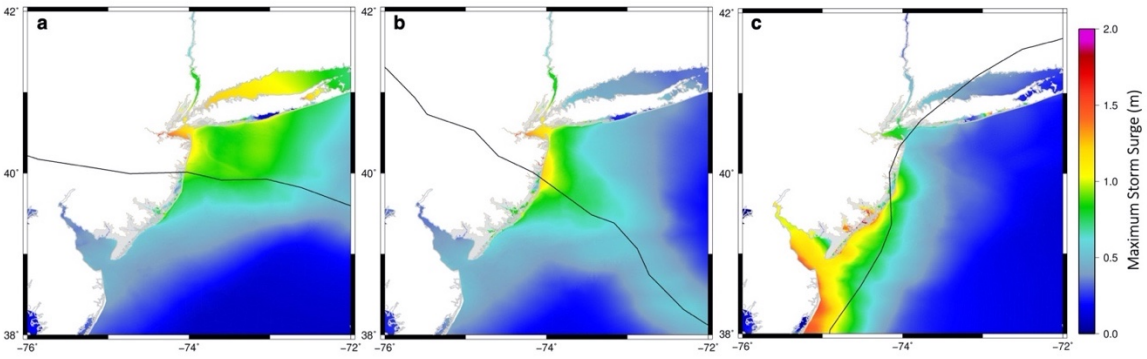

Figure 3-7. Maximum storm surge levels for the (a) perpendicular, (b) diagonal and (c) parallel tracks in the case study. Tracks are plotted near landfall at 3-hr intervals.

3.4.3.2 Ensemble Simulations to Assess the Effect of Cyclone Landfall on Storm Surge

To generalize the conclusions drawn for the case study, we specifically examined the HWCM-simulated tracks that made landfall in NJ and their corresponding average maximum storm surge. The simulated tracks were also classified into the same three storm types, namely, perpendicular, diagonal, and parallel, based on their initial storm placement in the real-world domain (i.e., points A-C respectively in Figure 3-3a). The filtering resulted in 59 perpendicular, 43 diagonal, and 11 parallel cases (Figures 3-8a - 3-8c).

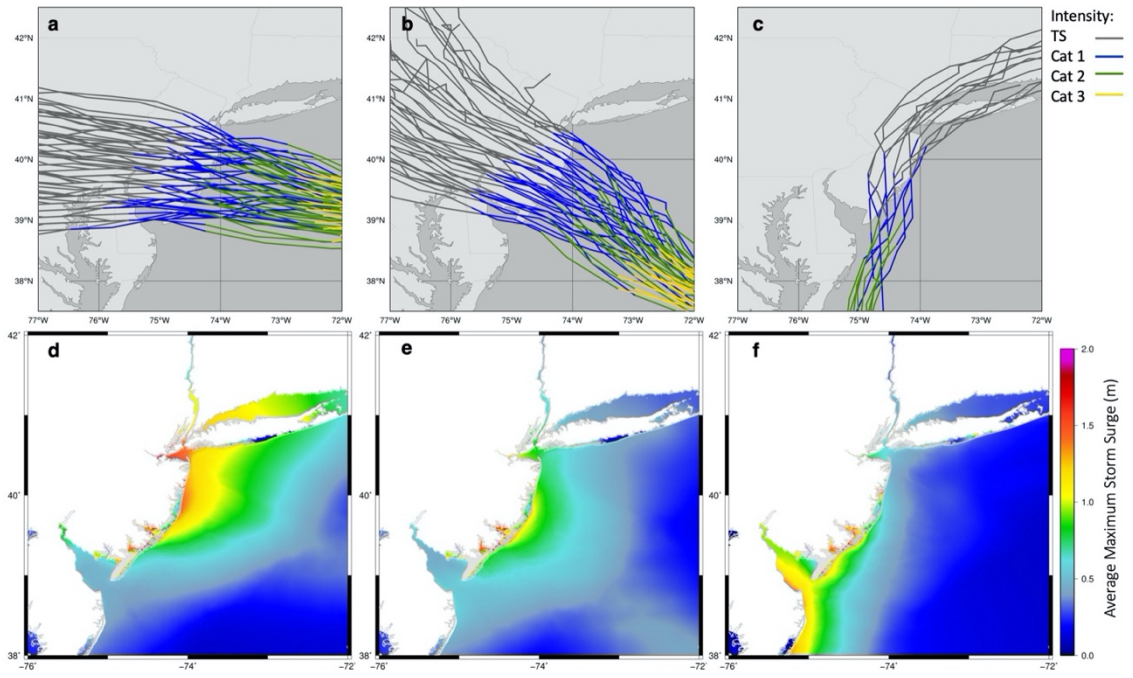

Figure 3-8. The tracks that made landfall in NJ were considered to investigate the effect of TC landfall angle and location on storm surge. The clustering resulted in (a) 59 perpendicular tracks, (b) 43 diagonal tracks, and (c) 11 parallel tracks with respect to the NJ coast. (d-f) The corresponding maximum storm surge levels, showing the differences in offshore extent.

The distributions of TC parameters in Figure 3-9 show the variability and spread among the individual cases in each directional category. These distributions have been normalized by the number of cyclones per directional category to account for the differences in the number of cyclones. With mean wind speeds of 34, 37, and 37.5 m/s for the parallel, diagonal, and perpendicular tracks, respectively, on average, they are all characteristic of a Category 1 TC (Figure 3-9a). The distributions for translation speed and radius of maximum winds (Figures 3-9c and 3-9d) show less variability than the intensity parameters. The peak in the distribution of R_{max} for each storm type cluster closely to each

other and have a large spread. The R_{max} distribution peaks between 32 and 36 km for the perpendicular and diagonal tracks and between 36 and 40 km for the parallel tracks. The distribution of translation speed shows the tendency of parallel tracks toward slower motions (mean of 7.5 m/s) and the perpendicular tracks toward faster motions (mean of 11.3 m/s).

While the magnitude of the resulting mean maximum storm surge is similar among the three groups, these mostly reflect an impact on the storm surge location and extent, as was previously seen in the case study (Figure 3-7) in section 3.3.1. On average, the parallel tracks had a larger effect in the Delaware Bay and along the southern NJ coast (Figure 3-8f). Since all the parallel tracks directly interact with land before reaching the NYH and LIS regions, little impact was seen in these areas from this type of storm. The perpendicular and diagonal tracks in Figures 3-8d and 3-8e share some similarities in terms of the location where the highest storm surge was produced. Their difference mostly lies in the offshore extent of storm surge. For the perpendicular cases, the average maximum storm surge resulted in a broader surge extent affecting more areas in NY such as LIS and the NYH region. For the diagonal tracks, the offshore storm surge extent was narrower than the average pattern resulting from the perpendicular tracks.

To assess inland flooding, we examined the inundated area and potential inundation volume. The inundation volume estimates consider both the extent of the area inundated, and the magnitude of the flooding. This metric provides a broader assessment of the impact associated with each storm direction. The mean inundation area for the parallel tracks is 469 km^2, which accounts for about 16% of the potential

flooding area (2,940 km^2). A larger sample of parallel cases would be useful to validate this result. The mechanisms behind this finding are likely due to two factors regarding the storm track itself and the region of impact. First, while the impact of parallel tracks on any specific region along the coast is of shorter duration, parallel tracks affect more of the coastline as they move alongshore and as such have a larger potential for inundation. In addition, the increase in inundation volume is due to the vulnerability of the area near landfall due to its low-lying topography. We have seen from the maximum water levels in Figure 3-8 that the region of inlets in southern NJ is particularly vulnerable to storm surge. The perpendicular and diagonal cases exhibited a wider range of inundation scenarios (Figure 3-9f), with most cases tending to inundate between 150 and 350 km^2.

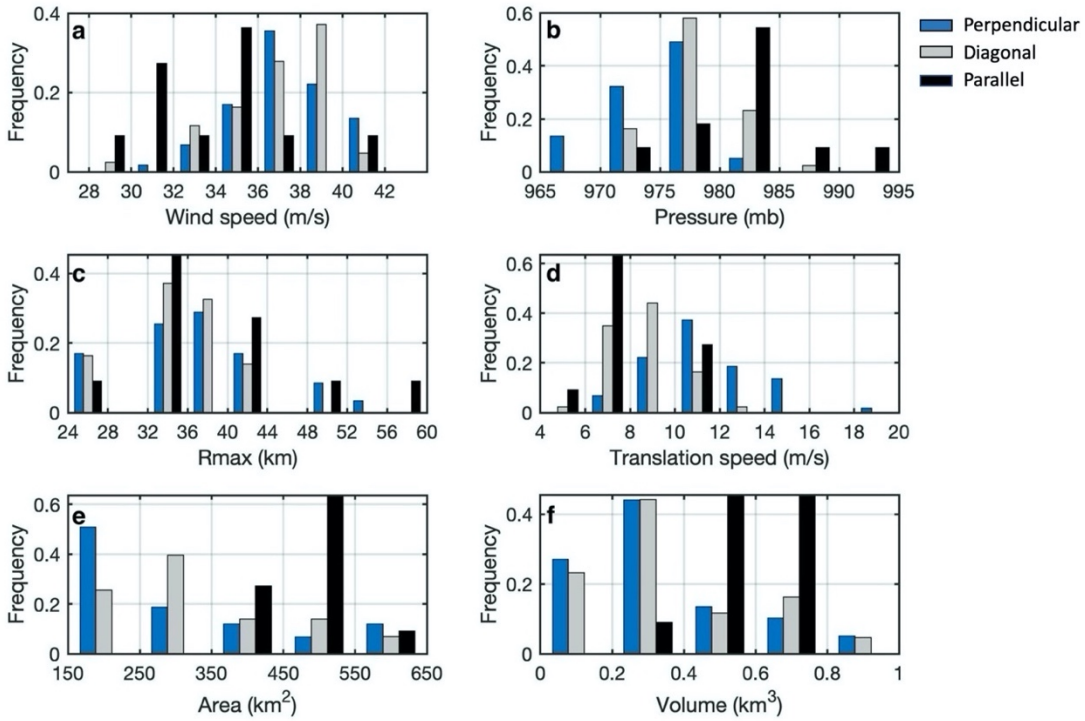

Figure 3-9. Distribution of (a) wind speed (m/s), (b) minimum pressure(mb), (c) radius of maximum winds (km), (d) translation speed, (e) inundation area (km^2), and (f) inundation volume(km^3). The distributions are normalized by the number of storms per category.

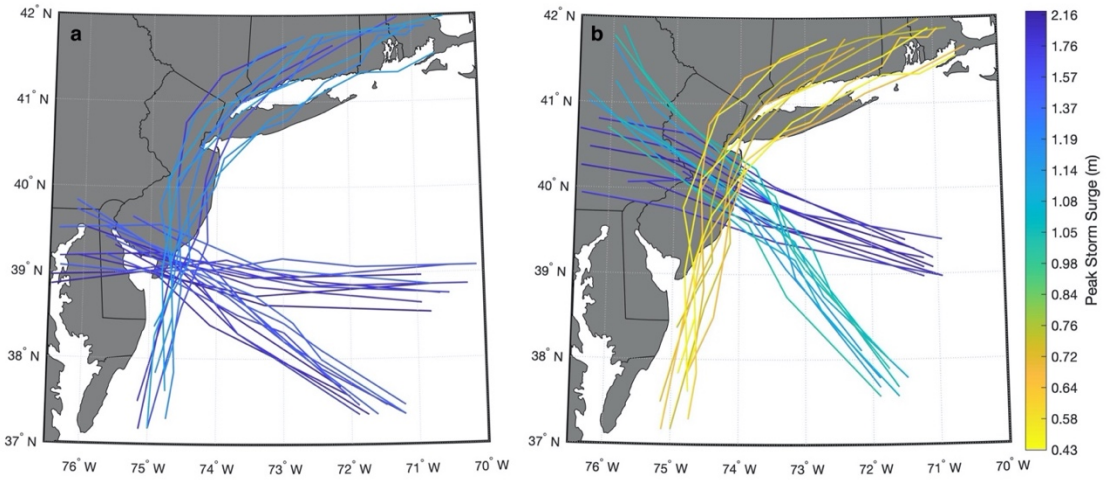

Figure 3-10. Simplified tracks for the storms that produced the top 10 highest storm surges for each of the categories at (a) Atlantic City and (b) The Battery stations. The tracks are identified based on the magnitude of the peak storm surge.

The parallel tracks produced the largest mean inundation volume of 0.57 ± 0.10 km^3. The mean volume estimates for the perpendicular tracks were lower (0.35 ± 0.22 km^3), albeit with a larger variability, than those for the diagonal cases (0.37 ± 0.21 km^3). The results for inundation area and volume prove somewhat unexpected and counterintuitive to what the maximum storm surge patterns depict in Figures 3-8d - 3-8f. While the maximum surge level patterns point to the highest potential for inland flooding for perpendicular tracks, the mean inundation values suggest that these storms produced the least inundation in terms of both the extent and the flood volume. However, the

perpendicular cases were actually responsible for the largest inundation area produced by any of the storms in the ensemble.

To address this further, we examined the top 10 surge-producing storms per directional category (Figure 3-10) and the corresponding inundation volume at two locations: The Battery and Atlantic City stations (NOAA/NOS/CO-OPS), chosen to correspond in the model with their actual placement as given by the NOAA Tides and Currents stations. At the Battery (Figure 3-10b), there is a clear distinction as to the effect of storm landfall angle on storm surge. Perpendicular tracks produced the highest storm surge impact, followed by the diagonal and parallel cases. At Atlantic City (Figure 3-10a), the sensitivity to landfall angle was not that apparent. While the perpendicular tracks did produce the highest peak storm surge at the Atlantic City station, all three storm types produced substantial and comparable peak surge heights relative to all the storms in the ensemble (between 0.84 and 1.71 m). When examining the top 10 storms producing peak levels at the Battery, the parallel cases caused the lowest peak surge (0.48m) but still exhibited a tendency to flood a larger volume than its counterparts. For Atlantic City the opposite was observed. Along the south coast of NJ, in the area of highest flooding potential, the perpendicular tracks had the highest flood volume estimates, while the parallel had the lowest. This result points to the relevance of landfall location in the assessment of storm surge sensitivity, which is explored in more detail in section 3.4.

3.4.4. Clustering by Storm Surge Scenarios

Initially, the HWCM ensemble of simulations were grouped in a subjective manner based on the general direction of the storm track. In this section, we present a different

approach by performing a K-means clustering on the spatial distribution of maximum storm surge levels rather than clustering by storm track direction. After the clustering, we examined the characteristics of the associated storms classified within each cluster. We were interested in using this tool to objectively examine the link between cyclone landfall angle and location with the resulting storm surge. The clustering was done for the 113 cases that made landfall in NJ. The variance ratio criterion (Caliński & Harabasz, 1974) was employed to determine the optimal number of clusters, which resulted in the use of four clusters (C1-C4).

The storm tracks associated with each cluster are shown in Figure A-2 of Appendix A. Two of the main features resulting from the cluster are (i) the fact that two out of the four groups are composed of tracks approaching the coast from different angles and (ii) the distinction between the TCs' landfall locations. Cyclones in clusters C1 and C3 have a similar landfall location along the southern coast of NJ (Figures A-2a and A-2e), while cyclones in C2 and C4 have an impact further north along the coast (Figures A-2c and A-2g). We further separated the clusters composed of different track categories such that for C3 we distinguish between C3 (diagonal) and C3 (parallel), and for C2 we distinguish between C2 (perpendicular) and C2 (diagonal) (Table 2). Upon inspection of the maximum storm surge levels for the individual categories, the patterns previously observed in the case study were repeated, as shown in Figures A-2b and A-2h for perpendicular cases.

While the cluster analysis was performed on the spatial distribution of the maximum water level, we were interested in examining how the characteristics of the storms producing such spatial patterns in each cluster are grouped. The characteristics of

the synthetic storms that generated the surge patterns in each of the clusters were examined. Table 2 presents the range and mean values for various TC parameters. Notable differences between the clusters and sub clusters are not immediately apparent. As shown for the maximum wind speed in Figure 3-11b, while some clusters (such as C4) tend to have slightly stronger storms, the resulting clusters do not appear to be primarily based on the maximum wind speed- or by any of the other physical characteristics inherent to the cyclones. Figure 3-11d also showed that clusters such as C2 and C3 have slower moving storms than have C1 and C4, which could point to the reason the perpendicular tracks of C2 and C4, with similar landfall location, are not clustered together.

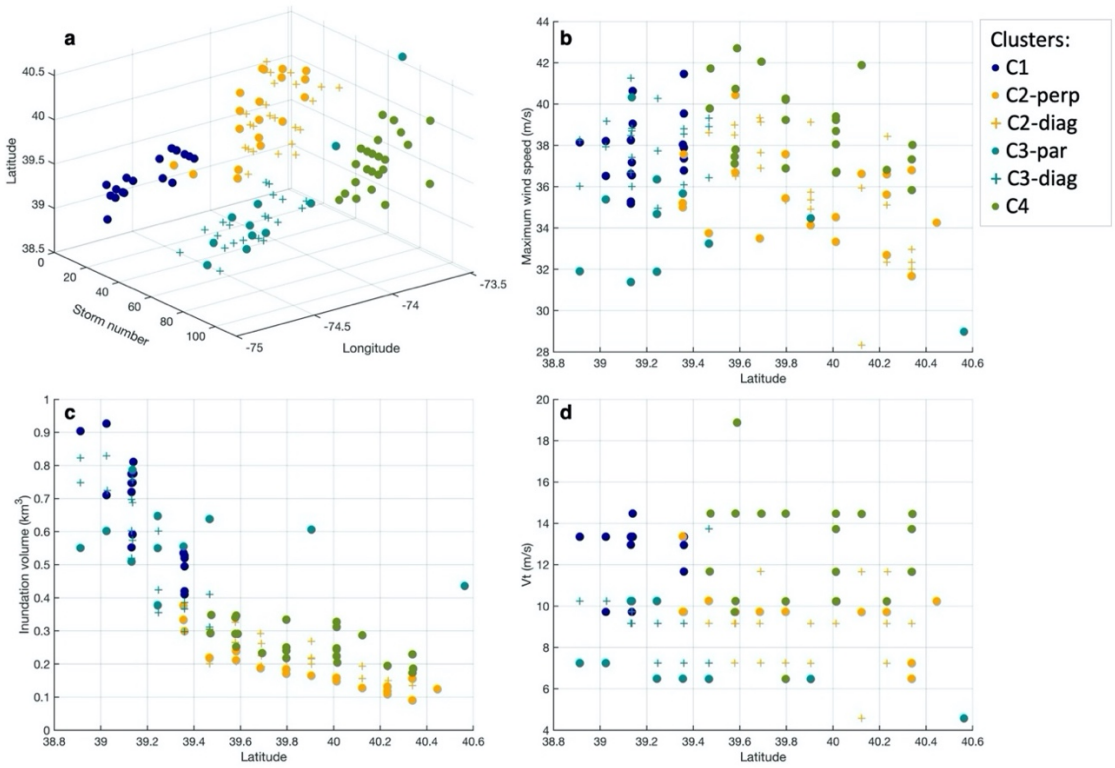

Figure 3-11. Tropical cyclone and storm surge properties identified by clusters. (a) Landfall location of storms, (b) maximum wind speed at landfall, (c) estimates of inundation

volume, and (d) translation speed. TC data in (b)-(d) have been sorted by increasing latitude coordinate at landfall.

As expected, the results highlight how each of the clusters was classified by various water elevation metrics such as the maximum storm surge estimate of overall inland flooding. Figure 3-11a shows the distinction of clusters by landfall location, separating the tracks that make landfall further north and south along the NJ coastline. The tracks that make landfall along the southern coast of NJ (C1 and C3) show a larger flooding volume than do the tracks that make landfall along the northern portion of the NJ coast (C2 and C4). The range of inundation volumes for the southern cases was 0.5496 - 0.6570 km^3. For the northern cases, the range was 0.1859 - 0.2636 km^3. On average, within each of the northern and southern cases, the perpendicular tracks were responsible for the highest inland flooding potential. Figure 3-11c highlights the pattern of decreasing flood volume with increasing latitude. The results from the clustering method highlight more directly the sensitivity of storm surge not only to the landfall impact angle but to landfall location.

Table 3-4. Range and Mean Values for Physical Parameters That Characterize the Cyclone Within Each Cluster.

Cluster number	Maximum wind speed (m/s)	Minimum pressure (mb)	Translation speed (m/s)	Radius of maximum wind (nm)
C1 (perpendicular)				
Range	35.18 - 41.46	969.5 - 979.2	9.71 - 14.48	13 - 27
Mean	37.80	974.35	11.95	20.29
C3 (parallel)				
Range	28.97 - 40.32	972.8 - 993.4	4.57 - 10.24	14 - 32
Mean	34.02	982.45	7.47	21.27
C3 (diagonal)				
Range	34.96 - 41.26	972.5 - 980.3	7.24 - 13.74	13 - 23
Mean	37.99	976.39	9.06	18.05
C2 (perpendicular)				
Range	31.66 - 40.42	974.3 - 980.8	6.47 - 13.35	14 - 29
Mean	35.33	977.98	9.65	21.21
C2 (diagonal)				
Range	28.32 - 39.33	973.7 - 988.4	4.57 - 11.67	14 - 23
Mean	35.81	979.11	8.53	19.48
C4 (perpendicular)				
Range	35.83 - 42.70	966.8 - 987.2	6.47 - 18.87	13 - 27
Mean	38.89	972.47	12.24	18.57

3.5 Discussion

The use of the HWCM in simulating synthetic tracks allowed us to control the characteristics of the cyclones, as the tracks responded to the external forcing imposed at the boundaries. This feature in the HWCM, allowed us to generate the desired spread in the ensemble to assess the sensitivity of storm surge to cyclone landfall angle.

We showed that the main difference between the TC directional groups manifested in the location and extent of the storm surge impacts. The parallel cases simulated in this study make landfall in south NJ, and the resulting storm surge mostly

impacts the Delaware Bay and southern NJ coast. If we considered parallel storms that moved along the coast without making landfall, we could expect these to have a higher and broader impact than would the parallel cases examined here. These tracks would likely continue their movement along the coast without the decrease in intensity they undergo after landfall. Given that the perpendicular and diagonal tracks do not interact with land prior to their landfall, we were able to compare them more directly. On average, the perpendicular tracks exhibited a more widespread extent of the storm surge signal, while the diagonal tracks were shown to impact a smaller region.

The three storm categories exhibited similarities in terms of the upper limit of the inundation extent and volume. On average, the parallel tracks exhibited the tendency to flood a broader area than did the other two directional categories. Nevertheless, the perpendicular tracks, particularly those making landfall in southern NJ, were responsible for the peak inundation within the domain. This result brought into question the potential influence of the mesh extent into the interpretation of the flooding of each category. However, since the mesh extent follows the 25-ft elevation contour, it is inherently designed to account for actual potential flooding areas based on the region's topographic features. Thus, the mesh represents the area that can be flooded in reality and does not bias the results presented. Storms impacting the southern NJ area have a higher flooding potential than those in other areas further north along the coast. The dependency of peak storm surge to the landfall angle in southern NJ was lower. Nevertheless, when comparing storms affecting the area of highest flooding potential, we found the perpendicular tracks have a greater effect, inundating a larger volume. More broadly, the flooding potential

along the NJ coast was not uniform and decreased with increasing latitude. The storm surge impact from TCs thus varied depending on its landfall location along the coast, pointing to the importance of geographical (e.g., coastal slope and complexity) and topographic features. The importance of these features in amplifying or reducing storm surge have been quantified in previous studies (Bilskie et al., 2014; Bloemendaal et al., 2019). TCs with landfall in areas with complex coastlines and shallow bathymetry are associated with higher storm surges. (Bloemendaal et al., 2019; Mori et al., 2014).

The cluster analysis provided further intuition as to the relationship between landfall angle and location and confirmed the conclusions previously drawn from the HWCM-ADCIRC ensemble. The cluster analysis raised the question of the factors contributing the most to the resulting storm surge. The clusters were not grouped by the TC physical parameters but by the direction of the storms and their general impact location. While it is beyond the scope of this paper, further study is needed to quantify the relative importance of each of the parameters to the resulting storm surge.

The study presented can be enhanced by considering other factors relevant to cyclone-induced inundation and coastal flooding. Results presented here only included the surge and wave components and are thus independent of the tidal cycle and its local effects and of rainfall-runoff contributing to flooding. In reality, the overall inundation volume depends on other factors such as the cyclone-induced precipitation. Rainfall-runoff can contribute to the already high inland flooding, pointing to the importance and need of including this process in storm surge and inundation assessment. While we do not delve into the mechanisms of flooding by both storm surge and rainfall-runoff, it is

interesting to note the differences among the cases. Rainfall totals calculated for the cyclones used in the case study (Figure A-3 in Appendix A) provide insight into the variations of the precipitation fields and the possible effects of the different storms on the overall flooding. More notable is the parallel case, which showed the highest rainfall totals along the entire coast of NJ and a vast area over Long Island and New York City. The parallel track seemed to have the most potential for inland flooding during the event due to its high precipitation totals along and in close proximity to the coastline. The perpendicular and diagonal cases might see a delay in the effect on flood heights due to precipitation runoff from distant regions.

TC landfall location and angle play a significant role in modulating storm surge magnitude and inundation. Determining the storm surge sensitivity of the NJ-NY Harbor region to cyclone landfall angle, and generalizing the conclusions to other regions, is complicated due to this dependency and relation to the landfall location of the storms. The methodology presented has the ability of providing further insight into the complex dependencies of storm surge peak heights and inundation volume to landfall angle and impact area while providing a framework applicable to other regions.

3.6 Concluding Remarks

In this study, we assessed the effect of TC impact angle on the magnitude and extent of storm surge and coastal inundation along the NJ coastline. The use of the HWCM, a recently developed modeling framework based on the WRF model, was implemented to create an ensemble of cyclones approaching the NJ-NY Bight at different angles.

The results of maximum storm surge highlight the difference in surge offshore extent for each of the three directional categories studied. Results indicate a sensitivity to both cyclone approach angle and landfall location. Cyclones with a perpendicular approach angle produce more widespread offshore surge and higher peak surges and have a higher potential for inland flooding, among the categories studied. The level of storm surge sensitivity to landfall angle, however, is not uniform along the coast as some regions were shown to be vulnerable to any type of storm regardless of approach angle (e.g., southern coast of NJ).

While the physical parameters of the storms are relevant, the approach angle and landfall location play a dominant role in the resultant storm surge. These results highlight the need to further quantify the contribution of each parameter to the overall storm surge. Ongoing research focuses on determining the importance of these parameters, at various lead times, in accurately forecasting storm surge.

3.7 References

Akbar, M. K., Kanjanda, S., & Musinguzi, A. (2017). Effect of Bottom Friction, Wind Drag Coefficient, and Meteorological Forcing in Hindcast of Hurricane Rita Storm Surge Using SWAN+ ADCIRC Model. Journal of Marine Science and Engineering, 5(3), 38.

Bennett, V. C., & Mulligan, R. P. (2017). Evaluation of surface wind fields for prediction of directional ocean wave spectra during Hurricane Sandy. *Coastal Engineering, 125*, 1-15.

Bilskie, M., Hagen, S., Medeiros, S., & Passeri, D. (2014). Dynamics of sea level rise and coastal flooding on a changing landscape. *Geophysical Research Letters, 41*(3), 927-934.

Blake, E. S., Kimberlain, T. B., Berg, R. J., Cangialosi, J. P., & Beven II, J. L. (2013). Tropical cyclone report: Hurricane Sandy. National Hurricane Center, 12, 1-10.

Bloemendaal, N., Muis, S., Haarsma, R. J., Verlaan, M., Irazoqui Apecechea, M., de Moel, H., et al. (2019). Global modeling of tropical cyclone storm surges using high-

resolution forecasts. *Climate Dynamics, 52*(7), 5031-5044. https://doi.org/10.1007/s00382-018-4430-x

Booij, N., Ris, R. C., & Holthuijsen, L. H. (1999). A third-generation wave model for coastal regions: 1. Model description and validation. Journal of Geophysical Research: Oceans, 104(C4), 7649-7666.

Booth, J. F., Rieder, H., & Kushnir, Y. (2016). Comparing hurricane and extratropical storm surge for the Mid-Atlantic and Northeast Coast of the United States for 1979–2013. *Environmental Research Letters, 11*(9), 094004.

Bruyère, C. L., Done, J. M., Jaye, A. B., Holland, G. J., Buckley, B., Henderson, D., et al. (2019). Physically-Based Landfalling Tropical Cyclone Scenarios in Support of Risk Assessment. Weather and Climate Extremes. https://doi.org/10.1016/j.wace.2019.100229

Caliński, T., & Harabasz, J. (1974). A dendrite method for cluster analysis. Communications in Statistics-theory and Methods, 3(1), 1-27.

Chen, F., & Dudhia, J. (2001). Coupling an advanced land surface-hydrology model with the Penn State-NCAR MM5 modeling system. Part I: Model implementation and sensitivity. Monthly Weather Review, 129(4), 569-585. <Go to ISI>://WOS:000168253900001

Cialone, M. A., Grzegorzewski, A. S., Mark, D. J., Bryant, M. A., & Massey, T. C. (2017). Coastal-storm model development and water-level validation for the North Atlantic Coast Comprehensive Study. Journal of Waterway, Port, Coastal, and Ocean Engineering, 143(5).

Colle, B. A., Bowman, M. J., Roberts, K. J., Bowman, M. H., Flagg, C. N., Kuang, J., et al. (2015). Exploring water level sensitivity for metropolitan New York during Sandy (2012) using ensemble storm surge simulations. Journal of Marine Science and Engineering, 3(2), 428-443.

Colle, B. A., Buonaiuto, F., Bowman, M. J., Wilson, R. E., Flood, R., Hunter, R., et al. (2008). New York City's vulnerability to coastal flooding: Storm surge modeling of past cyclones. *Bulletin of the American Meteorological Society, 89*(6), 829-841.

Dietrich, J., Tanaka, S., Westerink, J., Dawson, C., Luettich, R., Zijlema, M., et al. (2012). Performance of the unstructured-mesh, SWAN+ ADCIRC model in computing hurricane waves and surge. Journal of Scientific Computing, 52(2), 468-497.

Dietrich, J., Westerink, J., Kennedy, A., Smith, J., Jensen, R., Zijlema, M., et al. (2011a). Hurricane Gustav (2008) waves and storm surge: hindcast, synoptic analysis, and validation in Southern Louisiana. Monthly Weather Review, 139(8), 2488-2522.

Dietrich, J., Zijlema, M., Westerink, J., Holthuijsen, L., Dawson, C., Luettich Jr, R., et al. (2011b). Modeling hurricane waves and storm surge using integrally-coupled, scalable computations. Coastal Engineering, 58(1), 45-65.

FEMA. (2011). Redefinition of the Coastal Flood Hazard Zones in FEMA Region II: Analysis of the Coastal Storm Surge Flood Frequencies. In: Federal Emergency Management Agency.

FEMA. (2014a). Region II Storm Surge Project: Mesh Development. Washington, DC.

FEMA. (2014b). Region II Storm Surge Project: Model Calibration and Validation. Washington, DC.

Fossell, K. R., Ahijevych, D., Morss, R. E., Snyder, C., & Davis, C. (2017). The Practical Predictability of Storm Tide from Tropical Cyclones in the Gulf of Mexico. *Monthly Weather Review, 145*(12), 5103-5121.

Galarneau, T. J., Davis, C. A., & Shapiro, M. A. (2013). Intensification of Hurricane Sandy (2012) through extratropical warm core seclusion. *Monthly Weather Review, 141*(12), 4296-4321.

Garratt, J. (1977). Review of drag coefficients over oceans and continents. *Monthly weather review, 105*(7), 915-929.

Gonzalez, V. M., Nadal-Caraballo, N. C., Melby, J. A., & Cialone, M. A. (2019). Quantification of Uncertainty in Probabilistic Storm Surge Models: Literature Review. Retrieved from: https://apps.dtic.mil/dtic/tr/fulltext/u2/1067548.pdf

Hall, T. M., & Sobel, A. H. (2013). On the impact angle of Hurricane Sandy's New Jersey landfall. Geophysical Research Letters, 40(10), 2312-2315. Article. <Go to ISI>://WOS:000328840200076

Holland, G. J. (1980). An analytic model of the wind and pressure profiles in hurricanes. *Monthly weather review, 108*(8), 1212-1218.

Hong, S.-Y., & Lim, J.-O. J. (2006). The WRF single-moment 6-class microphysics scheme (WSM6). J. Korean Meteor. Soc, 42(2), 129-151.

Hong, S.-Y., Noh, Y., & Dudhia, J. (2006). A new vertical diffusion package with an explicit treatment of entrainment processes. Monthly Weather Review, 134(9), 2318-2341.

Hussain, M. A., Tajima, Y., Hossain, M. A., & Das, P. (2017). Impact of Cyclone Track Features and Tidal Phase Shift upon Surge Characteristics in the Bay of Bengal along the Bangladesh Coast. Journal of Marine Science and Engineering, 5(4), 52. http://www.mdpi.com/2077-1312/5/4/52

Iacono, M. J., Delamere, J. S., Mlawer, E. J., Shephard, M. W., Clough, S. A., & Collins, W. D. (2008). Radiative forcing by long-lived greenhouse gases: Calculations with the AER radiative transfer models. Journal of Geophysical Research: Atmospheres, 113(D13).

Irish, J. L., Resio, D. T., & Ratcliff, J. J. (2008). The influence of storm size on hurricane surge. Journal of Physical Oceanography, 38(9), 2003-2013. Article.

Jelesnianski, C. P., Chen, J., & Shaffer, W. A. (1992). SLOSH: Sea, lake, and overland surges from hurricanes.

Kalnay, E., Kanamitsu, M., Kistler, R., Collins, W., Deaven, D., Gandin, L., et al. (1996). The NCEP/NCAR 40-year reanalysis project. Bulletin of the American meteorological Society, 77(3), 437-472.

Kaplan, J., & DeMaria, M. (2003). Large-Scale Characteristics of Rapidly Intensifying Tropical Cyclones in the North Atlantic Basin. Weather and Forecasting, 18(6), 1093-1108.

Kimball, S. K. (2008). Structure and evolution of rainfall in numerically simulated landfalling hurricanes. *Monthly Weather Review, 136*(10), 3822-3847.

Kohno, N., Dube, S., K., Entel, M., Fakhruddin, S., H. M., Greenslade, D., Leroux, M.-D., et al. (2018). Recent progress in storm surge forecasting. Tropical Cyclone Research and Review, 7(2), 128-139. https://hal.archives-ouvertes.fr/hal-01727930

Lakshmi, D. D., Murty, P., Bhaskaran, P. K., Sahoo, B., Kumar, T. S., Shenoi, S., & Srikanth, A. (2017). Performance of WRF-ARW winds on computed storm surge using hydodynamic model for Phailin and Hudhud cyclones. *Ocean Engineering, 131*, 135-148.

Landsea, C., Franklin, J., & Beven, J. (2015). The revised Atlantic hurricane database (HURDAT2). United States National Oceanic and Atmospheric Administration's National Weather Service.[Available at http://www. nhc. noaa. gov/data/hurdat/hurdat2-format-atlantic. pdf.].

Li, Y., Cheung, K. K., & Chan, J. C. (2015). Modelling the effects of land–sea contrast on tropical cyclone precipitation under environmental vertical wind shear. Quarterly Journal of the Royal Meteorological Society, 141(687), 396-412.

Lin, N., & Chavas, D. (2012). On hurricane parametric wind and applications in storm surge modeling. *Journal of Geophysical Research: Atmospheres, 117*(D9). https://agupubs.onlinelibrary.wiley.com/doi/abs/10.1029/2011JD017126

Lin, N., Emanuel, K., Oppenheimer, M., & Vanmarcke, E. (2012). Physically based assessment of hurricane surge threat under climate change. Nature Climate Change, 2(6), 462-467. Article.

Lin, N., Emanuel, K. A., Smith, J., & Vanmarcke, E. (2010). Risk assessment of hurricane storm surge for New York City. Journal of Geophysical Research: Atmospheres, 115(D18).

Lin, N., Marsooli, R., & Colle, B. A. (2019). Storm surge return levels induced by mid-to-late-twenty-first-century extratropical cyclones in the Northeastern United States. *Climatic Change, 154*(1-2), 143-158.

Luettich, R., & Westerink, J. (2004). Formulation and Numerical Implementation of the 2D/3D ADCIRC Finite Element Model Version 44.XX. Retrieved from Chapel Hill, NC: http://www.unc.edu/ims/adcirc/adcirc_theory_2004_12_08.pdf

Luettich, R. A., Westerink, J. J., & Scheffner, N. W. (1992). ADCIRC: An Advanced Three-Dimensional Circulation Model for Shelves, Coasts, and Estuaries. Report 1. Theory and Methodology of ADCIRC-2DDI and ADCIRC-3DL. In Dredging Research Program Technical Report DRP-92-6 (pp. 137). Vicksburg, MS: COASTAL ENGINEERING RESEARCH CENTER.

Marsooli, R., & Lin, N. (2018). Numerical Modeling of Historical Storm Tides and Waves and Their Interactions Along the US East and Gulf Coasts. Journal of Geophysical Research: Oceans.

Mayo, T., & Lin, N. (2019). The Effect of the Surface Wind Field Representation in the Operational Storm Surge Model of the National Hurricane Center. Atmosphere, 10(4), 193. http://www.mdpi.com/2073-4433/10/4/193

Mori, N., Kato, M., Kim, S., Mase, H., Shibutani, Y., Takemi, T., et al. (2014). Local amplification of storm surge by Super Typhoon Haiyan in Leyte Gulf. *Geophysical research letters, 41*(14), 5106-5113.

Needham, H. F., Keim, B. D., & Sathiaraj, D. (2015). A review of tropical cyclone-generated storm surges: Global data sources, observations, and impacts. Reviews of Geophysics, 53(2), 545-591.

NOAA/NOS/CO-OPS. Tides and Currents. Retrieved from https://tidesandcurrents.noaa.gov

Orton, P., Vinogradov, S., Georgas, N., Blumberg, A., Lin, N., Gornitz, V., et al. (2015). New York City panel on climate change 2015 report chapter 4: dynamic coastal flood modeling. Annals of the New York Academy of Sciences, 1336(1), 56-66.

Peckham, S. E., Smirnova, T. G., Benjamin, S. G., Brown, J. M., & Kenyon, J. S. (2016). Implementation of a Digital Filter Initialization in the WRF Model and Its Application in the Rapid Refresh. Monthly Weather Review, 144(1), 99-106. https://journals.ametsoc.org/doi/abs/10.1175/MWR-D-15-0219.1

Quiring, S., Schumacher, A., Labosier, C., & Zhu, L. (2011). Variations in mean annual tropical cyclone size in the Atlantic. Journal of Geophysical Research: Atmospheres, 116(D9).

Ramos, A. (2019). Effect of Tropical Cyclone Landfall Angle on Storm Surge. DesignSafe-CI. https://doi.org/10.17603/ds2-9f5y-t459

Ramos-Valle, A., Curchitser, E., Bruyère, C., & Fossell, K. (2018). Simulating Storm Surge Impacts with a Coupled Atmosphere-Inundation Model with Varying Meteorological Forcing. Journal of Marine Science and Engineering, 6(2), 35. http://www.mdpi.com/2077-1312/6/2/35

Rego, J. L., & Li, C. (2009). On the importance of the forward speed of hurricanes in storm surge forecasting: A numerical study. Geophysical Research Letters, 36(7). https://agupubs.onlinelibrary.wiley.com/doi/abs/10.1029/2008GL036953

Rotunno, R., Chen, Y., Wang, W., Davis, C., Dudhia, J., & Holland, G. (2009). Large-eddy simulation of an idealized tropical cyclone. Bulletin of the American Meteorological Society, 90(12), 1783-1788.

Rotunno, R., & Emanuel, K. A. (1987). An Air–Sea Interaction Theory for Tropical Cyclones. Part II: Evolutionary Study Using a Nonhydrostatic Axisymmetric Numerical Model. *Journal of the Atmospheric Sciences, 44*(3), 542-561.

Skamarock, W., Klemp, J., Dudhia, J., Gill, D., Barker, D., Duda, M., et al. (2008). A description of the Advanced Research WRF Version 3, NCAR technical note, Mesoscale and Microscale Meteorology Division. National Center for Atmospheric Research, Boulder, Colorado, USA.

Smith, A. B., & Katz, R. W. (2013). US billion-dollar weather and climate disasters: data sources, trends, accuracy and biases | SpringerLink. Natural Hazards. http://link.springer.com/article/10.1007/s11069-013-0566-5

Thomas, A., Dietrich, J., Asher, T., Bell, M., Blanton, B., Copeland, J., et al. (2019). Influence of storm timing and forward speed on tides and storm surge during Hurricane Matthew. Ocean Modelling, 137, 1 - 19. http://www.sciencedirect.com/science/article/pii/S1463500318302609

Tiedtke, M. (1989). A comprehensive mass flux scheme for cumulus parameterization in large-scale models. Monthly Weather Review, 117(8), 1779-1800.

Torres, M. J., Reza Hashemi, M., Hayward, S., Spaulding, M., Ginis, I., & Grilli, S. T. (2018). Role of Hurricane Wind Models in Accurate Simulation of Storm Surge and Waves. *Journal of Waterway, Port, Coastal, and Ocean Engineering, 145*(1), 04018039.

Weisberg, R. H., & Zheng, L. (2006). Hurricane storm surge simulations for Tampa Bay. Estuaries and Coasts, 29(6), 899-913.

Yin, J., Lin, N., & Yu, D. P. (2016). Coupled modeling of storm surge and coastal inundation: A case study in New York City during Hurricane Sandy. Water Resources Research, 52(11), 8685-8699. <Go to ISI>://WOS:000393318600017

CHAPTER 4: IMPLEMENTATION OF AN ARTIFICIAL NEURAL NETWORK FOR STORM SURGE FORECASTING

4.1 Abstract

Accurate and timely storm surge forecasts are essential during tropical cyclone events in order to assess the magnitude and location of the storm surge impacts. Numerical weather prediction models provide accurate input data to drive storm surges in hydrodynamic models but are too computationally expensive to be run for real-time forecasting purposes. Therefore, real-time forecasting of storm surge impacts is usually conducted by means of a parametric vortex model, implemented within a hydrodynamic model, which decreases computational time at the expense of increased uncertainty. Recently, data-driven artificial neural networks are being implemented as an alternative due to their efficiency and high accuracy. This work seeks to examine how an artificial neural network can be informed to make accurate storm surge predictions. This work is thus concerned with determining the parameters needed to successfully implement a neural network model for the Mid-Atlantic Bight region. The neural network model was trained with modeled data resulting from coupling of the Hybrid WRF cyclone model (HWCM) and the Advanced Circulation Model (ADCIRC). An ensemble of synthetic, but physically plausible, cyclones was simulated using the Hybrid WRF cyclone model, and used as input for the hydrodynamic model. Tests of the artificial neural network were conducted to investigate the optimal lead-time configuration of the input data and the neural network architecture needed to minimize storm surge forecast errors. Results highlight the efficiency and accuracy of the neural network in forecasting moderate storm

surge levels, while indicating a deficiency in capturing the magnitude of the peak-values. Analysis of the feature importance ranked the cyclone minimum pressure and location as the most relevant variables for storm surge assessment.

4.2 Introduction

Recent tropical cyclone (TC) events have highlighted that TCs continue to be one of the most impactful natural phenomena in terms of loss of life and property- with storm surge as the primary cause of the fatalities resulting from TCs (Rappaport, 2014). The devasting nature of these events calls for timely and accurate inundation forecasts to ensure public safety. Emergency managers require information on the expected magnitude and the potential inundation area to make decisions on evacuation and planning for emergency response before, during and in the aftermath of a TC event.

Storm surge forecasting is challenging as it relies on the accuracy of the available meteorological data and can be a computationally intensive process (Elko et al., 2019; Mosavi et al., 2018). For real-time storm surge forecasting parametric wind models, such as the Holland model (Holland, 1980), are often used for their computational efficiency. These models use a set of track-based cyclone parameters to characterize the cyclone wind field. Despite the computational efficiency of parametric models, full-physics models have been shown to be more reliable than these in accurately forecasting a TC's wind field extent (Bennett & Mulligan, 2017; Ramos-Valle et al., 2018).

The use of machine learning (ML) methods applied to flood forecasting problems has been increasing in recent years (Mosavi et al., 2018). ML methods have been shown to be suitable for this type of application, achieving higher accuracy than the traditional

forecasting methods mentioned previously (Mosavi et al., 2018). Machine learning techniques, such as artificial neural networks (ANNs), provide a framework to obtain timely forecasts by training the network with a simulated or observed dataset. ANNs determine the non-linear and complex relationships between the parameters used for forecasting of a target variable. A more detailed description of ANNs is provided in section 4.3.

ANNs are commonly used for storm surge and flood forecasting, including forecasting of peak surges as well as time series (Kim et al., 2015; Mosavi et al., 2018). Hashemi et al. (2016) successfully developed an ANN model for Rhode Island based on a set of combined synthetic and historical cyclones with a root-mean-squared error of 35 cm. A neural network was also developed and implemented to forecast storm surge time series at stations around the Louisiana coast based on data from over 400 synthetic cyclones (Kim et al., 2015). Similarly, Wang et al. (2016) trained an ANN with atmospheric data from 153 synthetic cyclones to forecast storm surge along the Louisiana coast.

As a data-driven method, ANNs are able to produce forecasts without the need for knowledge of the underlying physical processes (Mosavi et al., 2018). However, after training, ANNs can shed light into the relationship between the variables used for training, often referred to as the input features, and the target variable. Commonly, for storm surge forecasting the input features are parameters that characterize the TCs including their intensity, size and location. Some studies also include atmospheric data recorded at the different stations in the training dataset (Tseng et al., 2007). These variables are used

to forecast the target variable, which for storm surge forecasting purposes is often the peak water levels or water level timeseries at a single or multiple locations.

Storm surge magnitude has been shown to be a function of various TC characteristics and physical parameters, including the cyclone intensity (Weisberg & Zheng, 2006), size (Irish et al., 2008), and forward speed (Hussain et al., 2017; Rego & Li, 2009; Thomas et al., 2019). Recent studies have also shown the dependency of storm surge on cyclone landfall angle and impact location (Bloemendaal et al., 2019; Ramos-Valle et al., 2020). Results from Ramos-Valle et al. (2020) highlighted the sensitivity of storm surge to cyclone landfall location and prompted questions such as: (i) What variables contribute the most to the resulting storm surge? (ii) What is the relative importance of each cyclone parameter in determining storm surge?

In this study, we determine the parameters and data needed to develop an ANN for the Mid-Atlantic Bight region. Furthermore, we implement an ANN that can successfully predict storm surge, on a testing dataset, with the goal of retrieving information that allows us to address the questions posed regarding the significance and relationships between the input variables.

An overview of artificial neural networks and the data used for training is provided in section 4.3. Results on the optimal architecture required to develop an ANN model, the evaluation of the ANN model configuration and the analysis of the input features are presented in sections 4.4. A discussion of the results is provided in section 4.5, followed by a summary of the study in section 4.6.

4.3 Data and Methods

An artificial neural network model is developed and used to accurately predict storm surge time series and understand the contribution of various TC parameters in forecasting storm surge. In this section, we briefly describe the atmospheric and hydrodynamic datasets used to train the ANN model. The datasets are publicly available through the DesignSafe-CI repository (Ramos, 2019). We also discuss the design of the ANN model, the metrics used to evaluate the storm surge predictions, and the methods used to analyze the individual contributions of the input variables in accurately forecasting storm surge.

4.3.1 Data

4.3.1.1 Synthetic Tropical Cyclones

Data from a pre-computed set of synthetic cyclones is used as input to the ANN. Simulations of tropical cyclones were conducted with the HWCM; an extension of the WRF model which enables the simulation of synthetic cyclones in a real-world environment. This hybrid approach provides the benefit of modeling physically plausible storm scenarios that have not been observed previously. Bruyère et al. (2019) provides an in-depth description and evaluation of the HWCM model setup. A description of the simulation configuration is available in Chapter 3 and published in Ramos-Valle et al. (2020).

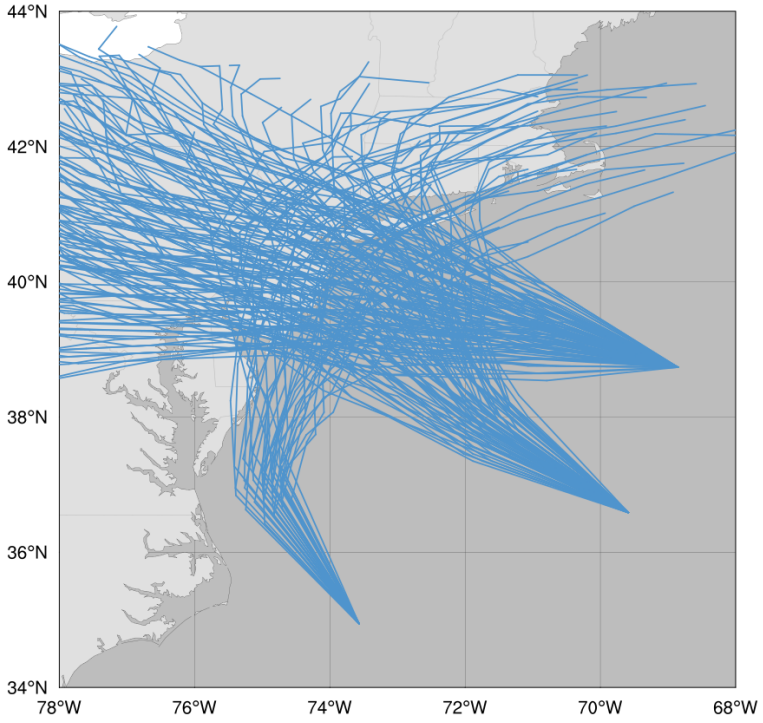

Figure 4-1. Tracks for the 198 synthetic cyclones used for training and testing of the ANN. These cyclones were simulated with the HWCM model (Ramos-Valle et al., 2020).

The atmospheric dataset consists of 198 synthetic cyclones impacting the New Jersey (NJ) and New York (NY) coastlines as depicted in Figure 4-1. Data for the TC's location, maximum wind speed, minimum pressure, radius of maximum wind and translation speed is available in a track-based format at an hourly-timestep for a length of four days. However, for the purposes of this study only 72 hours of data are used, since after the third day the cyclones are far inland, and no longer influence the water levels near the coast.

4.3.1.2. Storm Surge Simulations

In Ramos-Valle et al. (2020), storm surge impacts from the synthetic storms were assessed by using the two-dimensional depth integrated (2DDI) implementation of the

ADCIRC hydrodynamic model (Luettich & Westerink, 2004; Luettich et al., 1992), coupled with the Simulating Waves Nearshore (SWAN; Booij et al., 1999) wave model (SWAN+ADCIRC). The 10-m winds and surface pressure fields obtained from the HWCM simulated TC were used as atmospheric forcing to the hydrodynamic and wave models.

The target data used in the ANN is provided in terms of storm surge time series at an hourly time step at multiple station locations (Figure 4-2): Atlantic City, Sandy Hook, The Battery, Orient Harbor and Montauk (NOAA/NOS/CO-OPS).

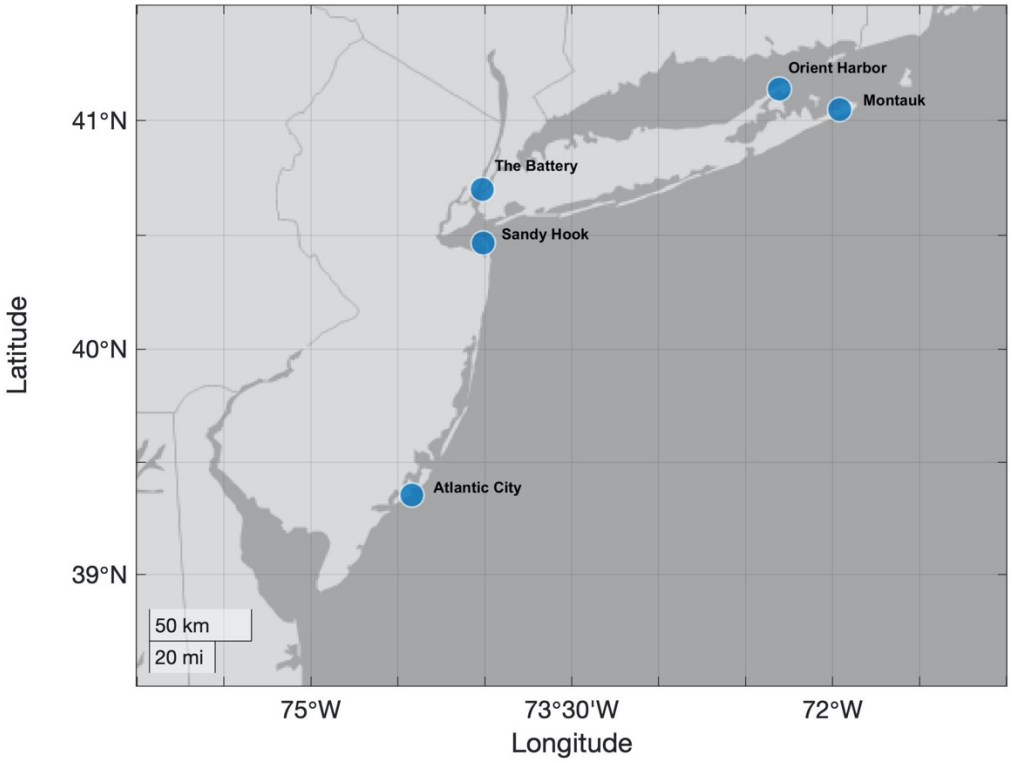

Figure 4-2. Region of study. The location of the stations examined in this study are highlighted. The ANN model is trained with storm surge levels at these five stations.

4.3.2 ANN Model Architecture

ANNs are classified as a supervised machine learning technique, in which both input and outputs are provided allowing the model to learn and determine the relationships between them. The ANN architecture is comprised of multiple layers: an input layer, a variable number of intermediate layers, known as hidden layers, and an output layer. The ANN implemented is a feedforward model in which the flow of information is in one direction, from the input to the output layer (Figure 4-3), such that a given layer receives information from the preceding layer. The input layer consists of a set of neurons representing the input variables. The output layer receives the data from the previous hidden layer and transforms them into output values. Computations and learning are carried out in the neurons of the hidden layers, where each neuron transforms the values from the previous layers. Each layer in the ANN is expressed as:

$$N = b_0 + \sum_{j=1}^{n} x_j^{in} w_j \quad (1)$$

$$x^{out} = f(N), \quad (2)$$

where x^{in} and x^{out} are the input and output data of the neurons, and N represents the input to the activation function. Each neuron calculates the weighted sum of its inputs and applies an activation function, f. The weights and the bias are given by w and b_0, respectively. The activation function is used to map the numerical value of a neuron, as it converts an input signal into an output. Common activation functions employed for ANNs are Sigmoid, Log-Sigmoid, Hyperbolic-Tangent, and Rectified Linear Units (ReLU). The activation function must be nonlinear for the ANN model to learn beyond linear relationships (McGovern et al., 2019).

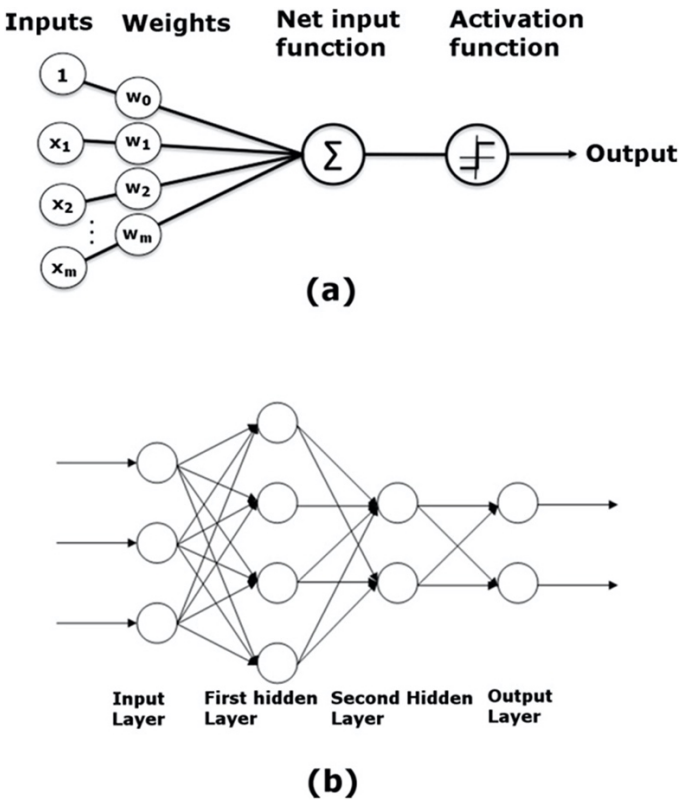

Figure 4-3. (a) Schematic of the architecture of a simple ANN with a single hidden layer. The input and their associated weights are combined into a net input function, as represented in Equation 1, and passed through the activation function to produce an output (Equation 2). (b) Schematic of an ANN with two hidden layers and multi-dimensional output as implemented in the current study. Source: Sahoo and Bhaskaran (2019).

Initially, the weights in the network are assigned a random value. The ANN model seeks to minimize the loss function between the model prediction and the observed values. The training process is then an optimization problem to determine the set of

weights that best describes the relationship between the input and output. The weights are updated by the process of backpropagation- which terminates when the loss is below a certain threshold or after a predefined number of iterations or epochs is reached. In the present study the number of epochs, or maximum training iterations, was set to 1000 and the tolerance for optimization was set to 0.0001.

The ANN presented in this study was implemented through the Scikit-Learn software in Python (Pedregosa et al., 2011). The input layer of the ANN model consisted of six input parameters related to the physical characteristics of the synthetic cyclones including the maximum wind speed, minimum pressure, radius of maximum winds, translation speed, and position as given by the latitude and longitude. The input parameters for each storm are provided as time series throughout the cyclone's lifetime. Each synthetic cyclone simulation consisted of 72 timesteps at an interval of 1 hour. The ANN model implemented is defined as multi-output since the model is designed to provide predictions at multiple station locations. The ANN model outputs the predicted storm surge at five station locations along the NJ and NY coastlines (Figure 4-2): Atlantic City (NJ), Sandy Hook (NJ), The Battery (NY), Orient Harbor (NY) and Montauk (NY).

The input and output data were randomly divided into 75% for training and 25% for testing. Additionally, the ANN algorithm used sets aside 10% of the training data for validation purposes. The distribution of the input parameters for the TC cases used for the training process in the ANN are shown in Figure 4-4. The distributions show a broad range for each of the input variables related to TCs. This is an optimal configuration as the ANN model can only make skillful predictions for cases that fall within the distribution of

the training data. The spatial coverage is broad ranging from about 35.9°N to 45°N latitude and expanding as far as -65.8°W. The maximum wind speed for the cyclones in the training set corresponds to intensities of tropical storms to Category-2, with the majority corresponding to Category-1 intensities, consistent with the historical record of observed TCs in the region of study (Marsooli & Lin, 2018).

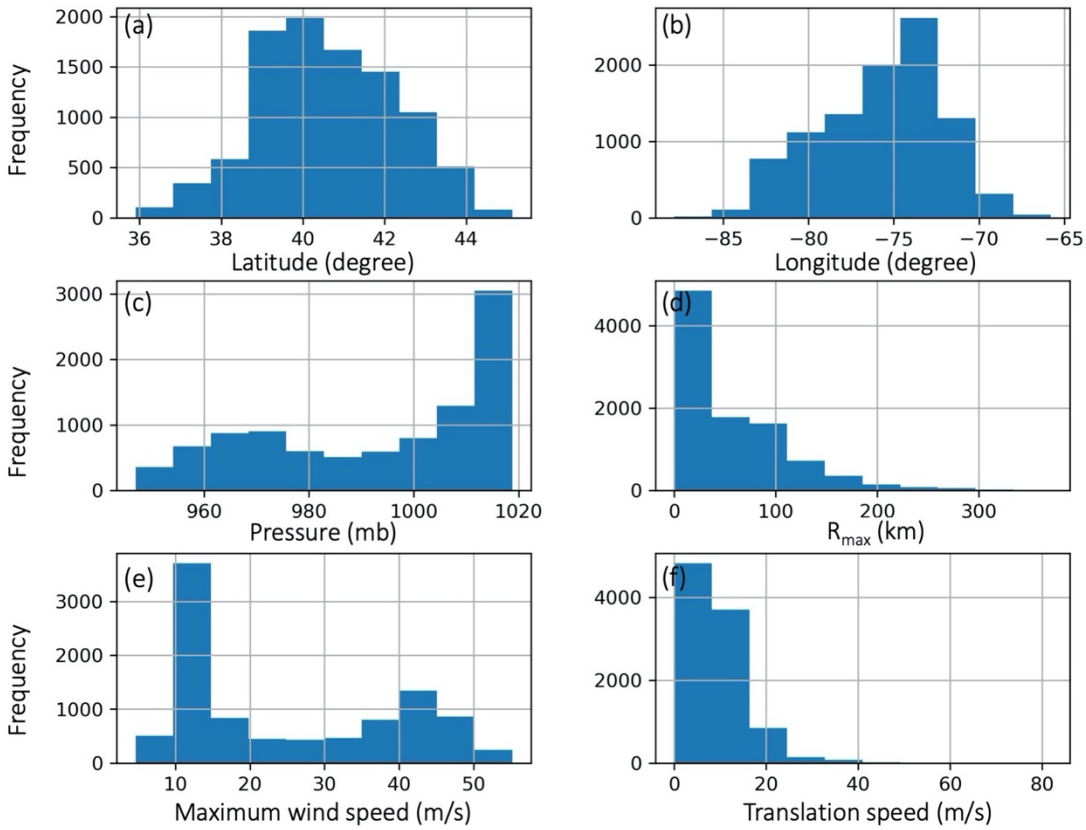

Figure 4-4. Distribution of various TC parameters for the 149 TCs used for training.

A k-fold cross-validation analysis was performed to determine the best set of additional hyperparameters (i.e., ANN model properties that control the training process) needed for the ANN, including the number of hidden layers and the number of neurons within each of these, the type of activation function and the type of learning rate used. A

10-fold cross validation was implemented in this case. The process consisted of splitting the training data into k=10 smaller subsets. The ANN model was then trained with k-1 folds and validated on the remaining set of the data. The cross-validation is an iterative process as it trains and validates models with a given set of hyperparameter settings. The model performance measure is then an average across all the k-fold trainings. The output from the cross-validation provides the best set of hyperparameters to use for the given dataset. In this study, we also tested the predictability of the data at various lead times including: no lag, 1-, 2-, 3-, 6- and 12-hr lead times. Six individual cross validations were carried out to test each of these configurations for the best hyperparameter settings.

Once the hyperparameters were selected, based on the error metrics, the best model from the six configurations was selected for further analysis. The ANN storm surge predictions for the test data were analyzed and compared to the hydrodynamic model predictions. Additionally, the importance and contribution of the individual input variables in accurately predicting storm surge was assessed.

4.3.3 Performance Metrics

The model performance is evaluated with the test data according to the mean squared error (MSE) in equation (3) and the correlation coefficient (R) in equation (4).

$$MSE = \frac{1}{N}\sum_{i=1}^{N}(y - \hat{y})^2 \quad (3)$$

$$R = \frac{N(\sum y\hat{y}) - (\sum y)(\sum \hat{y})}{\sqrt{[N\sum y^2 - (\sum y)^2][N\sum \hat{y}^2 - (\sum \hat{y})^2]}} \quad (4)$$

In equations (3) and (4), y and $\hat{y}$ represent the predicted and observed values, respectively. The optimal model will have MSE = 0 and R = 1. Additionally, the root-mean-squared error (RMSE = $\sqrt{MSE}$) is also used to describe the model performance.

4.3.4 Metrics for ANN Model Interpretation

One of the purposes of this study in designing and implementing an ANN is to interpret the relation between the input and output variables, which in this case are the TC parameters and storm surge levels. There are various interpretation and analysis methods available that provide a better intuition of the model structure such as the partial dependence plots (Friedman, 2001) and permutation feature importance (Breiman, 2001), which are employed in this work and described below.

4.3.4.1 Permutation Feature Importance

A key question that can be addressed by interpreting machine learning methods is: which input variable has the largest impact on the model predictions? The permutation feature importance method is an approach to rank the importance of the predictors used as input to the machine learning model (McGovern et al., 2019). It provides insight into how the model relies on each input feature to make its predictions. The method consists of randomly permuting the values of an input variable and evaluating how the model performance deteriorates when new predictions are made based on the permuted data compared to the unpermuted data. Larger errors indicate a higher importance of the variable in question.

An alternative to determining feature importance would be to remove a variable altogether, retrain the model with the remaining features and calculate the average loss.

However, by implementing this approach we would be creating individual ANN models and the loss comparison will not be made on the same model. An advantage of the permutation method is that it does not require the model to be retrained and it allows for comparison to be made on the same model estimator.

4.3.4.2 Partial dependence plots

The partial dependence indicates the average prediction for each possible value of the input variables. As such, it demonstrates the effect one or more input variables have on the machine learning model predictions. As their name suggests, PDPs depict how the predictions partially depend on the individual input features, showing whether the relation between them is linear or more complex.

4.4 Results

4.4.1 Test for Model Predictability at Various Lead Times

The 10-fold cross-validation was performed to determine the best set of hyperparameters to use in the ANN. The cross-validation process was repeated for different configurations of lead-times to assess the ANN model predictability. Table 4-1 presents the model hidden layer configuration that resulted in the lowest MSE for each of the lead-time configurations tested. Results from the cross-validation showed an agreement on three out of the four hyperparameters tested: the number of hidden layers, the activation function and the type of learning rate. The cross-validation results coincided on the use of a neural network with two hidden layers, on the use of the ReLU activation function and a constant learning rate set at 0.001. The hyperparameter that changed when testing for different lead times was the number of neurons in each of the

hidden layers, as shown in Table 4-1. Results do not indicate any clear pattern as to the change in number of neurons with increasing lead times.

Table 4-1 shows the mean squared error and the correlation at the five stations for each of the model configurations. The error is comparable for up to 3-hour lead time and increase for 6- and 12-hour lead time, respectively. The correlations are significant at all the stations and for the six different configurations. Only model 6, with lead time of 12 hours, has correlations below 0.90. There is not a notable difference in correlation between the different stations. On average, the Sandy Hook stations has the highest correlation of 0.95 for the configurations tested, while the Atlantic City station has the lowest of 0.94.

Table 4-1. Performance of the ANN Models Including MSE and Pearson Correlation Coefficient.

Model #	**(N_1, N_2)**	**Lead Time (hr)**	**MSE**	**R** Atlantic City	**R** Sandy Hook	**R** The Battery	**R** Orient Harbor	**R** Montauk
1	(140, 120)	0	0.007	0.95	0.96	0.95	0.94	0.94
2	(160, 100)	1	0.007	0.95	0.96	0.95	0.94	0.95
3	(100, 200)	2	0.007	0.96	0.96	0.96	0.96	0.96
4	(50, 200)	3	0.007	0.95	0.96	0.96	0.96	0.96
5	(160, 80)	6	0.009	0.93	0.94	0.94	0.96	0.95
6	(160, 140)	12	0.016	0.89	0.89	0.89	0.89	0.90

The Taylor Diagram (Taylor, 2001) in Figure 4-5 is used to compare the performance of the six models and select the most accurate model configuration. In this case, the correlation is presented for all the data in the test set. The majority of the models cluster close to each other, except for model 6 with 12-hour lead time. Model 3,

with 2-hour lead time was chosen as the most accurate model, with the highest correlation, and used for further testing. This model had the lowest MSE when tested with 100 and 200 neurons in the first and second hidden layers, respectively.

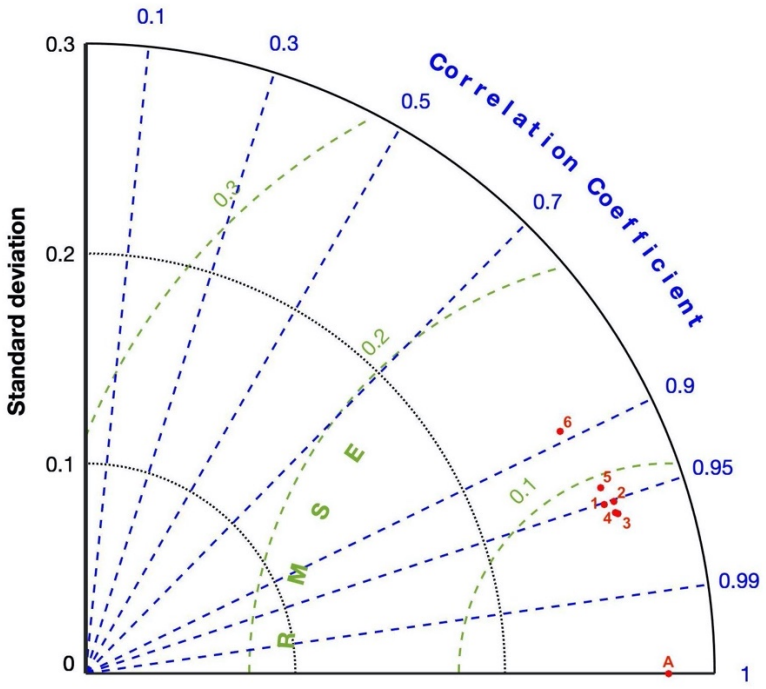

Figure 4-5. Taylor diagram showing relative performance of each ANN models in Table 4-1. Point A denotes the target model.

4.4.2 Storm Surge Forecast

Model 3 exhibited the highest average performance among the lead-time configurations tested. Figure 4-6 depicts the model performance at the five stations studied, comparing the ADCIRC predicted storm surge values against the predictions made by the ANN model 3. The identity line and the best fit of the data are plotted for reference. Results highlight the ANN model accuracy in predicting the water levels, with low MSE values and a significant correlation between the datasets. The correlation

coefficient is 0.96 for all the stations. The MSE varies from 0.003 to 0.009 for Montauk and Sandy Hook stations, respectively. This is equivalent to a storm surge error of 0.05 to 0.09 m.

The best fit line and the identity line are in close approximation to each other, pointing to the ANN model accuracy. However, one noticeable aspect that appears at all five stations is the slight underestimation of the ANN predicted water levels for the highest observed values. This behavior is not exclusive of the ANN model 3, as the pattern was observed for the other models tested (not shown).

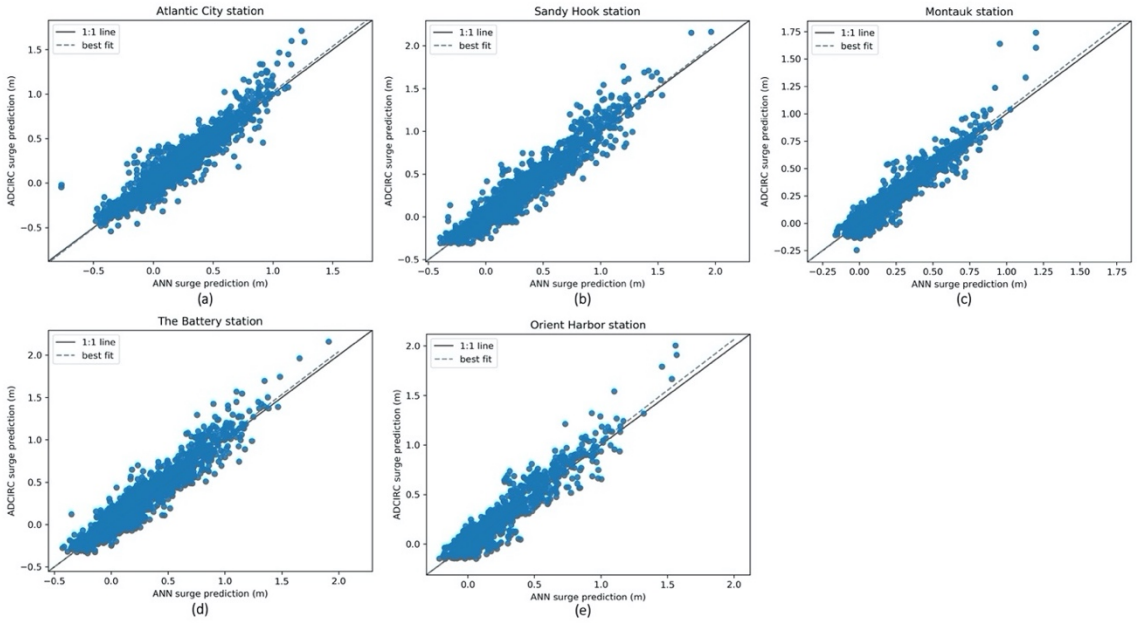

Figure 4-6. Scatter plots showing the ADCIRC model predictions vs the ANN model predictions. The dataset presented included every time step of the 49 cases in the testing set (N = 3,528 data points). The best fit line (dashed gray line) and the identity line (solid gray line) are plotted for reference.

We further investigated the ANN model performance by evaluating the storm surge time series forecast for the TCs used in the testing phase of the ANN. Figure 4-7 depicts the time series prediction by the ANN compared to the target ADCIRC simulated time series for one of the cases. As was observed in Figure 4-6, the ANN model underpredicts the peak values. In this case, the underprediction is about 0.10 to 0.15 m at the stations studied. However, the ANN predictions follow the general behavior and storm surge patterns. The ANN model can accurately capture the rise and consequent decline in water level as the storm moves through the area. It is also able to capture the behavior of double peaks observed at the Atlantic City station (Figure 4-7a).

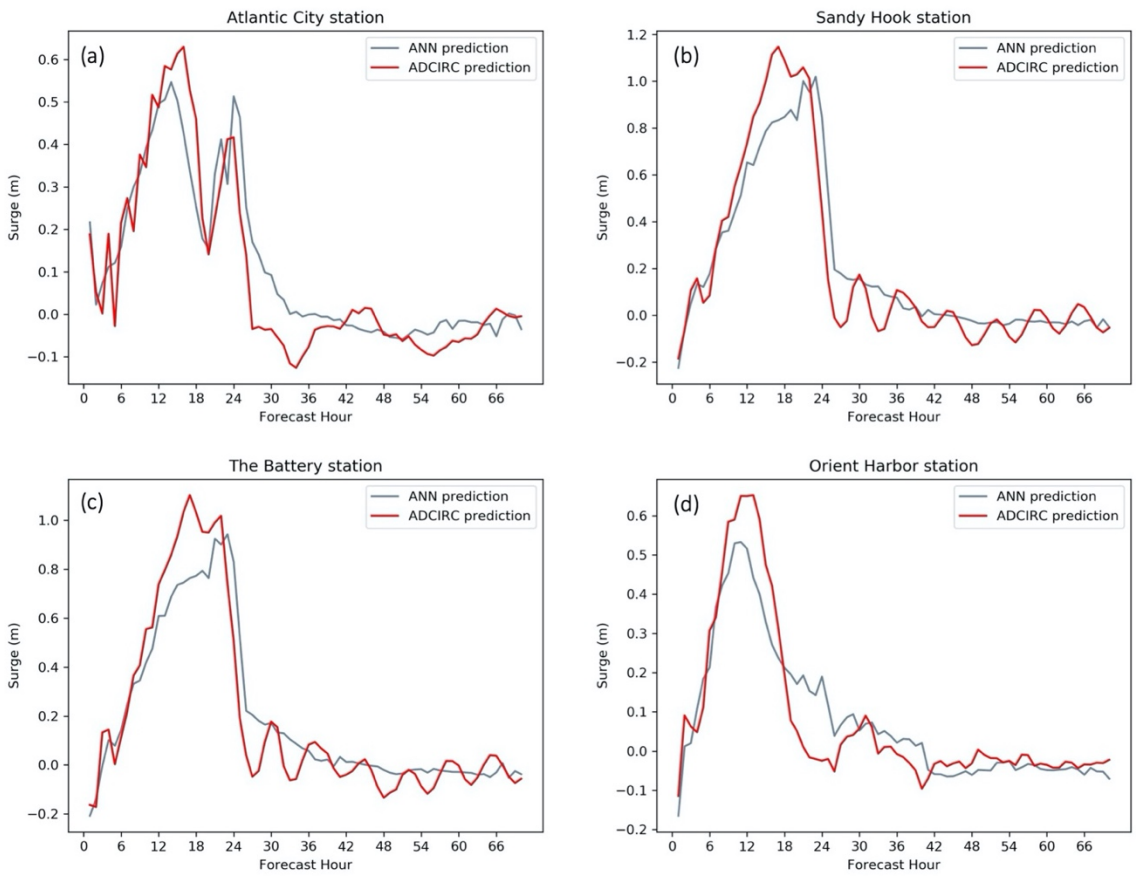

Figure 4-7. Storm surge time series for one of the TC test cases. The ANN storm surge time series prediction is compared to the verification data, the ADCIRC model predication, at (a) Atlantic City, (b) Sandy Hook, (c) The Battery, and (d) Orient Harbor stations.

4.4.3 Feature Importance

The ANN model was also used to determine the importance of the input variables in forecasting storm surge. The feature permutation importance analysis provides information as to the input variables that are most relevant. A guiding question to interpret the results of the permutation test is: How does the MSE change if we shuffle or randomize a given input variable? Results indicate that randomly permuting the values of minimum pressure produces the largest error of approximately 0.45 m (Figure 4-8),

pointing to its importance in assessing storm surge. The position of the cyclone, as given by its latitude and longitude rank second and third positions, respectively. Randomly perturbing the translation speed produced the lowest error of 0.10 m.

The permutation method does not account for correlations between the input variables, and as such can attribute a higher importance to one of the correlated features over the other. Figure 4-9 depicts a heatmap of the Pearson correlation coefficients between the input variables. The most significant correlation is between the cyclone minimum pressure and the maximum wind speed, which are negatively correlated, with a Pearson correlation coefficient of -0.98. This is an expected relation due to the known link between wind speed and minimum pressure. Another relevant relationship is the correlation between minimum pressure and the position of the cyclone as given by the latitude and longitude. For the input dataset this translates to weakening storms as they approach the coast and move northward.

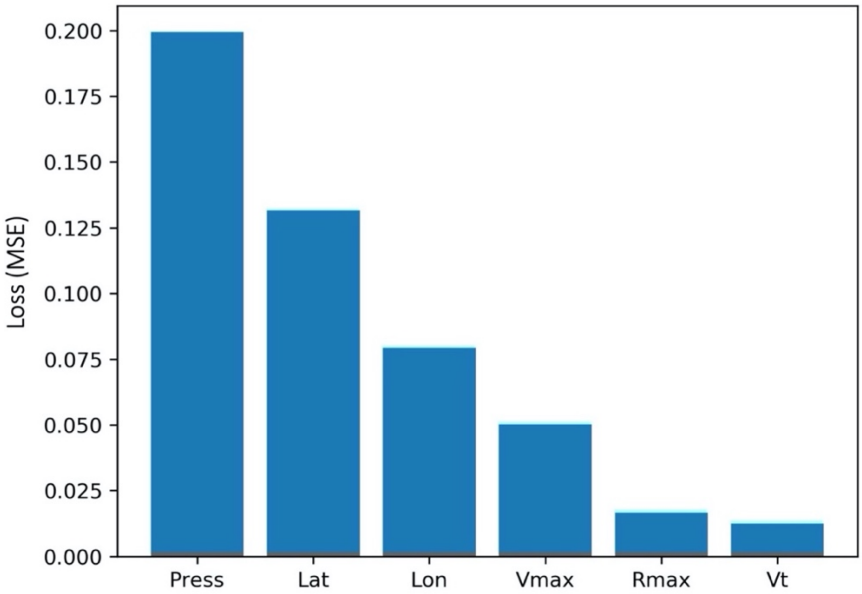

Figure 4-8. Feature permutation importance as given by the MSE loss function. The input variables are sorted in decreasing order of importance.

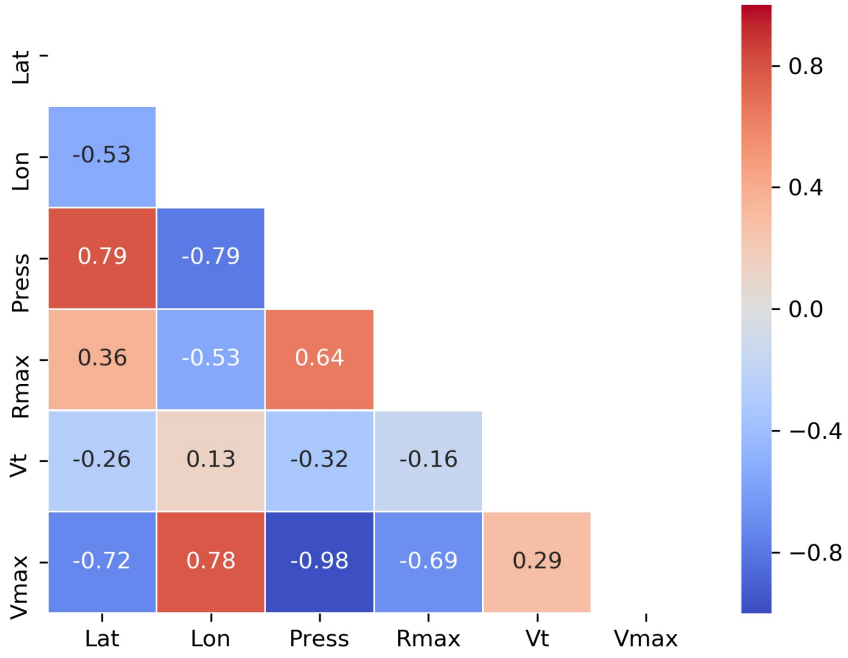

Figure 4-9. Correlation matrix between the input variables used in the ANN.

Another important relation to consider in assessing the results of the ANN is how the model predictions depend on a single input variable. The partial dependence provides further intuition into how and why each variable is important. The partial dependence of each variable corresponds to the average response of the model for each possible value of the input feature. The partial dependence plots in Figure 4-10 and Figure 4-11 depict these relationships at The Battery and Montauk stations, respectively. Regions of the PDP with nonzero slopes indicate where the ANN model prediction of storm surge is sensitive to each input variable.

A noticeable difference between the PDPs at the two stations is the dependence of storm surge on the storm's position as given by its latitude. At The Battery, the average storm surge response is proportional to the latitude. Generally, the storm surge response increases with latitude except for the region between about 40°N and 41.25°N, where the variables are inversely related. However, this is not the case at Montauk station where the average storm surge is seen to increase as the cyclone position shifts northward, increasing in latitude. The PDPs for the TC longitude further highlights the dependence of storm surge on storm location relative to the stations studied. At the Battery (Figure 4-10b), storm surge is expected to increase as the cyclone shifts westward closer to land. The peak storm surge is expected to occur when the cyclone is near -74°W, in close proximity to the station. As the position of the TC shifts further westward past the station, the storm surge values decrease. Similarly, at the Montauk station the peak storm surge is expected when the storm is near the station.

The partial dependence of storm surge on the cyclone's pressure is the most straightforward. The water levels are inversely proportional to the cyclone's minimum pressure. Above about 1000 mb the values of storm surge are negligible at both stations. It is noteworthy to point how the degree to which the storm surge depends on each of the input variables is lower at the Montauk station, possibly pointing to the influence of station location as Montauk is farther away from the paths of the cyclones.

Results indicate less sensitivity of storm surge to the TC's R_{max}, translation speed and maximum wind speed. In general, at both stations, the dependence of storm surge on the R_{max} is seen to slightly decrease with increasing storm size. The opposite pattern is seen at both stations for the cyclone translation speed and maximum wind speed. Storm surge values show a slight increase with increasing storm forward motion and intensity.

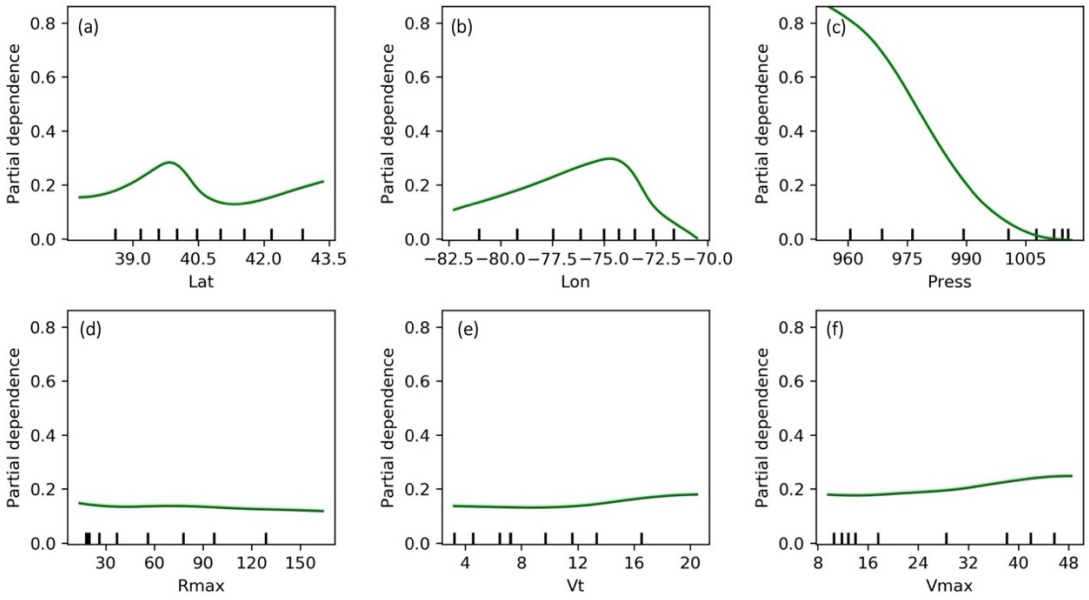

Figure 4-10. Partial dependence plots for the input variables: (a) latitude, (b) longitude, (c) pressure (mb), (d) R_{max} (km), (e) translation speed (m/s) and (f) maximum wind speed (m/s), examined at The Battery station.

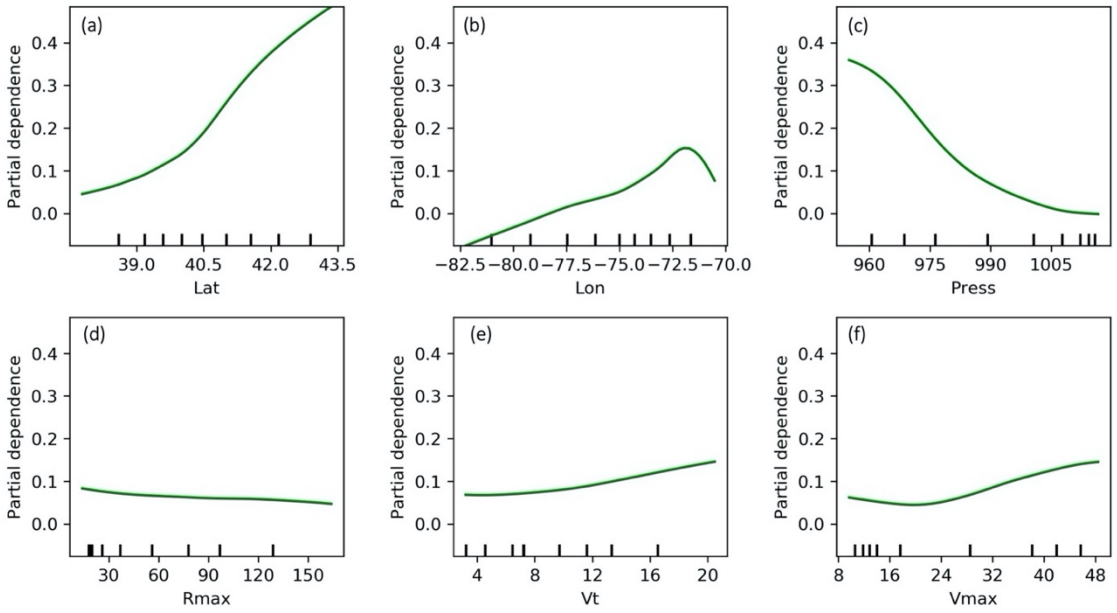

Figure 4-11. Partial dependence plots for the input variables: (a) latitude, (b) longitude, (c) pressure (mb), (d) R_{max} (km), (e) translation speed (m/s) and (f) maximum wind speed (m/s), examined at Montauk station.

4.5 Discussion

Data-driven ANNs are being used as a fast and accurate alternative for prediction of physical variables in storm surge assessment. ANNs are tuned to the dataset used for the training process. In this study, we determined the set of hyperparameters to use for the data given by a pre-computed set of synthetic tropical cyclones to forecast storm surge at multiple stations. A multi-output ANN is implemented to account for spatial correlations between five neighboring stations.

We tested various lead-time configurations (0-, 1-, 2-, 3-, 6- and 12-hour lead times) via a 10-fold cross-validation method. The training and validating process was repeated 10 times for each of the six lead-time configurations tested to determine the

best set of hyperparameters to use and obtain the average model performance. The most accurate model tested was Model 3 (2-hr lead time), which consisted of two hidden layers with 100 and 200 neurons, in each layer. The comparison between the ANN predicted water levels against the target values (simulated by the ADCIRC model), highlighted the accuracy of the ANN model in predicting storm surge. However, results indicated an underestimation by the ANN model of the peak storm surge values. The underprediction of storm surge by ANNs has also been shown in other studies (Hashemi et al., 2016; Sahoo & Bhaskaran, 2019). Several reasons are proposed to explain this behavior.

The data used for training might be skewed towards values that produce more moderate water levels. It is known that ANNs fail to make accurate predictions beyond the range of data used for training (Hashemi et al., 2016; Mosavi et al., 2018). The synthetic cyclones used as input for the ANN model were design to be constrained by the historical TC record. That is, the distributions of maximum wind speed, pressure, translation speed and radius of maximum winds are within the ranges observed for historical cyclones near the Mid-Atlantic Bight. The water levels simulated for these storms resulted in moderate levels. Specifically, the output data used for training has peak levels ranging between 1.56 and 2.24 m for the different stations. However, on average the output values used for training are much lower, mostly below 1.0 m. A broader distribution in the dataset used for training might result in more accurate predictions of the peak values evaluated here.

Another explanation for the underprediction of peak values is that in the configuration implemented, the ANN model only forecasts based on the data given at

each time step, $t_{i,}$ and does not consider the relationship between predictions at t_i and t_{i-1}. That is, the ANN has no memory of the values predicted in the prior time step. Long Short-Term Memory (LSTM; (Hochreiter & Schmidhuber, 1997) neural networks have the ability to learn long-term dependencies (Le et al., 2019), and as such it is an approach commonly implemented in time series forecasting to address this issue and account for correlations across timesteps.

Throughout the process of developing an ANN model we have been able to determine the parameters and infrastructure needed for its successful implementation. We have also been able to identify some of the model limitations and potential areas of improvement. The results presented have demonstrated the utility of ANNs as a powerful forecasting tool due to their computational efficiency and skill. ANN models show great potential to be implemented as a real-time storm surge forecasting system. However, to achieve this, consideration must be given to the limitations identified in this study. The results presented are an indication that more data should be included to support the training process. For storm surge assessment this implies a larger number of TCs that portray a wider range of both TC and storm surge scenarios. Specifically, the ANN model should be trained with a large number of samples of extreme storm surge events. The optimal number of TC cases needed for training is another topic of research that must be targeted in the consideration of using ANNs as real-time forecasting systems. The HWCM model used to simulate the synthetic tracks that served as input during training of the ANN model, facilitates the creation of additional cyclone scenarios which can be seamlessly included in the ANN model training process.

The assessment of permutation variable importance identified the cyclone minimum pressure as the most important variable in accurately predicting storm surge. While the ANN has no understanding of the underlying physics, our knowledge on storm surge validates this result. This is not to say, however, that the other input variables are not physically relevant or important. The magnitude of storm surge is known to depend on the cyclone's intensity as given by the minimum pressure, due to the inverse barometer effect (Pore, 1964). The maximum wind speed of the cyclone, which is known to be strongly correlated with storm surge, is ranked in fourth place. The fact that the maximum wind speed is ranked lower than the minimum pressure is somewhat unexpected. However, since these variables are highly correlated, the variable importance analysis may be giving a higher priority to one of the features, in this case the minimum pressure. While the permutation method provides useful insight, this is one of the drawbacks of the method when features are correlated. On the other hand, the calculated wind speeds have a higher variability than the pressure. Due to this inherent variability, the permutation of the maximum wind speed might not be exhibiting such a strong error response.

The cyclone position, given by the latitude and longitude, are ranked as the second and third most important variables, respectively. This result is not surprising. Recent studies have highlighted the importance of accounting for the cyclone's location, specifically their location at landfall, in assessing storm surge impacts. Based on the cyclone location, the cyclone will be affecting regions with different bathymetric and topographic features, which are important in accurately forecasting storm surge impacts.

The importance of the cyclone location is also highlighted in the results from the partial dependence analysis, which shows a high sensitivity of storm surge to the cyclones position, specifically the latitude. Results highlight the variation of storm surge from one station to the other. Results indicate a higher variability of the storm surge response relative to increasing latitude at The Battery station, compared to the Montauk station, which may point to the differences between the station locations. The Battery is an enclosed station near multiple channels and rivers, whereas the Montauk station is in a less geographically complex area (Figure 4-2). Generally, these results point to the importance of striving to obtain the most accurate atmospheric data available when assessing storm surge impacts.

The implementation of an ANN model for storm surge assessment proved to be a fast and reliable alternative to process-based methods. While we were able to develop and implement a skillful ANN model, the study and the methods presented are not without their limitations. As discussed, the study can be improved by including a broader range of TC scenarios that account for higher storm surge estimates, as well as implementing the LSTM method to improve the time series forecasts. Analysis of the ANN model input and output provided useful insight into the physics of storm surges and the variables needed for forecasting. The work presented thus alluded to the issues that need to be addressed in order to eventually rely on ANNs as real-time storm surge forecasting systems.

4.6 Conclusions

The goal of this study was to design an ANN model for the Mid-Atlantic Bight region, in order to understand the parameters needed for its successful implementation. We performed a cross-validation method to assess the ideal hyperparameters to use in configuring the ANN model and determine the most accurate lead-time configuration. The ANN was shown to be able to accurately forecast storm surge time series at multiple station locations. Results from the ANN were used to understand how each of the input variables relating to the cyclone physical parameters contributed to the overall storm surge forecast.

Results indicate that for out dataset, an ANN model used to forecast storm surge at a 2-hr lead time required the use of two hidden layers with 100 and 200 neurons in each layer, respectively. Assessment of the model performance in predicting storm surge levels, pointed to the skill of the model in accurately predicting moderate values of storm surge. The model, however, exhibited limitations in peak-value predictions. The cyclone minimum pressure and its position were identified as the top three most important variables for forecasting storm surge, supporting results from recent studies highlighting the dominant role of cyclone impact location in storm surge assessment.

ANNs show promise in their use for rapid and accurate storm surge predictions. The work presented highlighted the limitations and areas of improvement that must be addressed in order to implement ANNs as real-time forecasting systems.

4.7 References

Bennett, V. C., & Mulligan, R. P. (2017). Evaluation of surface wind fields for prediction of directional ocean wave spectra during Hurricane Sandy. *Coastal Engineering, 125*, 1-15.

Bloemendaal, N., Muis, S., Haarsma, R. J., Verlaan, M., Irazoqui Apecechea, M., de Moel, H., et al. (2019). Global modeling of tropical cyclone storm surges using high-resolution forecasts. *Climate Dynamics, 52*(7), 5031-5044. https://doi.org/10.1007/s00382-018-4430-x

Booij, N., Ris, R. C., & Holthuijsen, L. H. (1999). A third-generation wave model for coastal regions: 1. Model description and validation. *Journal of Geophysical Research: Oceans, 104*(C4), 7649-7666.

Breiman, L. (2001). Random forests. *Machine learning, 45*(1), 5-32.

Bruyère, C. L., Done, J. M., Jaye, A. B., Holland, G. J., Buckley, B., Henderson, D., et al. (2019). Physically-Based Landfalling Tropical Cyclone Scenarios in Support of Risk Assessment. In: Weather and Climate Extremes.

Elko, N., Dietrich, C., Cialone, M., Stockdon, H., Bilskie, M. W., Boyd, B., et al. (2019). Advancing the understanding of storm processes and impacts. *Shore & Beach, 87*(1), 37.

Friedman, J. H. (2001). Greedy function approximation: a gradient boosting machine. *Annals of statistics*, 1189-1232.

Hashemi, M. R., Spaulding, M. L., Shaw, A., Farhadi, H., & Lewis, M. (2016). An efficient artificial intelligence model for prediction of tropical storm surge. *Natural Hazards, 82*(1), 471-491. journal article. https://doi.org/10.1007/s11069-016-2193-4

Hochreiter, S., & Schmidhuber, J. (1997). Long short-term memory. *Neural computation, 9*(8), 1735-1780.

Holland, G. J. (1980). An analytic model of the wind and pressure profiles in hurricanes. *Monthly weather review, 108*(8), 1212-1218.

Hussain, M. A., Tajima, Y., Hossain, M. A., & Das, P. (2017). Impact of Cyclone Track Features and Tidal Phase Shift upon Surge Characteristics in the Bay of Bengal along the Bangladesh Coast. *Journal of Marine Science and Engineering, 5*(4), 52. http://www.mdpi.com/2077-1312/5/4/52

Irish, J. L., Resio, D. T., & Ratcliff, J. J. (2008). The influence of storm size on hurricane surge. *Journal of Physical Oceanography, 38*(9), 2003-2013. Article.

Kim, S.-W., Melby, J. A., Nadal-Caraballo, N. C., & Ratcliff, J. (2015). A time-dependent surrogate model for storm surge prediction based on an artificial neural network using high-fidelity synthetic hurricane modeling. *Natural Hazards, 76*(1), 565-585. journal article. https://doi.org/10.1007/s11069-014-1508-6

Le, X.-H., Ho, H. V., Lee, G., & Jung, S. (2019). Application of long short-term memory (LSTM) neural network for flood forecasting. *Water, 11*(7), 1387.

Luettich, R. A., & Westerink, J. (2004). *Formulation and Numerical Implementation of the 2D/3D ADCIRC Finite Element Model Version 44.XX*. Retrieved from Chapel Hill, NC: http://www.unc.edu/ims/adcirc/adcirc_theory_2004_12_08.pdf

Luettich, R. A., Westerink, J. J., & Scheffner, N. W. (1992). ADCIRC: An Advanced Three-Dimensional Circulation Model for Shelves, Coasts, and Estuaries. Report 1. Theory and Methodology of ADCIRC-2DDI and ADCIRC-3DL. In *Dredging Research Program Technical Report DRP-92-6* (pp. 137). Vicksburg, MS: COASTAL ENGINEERING RESEARCH CENTER.

Marsooli, R., & Lin, N. (2018). Numerical Modeling of Historical Storm Tides and Waves and Their Interactions Along the US East and Gulf Coasts. *Journal of Geophysical Research: Oceans*.

McGovern, A., Lagerquist, R., John Gagne, D., Jergensen, G. E., Elmore, K. L., Homeyer, C. R., & Smith, T. (2019). Making the black box more transparent: Understanding the physical implications of machine learning. *Bulletin of the American Meteorological Society, 100*(11), 2175-2199.

Mosavi, A., Ozturk, P., & Chau, K.-w. (2018). Flood prediction using machine learning models: Literature review. *Water, 10*(11), 1536.

NOAA/NOS/CO-OPS. Tides and Currents. Retrieved from https://tidesandcurrents.noaa.gov

Pedregosa, F., Varoquaux, G., Gramfort, A., Michel, V., Thirion, B., Grisel, O., et al. (2011). Scikit-learn: Machine learning in Python. *Journal of machine learning research, 12*(Oct), 2825-2830.

Pore, N. A. (1964). The Relation of Wind and Pressure to Extratropical Storm Surges at Atlantic City. *Journal of Applied Meteorology, 3*(2), 155-163. https://journals.ametsoc.org/doi/abs/10.1175/1520-0450%281964%29003%3C0155%3ATROWAP%3E2.0.CO%3B2

Ramos, A. (2019). *Effect of Tropical Cyclone Landfall Angle on Storm Surge*.

Ramos-Valle, A., Curchitser, E., Bruyère, C., & Fossell, K. (2018). Simulating Storm Surge Impacts with a Coupled Atmosphere-Inundation Model with Varying Meteorological Forcing. *Journal of Marine Science and Engineering, 6*(2), 35. http://www.mdpi.com/2077-1312/6/2/35

Ramos-Valle, A. N., Curchitser, E. N., & Bruyère, C. L. (2020). Impact of Tropical Cyclone Landfall Angle on Storm Surge Along the Mid-Atlantic Bight. *Journal of Geophysical Research: Atmospheres*, e2019JD031796. https://agupubs.onlinelibrary.wiley.com/doi/abs/10.1029/2019JD031796

Rappaport, E. N. (2014). Fatalities in the United States from Atlantic tropical cyclones: New data and interpretation. *Bulletin of the American Meteorological Society, 95*(3), 341-346.

Rego, J. L., & Li, C. (2009). On the importance of the forward speed of hurricanes in storm surge forecasting: A numerical study. *Geophysical Research Letters, 36*(7). https://agupubs.onlinelibrary.wiley.com/doi/abs/10.1029/2008GL036953

Sahoo, B., & Bhaskaran, P. K. (2019). Prediction of storm surge and coastal inundation using Artificial Neural Network – A case study for 1999 Odisha Super Cyclone. *Weather and Climate Extremes, 23*, 100196. http://www.sciencedirect.com/science/article/pii/S2212094718301695

Taylor, K. E. (2001). Summarizing multiple aspects of model performance in a single diagram. *Journal of Geophysical Research: Atmospheres, 106*(D7), 7183-7192. https://agupubs.onlinelibrary.wiley.com/doi/abs/10.1029/2000JD900719

Thomas, A., Dietrich, J., Asher, T., Bell, M., Blanton, B., Copeland, J., et al. (2019). Influence of storm timing and forward speed on tides and storm surge during Hurricane Matthew. *Ocean Modelling, 137*, 1 - 19. http://www.sciencedirect.com/science/article/pii/S1463500318302609

Tseng, C.-M., Jan, C.-D., Wang, J.-S., & Wang, C. (2007). Application of artificial neural networks in typhoon surge forecasting. *Ocean Engineering, 34*(11-12), 1757-1768.

Wang, Q., Chen, J., & Hu, K. (2016). *Storm surge prediction for Louisiana Coast using artificial neural networks.* Paper presented at the International Conference on Neural Information Processing.

Weisberg, R. H., & Zheng, L. (2006). Hurricane storm surge simulations for Tampa Bay. *Estuaries and Coasts, 29*(6), 899-913.

CHAPTER 5. SUMMARY

5.1 Summary and Implications

Atmospheric forcing is the main driver of storm surge (Dietrich et al., 2017; Lakshmi et al., 2017). In this study we examined the role of atmospheric forcing in driving storm surge, both from a physical and a modeling standpoint. The work presented was motivated by the need for improved storm surge forecasting methods that can help mitigate the damages and impacts from tropical cyclones (TCs).

First, we compared the use of different wind field models as atmospheric forcing for storm surge forecasting (discussed in Chapter 2). We coupled the Weather Research and Forecasting model (WRF; Skamarock et al., 2008) and the Advanced Circulation (ADCIRC; Luettich & Westerink, 2004; Luettich et al., 1992) models to perform a hindcast of Hurricane Sandy's storm surge for two meteorological forcing configurations. One simulation directly used the full wind and pressure field output from the WRF simulation. The other consisted of using track data derived from the WRF simulation, implemented within a parametric vortex model, such that the differences between the storm surge forecasts can be attributed to the differences in the wind field representations. Results indicate the effectiveness of using full wind and pressure fields derived from WRF over the implementation of the WRF-derived track within the parametric model. This has important implications for the future of storm surge forecasting since parametric models are most often implemented due to their computational efficiency. The higher accuracy achieved with fully-physics models prompts the need to optimize these for storm surge forecasting and quantify their limitations. We also show that a higher resolution

atmospheric simulation (i.e. 4 km against 12 km resolution), which has a much higher computational cost, is not necessary to accurately depict the storm surge magnitude and spatial extent. This is an important consideration for real-time storm surge forecasting, where timely predictions are needed.

We then used our findings to support the implementation of a novel method for simulating synthetic cyclones, the Hybrid WRF Cyclone Model (HWCM; Bruyère et al., 2019). We presented this approach to aid in the understanding of how different processes contribute to storm surge and inundation and by extension, improve storm surge predictability. We showed the first application of this advanced and novel model to study storm surge sensitivity to TC landfall angle, by coupling it with the ADCIRC hydrodynamic model. Our results indicate that cyclones with tracks perpendicular to the New Jersey coast produce the highest storm surge, the broadest offshore surge extent and cause more widespread inland flooding than cyclones approaching the coast at more oblique angles or parallel to the coast. This is also indicative of the sensitivity of storm surge to cyclone landfall location. The storm surge impact is not homogenous along the coast and strongly depends on the cyclone landfall location and the geographical characteristics of the impact region. Some regions are more vulnerable than others, exhibiting less sensitivity to changes in cyclone landfall angle. This result has implications for how mitigation efforts are carried out. Proposed solutions for planning and mitigation should begin at the local level as they must be tailored to the hazards and risks of each location (Helderop & Grubesic, 2019).

Finally, an artificial neural network (ANN) was implemented which produced timely and accurate storm surge forecasts. The ANN was trained with the ensemble of TCs and storm surge generated in Chapter 4. The use of an ANN also facilitated our understanding of the degree to which storm surge depends on various TC characteristics (e.g. cyclone location, maximum wind speed, minimum pressure, translation speed and size). We show that cyclone intensity, as given by the minimum pressure, is ranked as the most important variable for accurately predicting storm surge with the ANN. We also highlight the importance of the cyclone's position (as given by the latitude and longitude), in agreement with our previous findings on the dominant role of landfall location in the expected storm surge. The development of the ANN allowed us to determine the configuration needed to implement a successful model and determine its limitations. The ANN model had an average error of 0.08 m, considerably less than the error obtained with traditional process-based methods, which for the Mid-Atlantic Bight region can often be more than 0.5 m (FEMA, 2011). ANNs thus prove to be a useful method for rapid and accurate storm surge assessment and show promise in being implemented as a hazards assessment and forecasting tool in the future.

We developed a storm surge modeling framework that can be applied to other regions and extended to isolate and quantify the impact from other fundamental mechanisms that can impact surge (e.g. storm size, translation speed and intensity). Additionally, in the process of examining the response of storm surge to cyclone landfall angle, we created a set of 200 synthetic cyclones that can be used for other applications. The modeling framework and the data can be applied in numerous research areas

including, for example, studies of TC-induced precipitation events and studies on future climate scenarios. Understanding how storm surge is expected to respond to varying climate conditions is an important consideration for purposes of planning and construction of infrastructure along and near the coastline. Key areas of further research result from the development of this modeling framework, including: (i) the study of the effect of the projected climate change conditions on TC-induced storm surge in terms of changes to cyclone characteristics and the projected rise in sea level, (ii) the modification and development of the current modeling framework to include a hydrology model that can account for the compound effect of storm surge and precipitation.

The methodologies and results presented in this work, are a step towards a comprehensive assessment of storm surge that includes the evaluation of the physical and societal impacts. We developed a modeling framework, applicable to other regions, and demonstrated its utility in storm surge forecasting. The conclusions derived from this study will allow for more accurate assessment of storm surge, ultimately leading to better predictions in hopes of mitigating future damages from TC-induced storm surge.

5.2 References

Bruyère, C. L., Done, J. M., Jaye, A. B., Holland, G. J., Buckley, B., Henderson, D., et al. (2019). Physically-Based Landfalling Tropical Cyclone Scenarios in Support of Risk Assessment. http://www.sciencedirect.com/science/article/pii/S2212094718302123

Dietrich, J., Muhammad, A., Curcic, M., Fathi, A., Dawson, C., Chen, S., & Luettich Jr, R. (2017). Sensitivity of Storm Surge Predictions to Atmospheric Forcing during Hurricane Isaac. *Journal of Waterway, Port, Coastal, and Ocean Engineering, 144*(1), 04017035.

FEMA. (2011). Redefinition of the Coastal Flood Hazard Zones in FEMA Region II: Analysis of the Coastal Storm Surge Flood Frequencies. In. Washington, DC.

Helderop, E., & Grubesic, T. H. (2019). Social, geomorphic, and climatic factors driving US coastal city vulnerability to storm surge flooding. *Ocean & coastal management*, 104902.

Lakshmi, D. D., Murty, P., Bhaskaran, P. K., Sahoo, B., Kumar, T. S., Shenoi, S., & Srikanth, A. (2017). Performance of WRF-ARW winds on computed storm surge using hydodynamic model for Phailin and Hudhud cyclones. *Ocean Engineering, 131*, 135-148.

Luettich, R. A., & Westerink, J. (2004). *Formulation and Numerical Implementation of the 2D/3D ADCIRC Finite Element Model Version 44.XX*. Retrieved from Chapel Hill, NC: http://www.unc.edu/ims/adcirc/adcirc_theory_2004_12_08.pdf

Luettich, R. A., Westerink, J. J., & Scheffner, N. W. (1992). ADCIRC: An Advanced Three-Dimensional Circulation Model for Shelves, Coasts, and Estuaries. Report 1. Theory and Methodology of ADCIRC-2DDI and ADCIRC-3DL. In *Dredging Research Program Technical Report DRP-92-6* (pp. 137). Vicksburg, MS: COASTAL ENGINEERING RESEARCH CENTER.

Skamarock, W., Klemp, J., Dudhia, J., Gill, D., Barker, D., Duda, M., et al. (2008). A description of the Advanced Research WRF Version 3, NCAR technical note, Mesoscale and Microscale Meteorology Division. *National Center for Atmospheric Research, Boulder, Colorado, USA*.

APPENDIX A: SUPPORTING INFORMATION FOR CHAPTER 3

Text A-1. The Hybrid WRF Cyclone Model (HWCM) was evaluated to determine whether the behavior or the tracks was a response to the internal variability in the model or a response to the external forcing imposed at the boundaries. This evaluation was done by using the digital filter initialization (DFI) scheme in the Weather Research and Forecasting model (WRF) with filtering window of 0.5, 1, 2 and 3 hours. Two test cases were conducted using the same background wind flow of 8 m/s but different wind directional forcing at the boundaries.

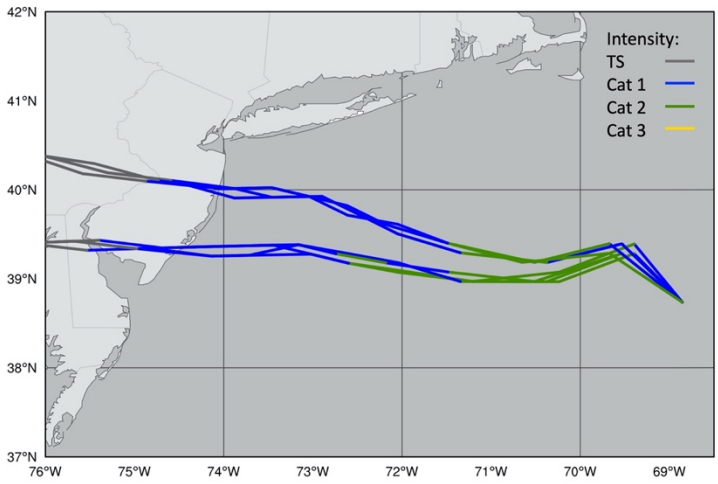

Figure A-1. Depicts the cases used to test for model variability in the HWCM. The DFI scheme, with integration time of 0.5, 1, 2 and 3 hours, was implemented within the HWCM to removed initial model instabilities by reducing high-frequency features. TC intensity is shown per each 3-hr time step.

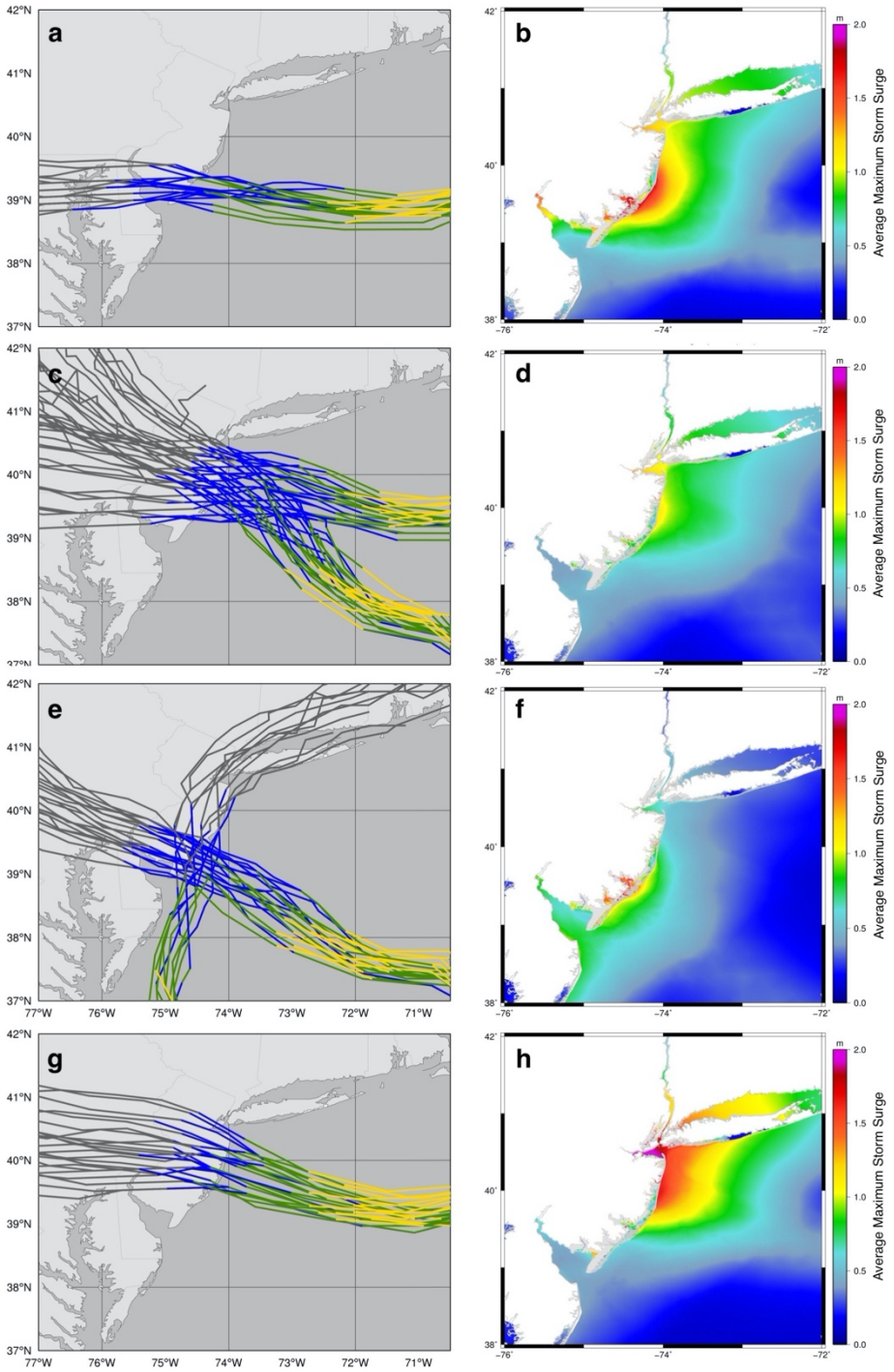

Figure A-2. K-means cluster analysis for the maximum storm surge distributions of the 113 cyclones in the HWCM ensemble that make landfall along the NJ coastline. The analysis resulted in the use of the four clusters presented here. (Left) Tracks for the

associated storm in each cluster and (right) the average maximum storm surge distributions are shown for Cluster 1, Cluster 2, Cluster 3 and Cluster 4, respectively.

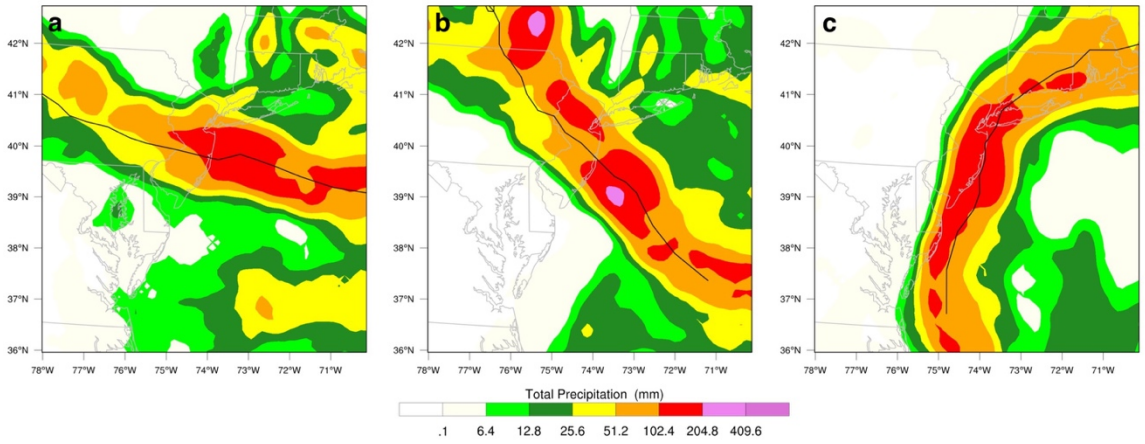

Figure A-3. Rainfall totals for the (a) perpendicular, (b) diagonal and (c) parallel tracks in the case study presented in Chapter 3, section 3.5.